

Chapter Title: DYNAMICS AND STRUCTURE OF THE URANIAN RINGS

Chapter Author(s): RICHARD G. FRENCH, PHILIP D. NICHOLSON, CAROLYN C. PORCO and ESSAM A. MAROUF

Book Title: *Uranus*

Book Editor(s): Jay T. Bergstrahl, Ellis D. Miner, Mildred Shapley Matthews

Published by: University of Arizona Press. (1991)

Stable URL: <https://www.jstor.org/stable/j.ctv1v7zdtq.13>

JSTOR is a not-for-profit service that helps scholars, researchers, and students discover, use, and build upon a wide range of content in a trusted digital archive. We use information technology and tools to increase productivity and facilitate new forms of scholarship. For more information about JSTOR, please contact support@jstor.org.

Your use of the JSTOR archive indicates your acceptance of the Terms & Conditions of Use, available at

<https://about.jstor.org/terms>



University of Arizona Press is collaborating with JSTOR to digitize, preserve and extend access to *Uranus*

JSTOR

PART IV

Rings

DYNAMICS AND STRUCTURE OF THE URANIAN RINGS

RICHARD G. FRENCH
Wellesley College

PHILIP D. NICHOLSON
Cornell University

CAROLYN C. PORCO
University of Arizona

and

ESSAM A. MAROUF
Stanford University

Since the discovery of the Uranian rings in 1977, a continuing series of Earth-based observations combined with results from the 1986 Voyager 2 encounter have provided a detailed picture of the kinematics and structure of this distant system. From multiple occultations, the Keplerian orbital elements of the rings have been established quite precisely, making it possible to identify telltale signatures of weak dynamical effects. Most of the ten known narrow rings are eccentric and inclined, and the γ and δ rings have self-excited normal modes. Several of the rings have a close connection with two small satellites, Cordelia and Ophelia, which straddle the ϵ ring and provide strong evidence for ring confinement by shepherds. A quantitative study of optical depth variations with wavelength and orbital phase provides information about the particle sizes and vertical extent of the rings. The rings are remarkably diverse in their radial structure and azimuthal variations, and a detailed comparison is presented of high-resolution ring profiles obtained from the Voyager 2 radio and stellar occultation observations. The central elements of the dynamics of ring confinement

ment by shepherding are presented. Despite the success of shepherding theories in accounting for many of the observed features of the rings, many troublesome and poorly understood elements of the dynamics of narrow rings remain. Significant progress in unravelling these mysteries can be expected during the coming years. The existing groundbased and Voyager observations will provide a solid foundation for new theoretical developments, and new Earth-based data will allow continued refinement of orbital and structural models of the rings.

I. INTRODUCTION

Since the serendipitous discovery of the Uranian rings in 1977, this remote system of narrow rings has inspired renewed interest in ring dynamics and structure. In nearly every respect, they behave contrary to seemingly reasonable and plausible expectations, most notably that rings should be broad, featureless sheets of particles in circular orbits confined to the equatorial plane of the central planet. The Uranian rings are narrow, elliptical, and inclined, forcing conventional wisdom to give way to theories of ring confinement, eccentricity maintenance, and the prevention of differential precession across the ring. Nature's imagination seems little constrained by adherence to Newton's law of gravitation, and the imaginations of scientists are stretched to account for the rich and varied phenomena revealed in planetary rings.

The ultimate goal of ring studies is to understand the origin of the rings and their subsequent evolution, but as in most physical systems, an appreciation of the present conditions must be gained before this more ambitious goal can be addressed. In this chapter, the current knowledge of the dynamics and structure of the Uranian rings is reviewed, with an emphasis on the observations that have allowed determination of accurate ring orbits and detailed radial structure. The chapter by Esposito et al. discusses the physical properties of ring particles, active physical processes, and the origin and evolution of the rings. Recent reviews of the Uranian rings are presented by Elliot and Nicholson (1984) and Elliot (1984); it will be assumed in this chapter that the reader is familiar with the overall characteristics of the Uranian rings as described therein.

The kinematics of the rings are discussed first: it will be shown that several of the Uranian ring orbits have a close connection with two small satellites, providing strong evidence for ring confinement by shepherds. A quantitative study of optical depth variations with wavelength and orbital phase leads to some tentative conclusions concerning particle sizes and the vertical structure of the rings. Next comes an examination of the structure of the rings. The rings are remarkably diverse in their radial structure and azimuthal variations, and it is clear that the underlying dynamics are still poorly understood. A basis for future work is provided through a detailed comparison of the high-resolution ring profiles obtained from the Voyager 2 occultation

tion observations. Next comes a review of the central elements of the dynamics of shepherding as currently understood, tempered by observational constraints. Finally, a selection of open questions and prospects for future progress is presented.

II. KINEMATICS OF THE RING ORBITS

A. Groundbased Observations

The Uranian rings were first observed during the stellar occultation of SAO 158687 on 10 March 1977, and for nearly a decade after their discovery most of the information about their orbits and radial structure came from more than a dozen similar stellar occultation observations. High-speed photometry is used to observe the fuzzy shadows cast by the rings on the Earth, providing a one-dimensional scan of the ring structure along the path of the occulted star as projected onto the ring plane. The occultation technique and early Uranian ring observations are reviewed in some detail by Elliot and Nicholson (1984).

The precise timing of the observed ring-occultation profiles makes it possible to determine quite accurate models of the ring orbits. Such models are of interest because the rings both contribute and respond to the gravitational field of the Uranian system: the kinematical properties of the rings reflect the underlying dynamical processes responsible for ring confinement and ring structure. As the ring plane radii of the midpoints of individual ring profiles can be determined to better than a few hundred m, corresponding to precisions of approximately one part in 10^5 , even very weak dynamical effects might leave recognizable signatures in the ring orbits. Additionally, as discussed below, some of the rings are located at resonances with small satellites, but in order to determine the dynamical significance of these resonances it must first be demonstrated that the rings or their edges do in fact lie at the appropriate resonant radii. Thus, there has been a strong impetus for continual improvement in the models of the ring orbits.

A full decade of worldwide Uranus ring occultation observations has produced a rich data set characterized by a long time baseline, broad coverage of a wide range of ring longitudes, and multiple-station observations of several individual occultations. Recent surveys of these observations were published by Elliot and Nicholson (1984), French et al. (1986a) and French et al. (1988a). From these groundbased data alone, a reasonably accurate kinematical model of the ring system was obtained, but information about internal ring structure was severely restricted by the diffraction-limited resolution of the ring profiles. Prior to the Voyager encounter with Uranus in 1986, the following picture had emerged of the orbital characteristics of the 9 known Uranian rings (French et al. 1986a,b):

1. Accurate inclined, precessing elliptical ring orbits were determined for 7 of the 9 known rings (i.e., for all but the γ and δ rings), with typical uncertainties in the orbital elements of $\sigma(a) \approx 5$ km, $a\sigma(e) \approx 1$ km, and $\sigma(i) \approx 0^\circ 005$;
2. Typical post-fit ring plane orbital radius residuals of 0.2 to 0.6 km for these rings were comparable to the uncertainties in the midpoints of the ring profiles for many data sets;
3. The δ ring was shown to have a wavenumber $m = 2$ azimuthal distortion with an amplitude of several km, but its cause was not established;
4. The γ ring showed *rms* radius residuals ≈ 3 km, well above the uncertainties in the data, but of unknown origin.

B. Voyager Observations

The passage of Voyager 2 through the Uranus system in January 1986 (Stone and Miner 1986) provided crucial complementary information about the Uranian rings. Images during the approach phase (Fig. 1) confirmed the overall characteristics of the rings as inferred from groundbased observations, and revealed previously undetected features. These included 2 new rings (the faint narrow λ ring, formerly known by its preliminary designation of 1986U1R, lying between rings δ and ϵ , and a broad diffuse feature inside ring 6) and a retinue of ten small satellites (Smith et al. 1986). Furthermore, forward scattering images clearly revealed a very tenuous dust sheet spanning the entire ring system. Owing to their limited spatial resolution (≈ 10 km per line pair), the Voyager images impose only weak constraints on the orbits of the rings. Nevertheless, they have been used to constrain the visual photometric properties of the ring material (Ockert et al. 1987) and to characterize the dust in the ring system. These results are discussed in the chapter by Esposito et al.

Of greater significance for an understanding of the kinematics and structure of the rings was a series of high-resolution occultation measurements made during the Voyager encounter. Two stellar occultations were observed by both the Photopolarimeter (PPS) and Ultraviolet Spectrometer (UVS) instruments, at effective wavelengths of $0.27 \mu\text{m}$ and $0.11 \mu\text{m}$, respectively (Lane et al. 1986; Holberg et al. 1987). The event geometry for the Voyager occultations is shown in Fig. 2. The azimuthally near-grazing occultation of σ Sagittarii spanned the region of the δ and ϵ rings only, but the unusually small projected radial velocities of 0.3 to 1.0 km s^{-1} resulted in profiles for these two rings of good signal-to-noise ratio and extremely high sampling resolution: 3 to 10 m for the PPS experiment and 100 to 300 m for UVS. (Large, abrupt changes in ring opacity can be localized with this spatial precision, although the data must be averaged to reveal more subtle structural variations in the presence of noise.) This occultation also resulted in the only such detection to date of λ , the tenth Uranian ring, located between the δ and ϵ rings and first discovered in Voyager images (Smith et al. 1986).

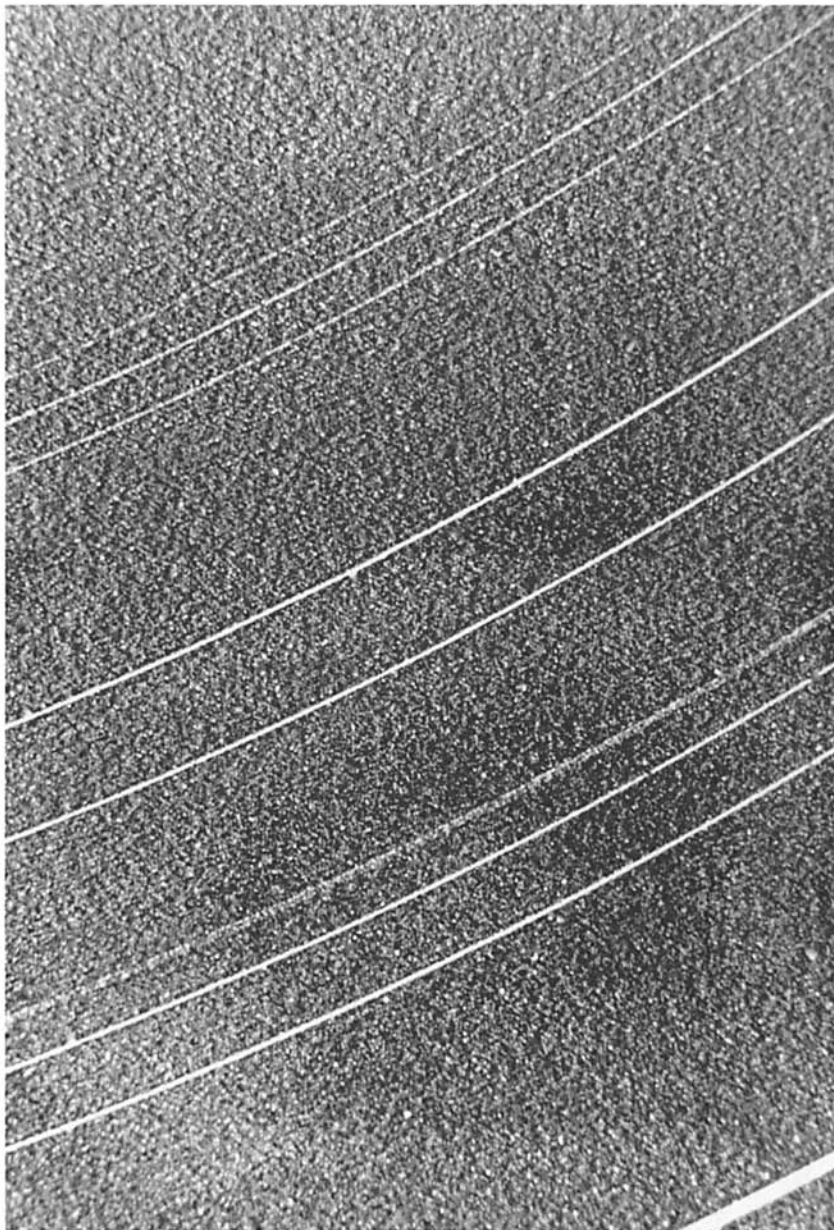


Fig. 1. The Uranian rings in backscattered light. This mosaic is composed of 2 Voyager images taken through the broadband clear filter (effective wavelength of $0.48 \mu\text{m}$) from a distance of approximately $1.1 \times 10^6 \text{ km}$, at a phase angle of 18° and an emission angle of 21° . The image scale is 10 km pixel^{-1} . The frames have been processed to enhance narrow features. The 9 classical Uranian rings are clearly visible. The 10th ring λ (formerly known as 1986U1R), can be seen faintly midway between the broad ϵ ring, imaged here at apoapse, and the δ ring. Both the bright, narrow inner component and the fainter, extended outer component of the η ring are distinct. Only the ϵ ring, which reaches its greatest width of 96 km at this azimuth, and the broad η ring component are resolved.

The occultation of β Persei provided two complete sets of ring profiles, at an average radial resolution of 120 meters for PPS and 4 km for UVS. Regrettably, the UVS data from this occultation were rendered almost unusable by a very high charged-particle background in the instrument, and only the ϵ ring egress profile was salvaged. Although more comprehensive, the PPS data from this occultation are of lower signal-to-noise ratio than the σ Sgr data, owing to the comparative faintness of β Per in the ultraviolet and to the higher radial velocity.

Two additional occultation cuts through the entire ring system were obtained by the Voyager radio-occultation experiment using the Radio Science Subsystem (RSS), each at wavelengths of 3.6 cm (X band) and 13 cm (S band) (Tyler et al. 1986; Gresh et al. 1989). The occultation track as seen from above the ring plane is shown in Fig. 2. While the radio-occultation technique is similar in principle to groundbased and spacecraft-based stellar occultations, it differs fundamentally in several important respects due to the different nature of the illuminating source. For the radio occultations, coherent radio signals generated onboard Voyager referenced to an ultra-stable oscillator were used to illuminate the rings. Both the intensity and relative phase change (retardation or advance) of the signal diffracted by the rings were

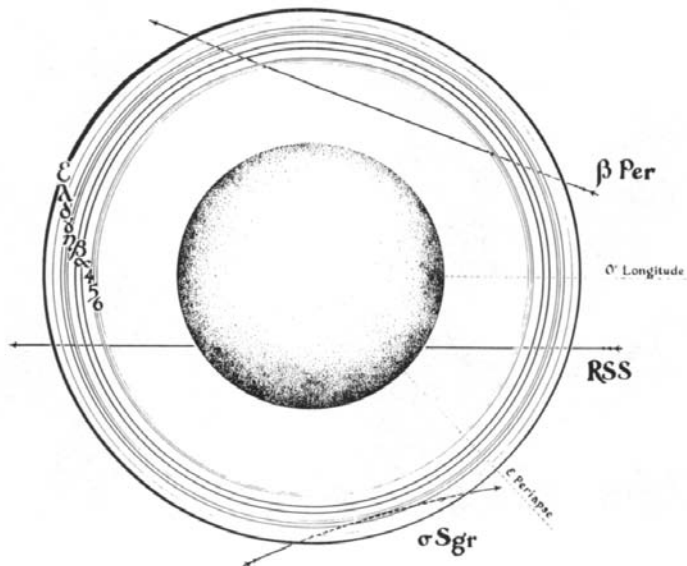


Fig. 2. Geometry of the Voyager stellar and radio occultations, as projected onto the ring plane, and viewed from the north rotational pole of Uranus. The dual-frequency radio occultation cuts are designated RSS, while the 2 stellar occultations observed by the PPS and UVS instruments are identified by the star names. The location of zero longitude (ascending node of the ring plane on the Earth's equator) and the direction to the ϵ ring's periapse are shown for reference (figure courtesy of M. Cooke).

observed on the Earth. The availability of the phase shift information distinguishes the radio-occultation observations and permits subsequent reconstruction to remove diffraction effects (Marouf et al. 1986), yielding ring profiles at radial resolutions as fine as 50 m at X band and 500 m at S band (Gresh et al. 1989), under the assumption that the ring structure does not vary strongly in azimuth over a distance of several Fresnel scales (tens of km at S band) along the ring. The reconstructed ring profiles have the highest signal-to-noise ratio of any Voyager data set, and greatly surpass in radial resolution (though averaged over many km in azimuth) any of the groundbased data.

To illustrate the utility of the phase shift information for diffraction removal, the example of the δ ring is depicted in Fig. 3 (Gresh et al. 1989).

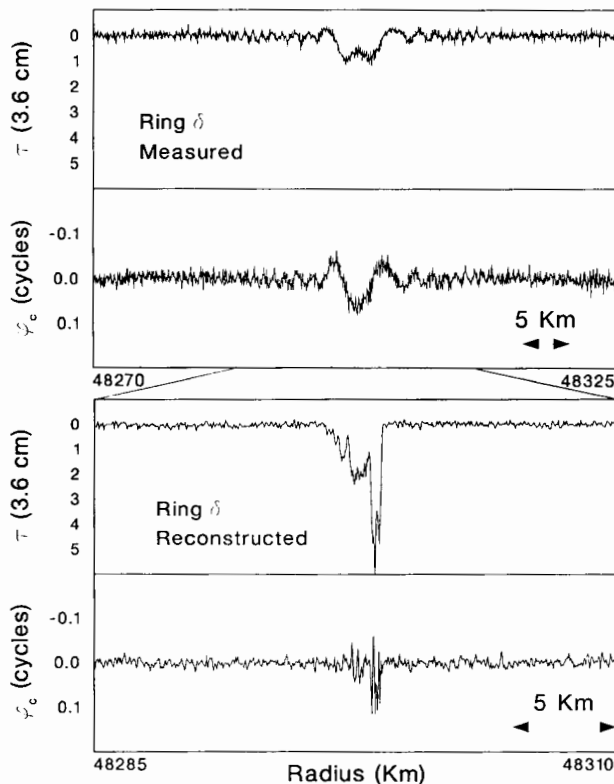


Fig. 3. Diffraction reconstruction of the RSS δ ring egress profile. Voyager radio-occultation observations are initially diffraction limited, as optical depth and phase shift profiles of the δ ring (top two panels) clearly show. The phase information, unique to radio occultation, makes it possible to reconstruct the profiles to remove diffraction effects (bottom two panels), revealing detailed ring structure (Marouf et al. 1986; Gresh et al. 1989). Note that while the initial diffraction pattern closely resembles classical diffraction by an opaque strip (square-well model), marked asymmetry characterizes the actual ring profile.

The top two panels show the initial X-band diffraction-limited profiles of optical depth τ and phase shift ϕ_c . Because the ring width is comparable to the experiment Fresnel scale (~ 2 km), the large-scale behavior of the τ and ϕ_c profiles resembles classical diffraction by an opaque narrow strip, analogous to the “square-well” model usually used to interpret diffraction-limited groundbased observations (see below). The true τ and ϕ_c profiles can be recovered from the observations through an inverse Fresnel transform operation (Marouf et al. 1986). Results for the δ ring are depicted in the two lower panels of Fig. 3, where significant detailed structure is clearly revealed. All radio occultation profiles presented below were reconstructed using similar inverse Fresnel transform procedures, generalized to include finite ring ellipticity (Gresh et al. 1989). Note that the reconstructed phase shift profiles provide information about ring particle size distributions that is not available from other occultation observations (Marouf et al. 1982). Further discussion of the phase shift observations at Uranus can be found in the chapter by Esposito et al.

C. Ring Orbit Models

In practice, ring orbits are determined by comparing the observed mid-times of ring occultations with calculations based on an assumed ring orbit model, which is then iteratively refined until the best match is found between the model and the data. The model parameters of the fit include the Keplerian orbital elements of the rings, the direction of the pole of Uranus, harmonic coefficients of the planet’s gravitational field, and offsets in right ascension and declination between the predicted and observed relative positions of the planet and the occulted star at the epoch of the occultation. The latter are due to uncertainties in the planetary ephemeris and the positions of the stars. It is essential that the observations be accurately timed and well calibrated, as emphasized by Elliot and Nicholson (1984) in their summary of techniques for groundbased observations.

The geometric characteristics of the occultations are also important. The large obliquity of Uranus and the nearly pole-on aspect of the planet as viewed from the Earth during recent years are favorable for the determination of the shapes of the ring orbits, but not for estimating inclinations of the rings or the direction of the planetary pole. The uncertainty in the pole direction and its strong correlation with the absolute radius scale of the rings was the most severe limitation of pre-Voyager orbit models. The situation was dramatically improved by the Voyager occultation observations, which provided a range of viewing geometries quite different from those obtainable from the Earth during the previous decade of observations. The stellar occultations viewed the rings at angles with respect to the mean ring plane of 62.9° for σ Sgr and -53.2° for β Per, providing particularly strong constraints on ring inclinations and the direction of the planetary pole. The pole-on geometry for the radio occultation was similar to that of groundbased observations, but

because the position of the spacecraft relative to Uranus was known throughout the event to an accuracy of about 1 km, the radio results provided an accurate determination of the absolute radius scale of the ring system.

Using the full set of spacecraft occultation results, along with previous groundbased data, French et al. (1988a) performed a least-squares fit for the Uranian ring system geometry and orbital elements. Rings 6, 5, 4, α , β , η , and ϵ were modeled as inclined, elliptical rings, with free apsidal precession and nodal regression rates determined by Uranus' gravitational harmonic coefficients J_2 and J_4 . The newly discovered narrow ring λ was modeled as circular and in the equatorial plane, since only two spatially independent occultation observations were made of this faint ring. The derived orbital elements for these rings are given in Table I, along with the fitted values for J_2 and J_4 and the direction of the planetary rotation axis. Note that the formal uncertainties in the ring semimajor axes are now well under 1 km.

D. Normal Modes

An important result from the Voyager observations was the discovery of the existence of self-excited normal modes in narrow rings. Borderies et al. (1985) found that, for a model of a densely packed differentially rotating disk in which the particles' collective behavior is more like a liquid than a gas, free density waves of arbitrary m become unstable. In the presence of a feedback mechanism, these waves can, in principle, amplify, become self-sustaining and eventually become detectable. A self-gravitating ring with sharp edges can provide a resonant cavity in which such a disturbance might grow, so long as it is sufficiently narrow.

In general, the resulting systematic distortion of the particle streamlines can be written in the form

$$r(\theta, t) = a[1 - e \cos m(\phi - \phi_0)] \quad (1)$$

where

$$\phi = \theta - \Omega_p t \quad (2)$$

a is the mean radius, ae is the amplitude of the distortion, ϕ_0 is an arbitrary phase, and Ω_p is the 'pattern speed', i.e., the rate at which the distortion rotates relative to inertial space. By simultaneously requiring that individual ring particle orbits correspond to the usual Keplerian ellipses,

$$r(\theta, t) \approx a[1 - e \cos (\theta - \bar{\omega})] \quad (3)$$

where $\bar{\omega}$ is the longitude of pericenter, we find (cf. Borderies and Longaretti 1987) that we must have

TABLE I
Eccentric Ring Orbit Solution from Earth-Based and Voyager 2 Occultation Observations

Ring	Eccentric Ring Orbital Elements ^a					
	Semimajor Axis <i>a</i> (km)	Eccentricity <i>e</i> ($\times 10^3$)	Longitude of Periape $\bar{\omega}_0$ (deg) ^b	Inclination <i>i</i> (deg)	Longitude of Ascending Node Ω_0 (deg) ^b	rms Ring Orbit Residual (km)
6	41837.15 ± 0.26	1.013 ± 0.004	242.80 ± 0.34	0.0616 ± 0.0010	12.12 ± 0.62	0.23
5	42234.82 ± 0.27	1.899 ± 0.005	170.31 ± 0.29	0.0536 ± 0.0013	286.57 ± 0.74	0.27
4	42570.91 ± 0.28	1.059 ± 0.004	127.28 ± 0.29	0.0323 ± 0.0006	89.26 ± 1.70	0.27
α	44718.45 ± 0.22	0.761 ± 0.004	333.24 ± 0.27	0.0152 ± 0.0006	63.08 ± 2.92	0.32
β	45661.03 ± 0.13	0.442 ± 0.003	224.88 ± 0.56	0.0051 ± 0.0006	310.05 ± 11.50	0.26
γ	47175.91 ± 0.14	(0.004 ± 0.003)	(228.1 ± 57.7)	(0.0011 ± 0.0008)	(188.73 ± 30.81)	0.49
λ	50023.94 ± 0.34	(0.0)	(0.0)	(0.0)	(0.0)	0.51
ϵ	51149.32 ± 0.13	7.936 ± 0.005	214.97 ± 0.06	(0.0002 ± 0.0008)	(246.6 ± 155.2)	0.60
Harmonic Coefficients of the Gravity Potential ^c			Pole of the Equatorial Plane (deg)			
$J_2 = (3.34343 \pm 0.00032) \times 10^{-3}$			$\alpha(1950.0) = 76.5969 \pm 0.0034$			
$J_4 = (-2.885 \pm 0.045) \times 10^{-5}$			$\delta(1950.0) = 15.1117 \pm 0.0033$			

^aFor $GM = 5.79393 \times 10^{21} \text{ cm}^3 \text{ s}^{-2}$. The orbital elements for the γ and δ rings include normal modes, as given in Table II.

^bAt 20:00 UT on 10 March 1977 at Uranus. Longitudes are measured in the prograde direction from the ascending node of Uranus' equator on the Earth's equator of 1950.0.

^cFor a reference radius $R = 26,200 \text{ km}$.

$$\theta - \tilde{\omega} = m(\phi - \phi_0). \quad (4)$$

This expression specifies the necessary value of $\tilde{\omega}$ at each (θ, t) such that the combined effect of the individual particle orbits yields the overall ring distortion given by Eq. (1). Differentiating Eq. (4), we obtain an expression for the pattern speed corresponding to Eq. (1):

$$m\Omega_p = (m-1)n + \dot{\tilde{\omega}} \quad (5)$$

where n is the Keplerian mean motion. By the term "normal mode" is meant any global distortion of a ring described by Eqs. (1) and (5), for which ϕ_0 is approximately constant across the ring (Longaretti 1989). For $m=1$, Eq. (1) describes a simple eccentric ring, such as the ϵ ring, and $\Omega_p = \dot{\tilde{\omega}}$, as expected. For $m=0$, the distortion of the ring is axisymmetric (i.e., a simple radial oscillation) with an oscillation frequency $\omega = -m\Omega_p = n - \dot{\tilde{\omega}} = \kappa$, the epicyclic frequency.

Equation (5) is identical to the condition satisfied at the inner Lindblad resonance with an external satellite of mean motion Ω_p (Goldreich and Tremaine 1982), and Eq. (1) describes the distortion of streamlines associated with such a resonance. The trailing density wave driven at the resonance may also be described by Eq. (1), but with a suitable negative radial gradient in $\phi_0(a)$ (Borderies and Longaretti 1987).

In an unperturbed ring, Eq. (5) can be satisfied, for any given value of Ω_p , at only a single mean radius a , referred to as the "resonant radius." If all streamlines in a narrow ring of finite radial width δa are to obey Eq. (1) with a single pattern speed, then n (or $\dot{\tilde{\omega}}$ in the case $m=1$) for the nonresonant streamlines must be perturbed such that Eq. (5) is satisfied for all a . This may be accomplished either by the self-gravity of the ring itself (Goldreich and Tremaine 1979a; Borderies et al. 1983a), or by collisions associated with close packing of the ring particles at pericenter, $\phi = \phi_0$ (Dermott and Murray 1980). Because the Keplerian gradient in $\dot{\tilde{\omega}}$ is less than that in n by a factor of order $J_2(R/a)^2$, compliance with Eq. (5) may be forced over a much wider range of a for $m=1$ than for any other value of m . For this reason, distortions with $m \neq 1$ are expected to be confined to the narrowest and densest rings.

The γ and δ rings both fit this description, and were found to deviate significantly from simple $m=1$ ellipses (French et al. 1986b). They investigated a number of possible perturbations and found that the δ ring could be matched by a wavenumber $m=2$ distortion, corresponding to an ellipse with the planet at the center rather than at the focus, rotating relative to inertial space at a rate of 23.4383 ± 0.0001 deg hr⁻¹. They initially attributed this distortion to a Lindblad resonance with an unseen small satellite. Corrections to the planetary mass GM_{\oplus} determined from Voyager tracking (Tyler et al. 1986), and revisions to the ring radius scale suggested by Porco and Gold-

reich (1987) and confirmed by French et al. (1988a), have established that the noncircularity of the δ ring is due primarily to an excited normal mode with $m = 2$ and an amplitude $ae = 3.11 \pm 0.09$ km. Figure 4a shows the best-fitting $m = 2$ normal mode as a function of orbital phase for the δ ring. The fitted semimajor axis for the ring is 48300.12 ± 0.08 km. The predicted resonant radius for an $m = 2$ distortion rotating with the observed pattern

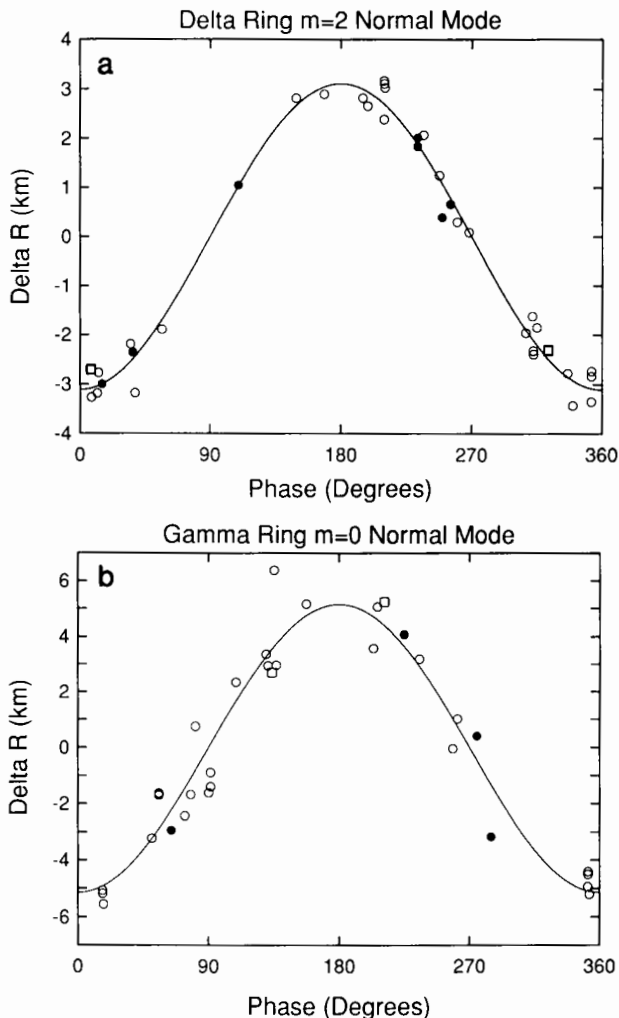


Fig. 4. Normal modes of the δ and γ rings (adapted from Figs. 9 and 12 of French et al. 1988a). The open symbols represent Earth-based occultation data and the filled symbols are Voyager data. (a) The best-fitting $m = 2$ normal mode for the δ ring, as a function of orbital phase. The data points are the observed radius residuals from a circular, equatorial ring orbit. (b) The best-fitting $m = 0$ normal mode for the γ ring, as a function of orbital phase. The data points are the observed radius residuals from an inclined, precessing elliptical orbit ($m = 1$ mode).

speed $\Omega_p = 23.43821 \pm 0.00004 \text{ deg hr}^{-1}$, calculated from Eq. (5), is $a_{\text{res}} = 48300.19 \pm 0.09 \text{ km}$. The excellent agreement between these two radii confirms that the distortion of the δ ring is indeed associated with an excited normal mode.

Similar analysis shows that the γ ring distortions stem from a combination of a precessing ellipse (equivalent to an $m = 1$ normal mode) and an $m = 0$ mode (French et al. 1988a). The best-fitting $m = 0$ normal mode for the γ ring is shown in Fig. 4b as a function of the phase of the radial oscillation. Its amplitude, $ae = 5.15 \pm 0.33 \text{ km}$, is nearly identical to the amplitude of the $m = 1$ mode of $ae = 5.19 \pm 0.33 \text{ km}$. The resonant radius for a particle with an epicyclic frequency corresponding to the observed radial oscillation frequency of $47.73198 \pm 0.00019 \text{ deg hr}^{-1}$ is $a_{\text{res}} = 47626.24 \pm 0.14 \text{ km}$, within 0.63 km of the fitted semimajor axis of the ring, $47626.87 \pm 0.28 \text{ km}$, confirming the identification of the mode. The parameters of the normal mode fits to the δ and γ rings are given in Table II.

E. Shepherd Satellite Resonances

Ten small satellites were discovered during the Voyager encounter, and two of these, Cordelia (1986U7) and Ophelia (1986U8), appear to have resonances associated with several of the rings. Porco and Goldreich (1987) used the satellite mean motions determined by Owen and Synnott (1987) and GM_U derived from Voyager Doppler tracking data to compute resonance locations in the vicinity of the known rings. They noted that several first-order resonances were located near the nominal locations of the γ , δ and ϵ rings (or

TABLE II
Normal Modes of the γ and δ Rings

Parameter	γ Ring	δ Ring
Wavenumber m	1	1
Semimajor axis a (km)	47626.87 ± 0.28	48300.12 ± 0.08
Eccentricity e ($\times 10^3$)	0.109 ± 0.007	0.004 ± 0.002
Longitude of periapse ω_0 (deg)	132.1 ± 4.3	216.7 ± 29.3
Inclination i (deg)	(0.0015 ± 0.0018)	0.0011 ± 0.0004
Longitude of ascending node Ω_0 (deg)	(251.3 ± 84.8)	260.7 ± 39.0
Wavenumber m	0	2
Amplitude (km)	5.15 ± 0.33	3.11 ± 0.09
Phase ϕ_0 (deg)	122.7 ± 11.7	13.6 ± 2.5
Frequency (deg hr^{-1}) ^a	47.73198 ± 0.00019	23.43821 ± 0.00004
Period (hr)	7.54211 ± 0.00003	15.35953 ± 0.00003
Resonance radius a_{res} (km)	47626.24 ± 0.14	48300.19 ± 0.09
$a - a_{\text{res}}$ (km)	$+ 0.63$	$- 0.07$
rms ring orbit residual (km)	0.99	0.31

^aFor $m = 2$, the frequency is Ω_p . For $m = 0$, the frequency is $m \Omega_p$ (the product is finite even though $\Omega_p = \infty$ for $m = 0$).

their edges), and they proposed that a systematic reduction in the pre-Voyager ring orbital radii of $(0.0124 \pm 0.0021)\%$ would bring the locations of the resonances and rings into accord. These identifications were confirmed by French et al. (1988a) in their post-Voyager ring orbit solution. Table III presents the correspondence between ring locations and shepherd satellite resonances. These resonances will be discussed later in the review of the kinematics and dynamics of the shepherding mechanism (Sec. V.B).

The accuracy of the derived orbits is ultimately determined by the validity of the assumed kinematical model and the accuracies of the ring event times, GM_U and Voyager's trajectory during the Uranus encounter. French et al. (1988a) concluded that the *absolute* radius scale of the rings (Tables I and II) is accurate to about ± 1 km, comparable to the uncertainty in calculating the radial positions of resonances with Cordelia and Ophelia due to imprecise satellite orbital periods and the uncertainty in GM_U . On the other hand, the *relative* radii of the rings are less susceptible to systematic errors, and are probably accurate at the level of the errors quoted in the tables. The comparative quality of the orbit models for individual rings can be seen in Fig. 5, which shows the post-fit radius residuals. A more quantitative measure is given by the *rms* radius residual for each ring (Tables I and II), which ranges from 0.26 to 0.60 km for the eccentric rings to a maximum of 0.99 km for the γ ring. In some cases, these residuals are clearly larger than the uncertainty in the observed location of the ring. At the same time, the set of ring event times used in the orbit model is based on a model that represents each ring as sharp edged and uniformly translucent, clearly an oversimplification.

F. Weak Dynamical Effects

The ring orbit model described above does not include a number of potentially significant dynamical effects, such as the motion of Uranus with respect to the system barycenter during groundbased occultations, wave-like perturbations of the ring edges associated with shepherd satellites, the possible simultaneous presence of multiple normal modes in some rings, forced precession of the rings by either the shepherd satellites or the 5 major Uranian satellites, and the contribution of J_6 and higher gravitational moments to the

TABLE III
Shepherd Satellite Resonances

Ring	Satellite	Resonance ^a	Feature	a_{res}	a_{obs}	Δa
ϵ	Cordelia	24:25 OER	inner edge	51121.2 ± 0.3	51120.8 ± 0.4	0.4
	Ophelia	14:13 IER	outer edge	51178.1 ± 1.8	51177.8 ± 0.4	0.3
λ	Cordelia	122:123 OER	inner edge	50022.5 ± 0.3	50023.1 ± 0.5	-0.6
δ	Cordelia	23:22 IER	outer edge	48302.5 ± 0.3	48302.4 ± 0.2	0.1
γ	Ophelia	6:5 IER	inner edge	47625.7 ± 1.8	47625.5 ± 0.4	0.2

^aOER = outer eccentric resonances; IER = inner eccentric resonances.

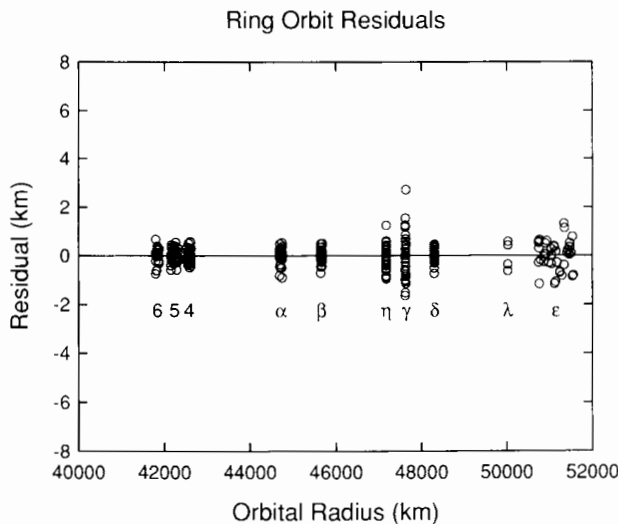


Fig. 5. Ring plane radius residuals from the best-fitting orbit models given in Tables I and II (figure from French et al. 1988a).

free precession of the rings. In the future, the observations can be used to place limits on or allow identification of weak dynamical effects in the Uranian system. Freedman et al. (1983) identified a number of such effects, including the radial perturbations in the rings expected from shepherd satellites. The *rms* ring orbit residuals can be used to set upper limits on the properties of unseen shepherd satellites in the Uranian system. The characteristic amplitude of forced radial oscillations Δr due to a shepherd satellite of mass M_s , orbiting at a radius r , near a circular ring of radius a is

$$|\Delta r| = \frac{8GM_s}{9n^2|a-r|^2} \left[2K_0\left(\frac{2}{3}\right) + K_1\left(\frac{2}{3}\right) \right] \quad (6)$$

where n is the mean motion of the ring particle, and K_0 and K_1 are modified Bessel functions. Numerically,

$$|\Delta r| = 3 \text{ km} \left(\frac{M_s}{10^{19} \text{ g}} \right) \left(\frac{r}{50,000 \text{ km}} \right)^3 \left(\frac{100 \text{ km}}{a-r} \right)^2 \quad (7)$$

and the corresponding satellite diameter d is

$$d = \frac{9 \text{ km}}{\rho^{1/3}} |\Delta r(\text{km})|^{1/3} \left(\frac{|a-r|}{100 \text{ km}} \right)^{2/3} \left(\frac{50,000 \text{ km}}{a} \right) \quad (8)$$

where ρ is its density in g cm^{-3} . The *rms* ring orbit residuals thus set upper limits on the diameters of shepherds located within a few hundred km of the rings at ~ 10 to 20 km. Shepherd satellite searches using the Voyager images give upper limits on the diameters of unseen satellites of order 10 km (Smith et al. 1986).

Precession rates of the individual rings can also be used to place useful limits on possible shepherd masses, as well as to investigate a number of other weak dynamical effects. When the occultation data are fitted with the apsidal precession and nodal regression rates as free parameters, rather than being determined from J_2 and J_4 , one obtains the results given in Table IV. The differences between the rates calculated by J_2 and J_4 and those obtained from the individual ring fits represent anomalous precession and regression rates. Since the precession rates are known more accurately than the regression rates, owing to the small inclinations of the rings and the current face-on geometry of the ring system, we focus our attention on the former.

Freedman et al. (1983) found the forced precession rate due to a shepherd satellite of mass M_s orbiting a planet of mass M_u at a distance r to be

$$\Delta\dot{\omega} = -\frac{1}{2\pi}\left(\frac{GM_u}{r^3}\right)^{1/2}\left(\frac{M_s}{M_u}\right)\left(\frac{a}{a-r}\right)^2 \quad (9)$$

with a corresponding shepherd diameter of

$$d = \frac{3.7 \text{ km}}{\rho^{1/3}} \left(\frac{|\Delta\dot{\omega}|}{0.0001 \text{ deg day}^{-1}} \right)^{1/3} \left(\frac{|a-r|}{100 \text{ km}} \right)^{2/3} \left(\frac{50,000 \text{ km}}{a} \right)^{1/6}. \quad (10)$$

For a typical anomalous precession of $0.0002 \text{ deg day}^{-1}$ (Table IV) and a density of 1.5 g cm^{-3} , one finds $d = 4$ to 10 km, comparable to the limits obtained from radial perturbations (Eq. 8).

The relatively large estimated diameters of the shepherds Cordelia and Ophelia (26 and 30 km, respectively [Thomas et al. 1989]) raise the possibility that they force measurable precessions on the nearby eccentric rings. From Eq. (9), the forced precession rates induced in the ϵ ring by Cordelia and Ophelia are 0.000035 and $0.000015 \text{ deg day}^{-1}$, respectively, rather larger than the formal uncertainty in the individually fitted precession rate of the ϵ ring. One must conclude that the fitted values for J_2 and J_4 are contaminated by the unmodeled influence of shepherd satellites, and possibly by other unmodeled dynamical effects as well.

Figure 6 compares several currently unmodeled predicted contributions to the apsidal precession rates with the anomalous rates from Table IV. The largest unmodeled contributions are due to the 5 major satellites, whose masses have only recently become well determined (Dermott and Nicholson 1986; Tyler et al. 1986; Laskar and Jacobson 1987), and perhaps J_6 . (A nom-

TABLE IV
Precession and Regression Rates

Ring	Apsidal Precession Rate (deg day^{-1})			Nodal Regression Rate (deg day^{-1})		
	from J_2, J_4	Fit	Difference	from J_2, J_4	Fit	Difference
6	2.76187	2.76156 ± 0.00023	+ 0.00031	- 2.75648	-2.75629 ± 0.00040	- 0.00019
5	2.67151	2.67151 ± 0.00009	- 0.00000	- 2.66640	-2.66604 ± 0.00034	- 0.00036
4	2.59807	2.59816 ± 0.00015	- 0.00009	- 2.59318	-2.59271 ± 0.00087	- 0.00047
α	2.18531	2.18574 ± 0.00023	- 0.00043	- 2.18157	-2.18326 ± 0.00219	+ 0.00169
β	2.03084	2.03083 ± 0.00039	+ 0.00001	- 2.02751	-2.02778 ± 0.00444	+ 0.00027
γ	1.75066	1.75075 ± 0.00427	- 0.00009			
ϵ	1.36325	1.36325 ± 0.00002	+ 0.00000			

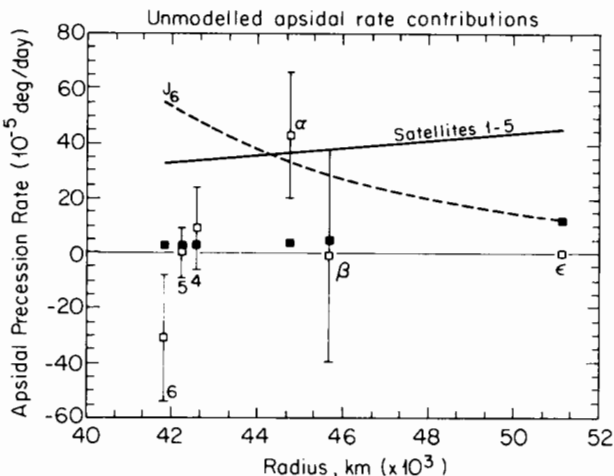


Fig. 6. Unmodeled effects on ring apsidal precession rates. The open squares are the difference between individually fitted apsidal rates (with their uncertainties) for the eccentric rings, and the rates determined by the best-fitting gravitational harmonics J_2 and J_4 (see Tables I and IV). The solid line shows the apsidal rate contribution due to the 5 main Uranian satellites. The filled squares are the predicted contribution from the 10 small satellites discovered by Voyager, assuming a mean density of 1.5 g cm^{-3} and the satellite diameters obtained by Thomas et al. (1989). The dashed curve is the predicted contribution from $J_6 = 1 \times 10^{-6}$.

inal value for J_6 of 10^{-6} has been assumed, based on interior models calculated by W. B. Hubbard [personal communication].) Uncertainties in the current model's precession rates associated with the $1 - \sigma$ uncertainties in J_2 and J_4 are comparable in magnitude to the expected J_6 contribution. It appears likely that the current value for J_4 may well be overestimated (in absolute value) by the omission of J_6 , although it is not yet clear that the data are of sufficient accuracy to permit a solution for all 3 harmonic coefficients. The inclusion of the 5 major satellites, on the other hand, will probably lead to an increase in the absolute value of J_4 because of the opposing trends of these two effects with increasing radius. The contributions by the 10 newly discovered satellites, based on the photometric radii (Thomas et al. 1989) and an assumed density of 1.5 g cm^{-3} , are currently negligible for all rings except ϵ . About 40% of the total contribution to the ϵ ring precession rate is due to the 2 nearby shepherds, and 60% to the 8 more distant, although larger, satellites. Additional constraints on the gravity harmonics may also come from the fitted pattern speeds of the γ and δ ring normal modes, although these rates are primarily sensitive to GM_U and the absolute ring semimajor axes, and from the nodal regression rates of rings 6, 5 and 4. A comprehensive examination of these effects may permit a direct estimate of the shepherd satellite masses, which would be of considerable dynamical interest. A meaningful estimate for J_6 would constrain models of the outer envelope of Ur-

anus, and perhaps the depth to which the observed differential atmospheric rotation extends (Smith et al. 1986).

III. INTEGRAL PROPERTIES OF THE RINGS

In this section, constraints are explored on the vertical thickness of the rings and on the particle size distribution imposed by measurement of integral quantities, chiefly the radially integrated optical depths, at a variety of ring longitudes and wavelengths. Section IV discusses the internal structure of individual rings as revealed by the Voyager observations, and the systematics of the observed width variations with longitude.

A. Equivalent Widths and Equivalent Depths

The earliest estimates of ring widths and optical depths were based on comparisons of the observed occultation lightcurves with model ring diffraction profiles, convolved with the appropriate stellar brightness distribution and instrumental response function (Nicholson et al. 1982). These estimates formed the basis of the width and optical depths tabulated by Elliot and Nicholson (1984).

A more systematic method for estimating these two quantities was developed by Elliot et al. (1984), who employed a least-squares procedure to find the best-fitting "square-well" model consistent with the observed ring profiles. In this approach, the diffraction pattern of a model ring segment of specified width and (uniform) optical depth is calculated, convolved with the limb-darkened stellar brightness profile and with the known instrumental impulse response function, and then the parameters of the model are iterated until an optimal fit to the observed occultation lightcurve is obtained. Parameters fitted typically include ring width and optical depth, stellar diameter (fixed for a given occultation for all rings), and stellar and background flux levels. There is an unavoidable tradeoff, in that the brightest stars yield the data of highest signal-to-noise ratio and thus the best determined ring parameters, but also typically have relatively large angular diameters, limiting the retrieval of very narrow ring widths. A second common limitation is due to uncertainties in the fitted background flux level, which effectively prevent accurate determinations of optical depths from the more opaque ring profiles. This square-well fitting procedure nevertheless has the advantage of consistency of application, is objective, and provides some idea of the uncertainties in the fitted parameters. The limitations outlined above must be kept in mind, however, in assessing the reliability of the results.

For the narrowest rings, with widths appreciably less than one Fresnel zone (≤ 3.5 km), the computed diffraction profiles are almost independent of the exact width and optical depth, and depend only on the total quantity of incident starlight blocked by the ring. This quantity is denoted equivalent

width E by analogy with spectroscopic terminology, and is defined by the relation (Elliot et al. 1984):

$$E = \mu W(1 - f_0) \quad (11)$$

where W is the radial width of the ring segment, f_0 is the observed fractional transmission of starlight through the ring, and $\mu = \sin B$, where B is the inclination of the ring plane to the line of sight. (The factor of μ is included in the definition to facilitate comparison of observations made at different ring inclinations.) It can be shown that the equivalent width of a square-well ring is unaffected by either diffraction or the effects of a finite stellar diameter, and is directly related to the integrated light loss of the observed occultation profile:

$$E = v_r \mu \int [1 - \phi(t)] dt \quad (12)$$

where $\phi(t)$ is the observed lightcurve, background corrected and normalized to unity for the unocculted star, and v_r is the projected radial velocity of the star in the ring plane. The equivalent width is thus reliably determined even for very narrow rings, although the ring width itself may be indeterminate.

A related quantity, and one of greater physical significance, is the integrated normal optical depth across a ring segment, denoted A , also referred to as the equivalent depth (Elliot et al. 1984). For a square-well ring of uniform transmission $f_0 = e^{-\tau/\mu}$, the equivalent depth is defined by

$$A = W\tau. \quad (13)$$

The generalization to an arbitrary optical depth profile is straightforward:

$$A = v_r \int \tau dt \quad (14)$$

where $\tau = -\mu \ln [\phi(t)]$, and is used below in the discussion of the Voyager data. Although the equivalent depth is more directly related to the total cross section of material per unit of ring length than is the equivalent width, it can be difficult to determine accurately if either (1) the ring is almost opaque, or (2) significant optical depth variations exist at a scale below the resolution limit of the experiment. The latter particularly affects groundbased observations.

The definitions of E and A are also motivated by two alternative views of ring structure, and their implications for the dependence of the observed

transmission on inclination B and local ring width W . For a monolayer ring composed of nonshadowing spherical particles, the total area blocked by a segment of the ring is independent of both B and W , while the projected area of the segment scales as μW . Thus the fraction of incident starlight blocked, $1 - f_0$, goes as $(\mu W)^{-1}$, and the equivalent *width* of the ring is independent of B and W . (This constancy of E eventually breaks down as $\mu W \rightarrow 0$, when mutual shadowing within the monolayer becomes important.)

For a ring whose thickness is many times the radius of a typical particle $\langle r \rangle$, and in which the interparticle separations D are large enough for diffraction to "fill in" the shadows behind individual particles (i.e., $D \geq 2 \langle r \rangle^2/\lambda$, where λ is the wavelength of observation), the extinction follows a classical radiative transfer law in which the normal optical depth is proportional to the vertically integrated total particle cross section per unit of ring area. In this situation, because one expects the total number of particles per unit length of ring to be constant (ring eccentricities are ≤ 0.01 in all cases), $\tau \propto W^{-1}$ and the equivalent *depth* of the ring should be independent of B and W .

Substantial information on the particle size distribution and volume packing density of the rings can be gleaned from comparisons of equivalent widths and depths measured at different wavelengths and orbital phases. The definitive studies of this type have yet to be completed, but some interesting preliminary results are available (see also the chapter by Esposito et al.). Theoretical considerations suggest that the rings should exhibit a broad size distribution extending down to micron sizes (owing to collisional comminution of the larger particles), cut off at the lower end by Poynting-Robertson or exospheric drag (Broadfoot et al. 1986), and be flattened into what can be called a "dynamical monolayer." The latter refers to a state in which the largest particles, which control the mass distribution in the ring, are confined to a layer whose thickness is several (≤ 10) particle diameters, while the smaller particles are stirred into a thicker layer (relative to their diameters) by the gravitational effects of the large particles (Cuzzi et al. 1979). The data at hand for the Uranian rings seem to contradict at least the former of these simple notions: the rings are apparently composed almost exclusively of particles many centimeters in size and larger.

B. Azimuthal Variations and the Thickness of the Rings

The most complete discussion of ring widths and mean optical depths obtained from fitting square-well models to groundbased data is given by French et al. (1986a), and represents the state of knowledge immediately prior to the Voyager encounter. In most cases, the quantities directly fitted to the observed lightcurves were the width W and the equivalent depth A , with the fractional transmission f_0 and mean optical depth τ inferred from Eq. (13) above.

Combining Eqs. (11) and (13), we see that the equivalent width and depth are related for a square-well ring by

$$E = \frac{(1 - e^{-\tau/\mu})}{\tau/\mu} A. \quad (15)$$

If $\tau/\mu \ll 1$, then $E \approx A$, and it follows that A is also well determined from the diffraction profile of the ring. If $\tau/\mu \gg 1$, however, then A becomes effectively indeterminate. Both τ and the equivalent depth derived from groundbased observations of highly opaque rings, such as the γ and δ rings, and the ϵ ring near periape, must therefore be treated with some caution. Furthermore, it should be noted that E refers to the radially averaged *transmission* through the ring, while A refers to the radially averaged *optical depth*. If there are significant variations in optical depth across the ring, then E and A are connected via the more general relation

$$E = \mu A \frac{\int (1 - e^{-\tau(r)/\mu}) dr}{\int \tau(r) dr} \quad (16)$$

The mean τ derived from the square-well-fitted equivalent width of a ring exhibiting unresolved internal structure will therefore underestimate somewhat the true mean optical depth of the ring. The considerable variations in optical depth in even the narrowest rings revealed by the Voyager occultation data thus cast some doubt on the accuracy of the mean optical depths obtained from square-well models. It appears likely that the most reliable quantities derived from such models are the ring widths (at least for moderately sharp-edged rings) and the equivalent widths.

French et al. (1986a) analyzed the variation of equivalent width and equivalent depth as functions of true anomaly and radius for each ring. Using Eq. (15) above, they fitted the observed variation of E with width and true anomaly on the assumption that A is independent of ring width. It was found that, for every ring, this model produced smaller residuals in E than were obtained on the assumption that E itself was conserved, as illustrated in Fig. 7. Their results thus favored the classical radiative transfer, or many-particle-thick, ring model over the monolayer description.

This conclusion is further reinforced by the Voyager observations, which in most cases show no significant variations in equivalent depth between ingress and egress for any of the three occultation data sets (see Table VI below). The conservation of equivalent depth is best documented for the ϵ ring, for which Holberg et al. (1987) demonstrated that A is constant (to within an *rms* dispersion of 6%) for ring widths varying from 21 to 89 km (Fig. 8). Tyler et al. (1986) and Gresh et al. (1988b) concluded from the radio-science data alone that the constancy of 3.6 cm equivalent depths ($\pm 4\%$ for the ϵ

ring) requires that the volume filling fraction of ring particles be no greater than 0.01, or that the particles are separated by at least 5 times their typical diameter. For the ϵ ring at periape, Gresh et al. (1988b) utilized the multi-layer model of Zebker et al. (1985) to estimate a lower bound of $N > 10$ on the number of possible thin layers, corresponding to a physical thickness > 30 m for an effective particle size, $a_{\text{eff}} > 70$ cm (see also Gresh 1990; chapter by Esposito et al.).

In a similar vein, Lane et al. (1986) pointed out that the optical depths in excess of 2.5 encountered in the stellar occultations by the γ and ϵ rings almost certainly require that the rings are at least 4 to 5 particle layers thick in some locations. Additional evidence for the constancy of equivalent depth, and thus the classical thick-ring model, is provided by the observed variation

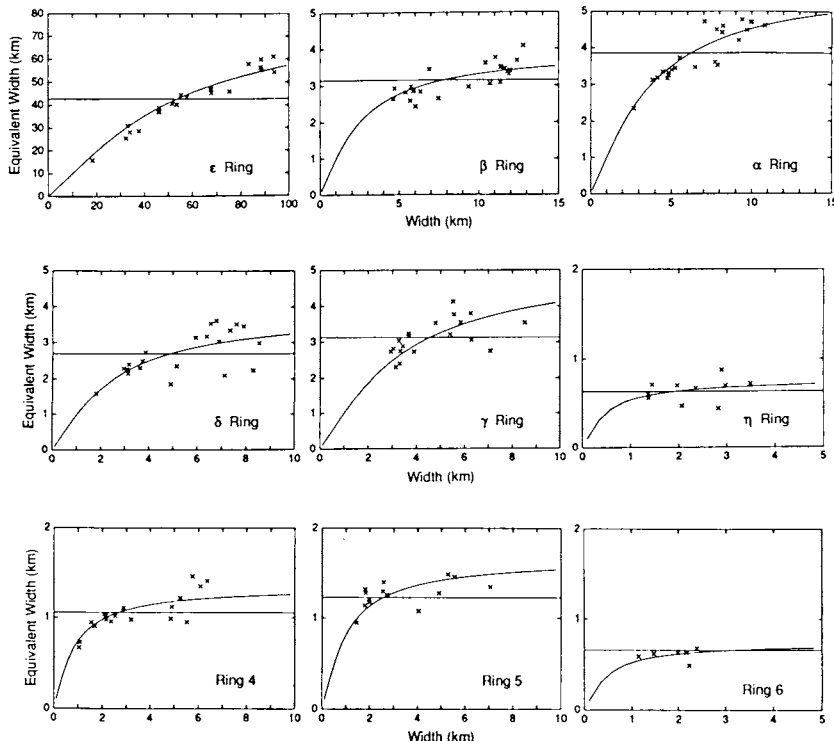


Fig. 7. Equivalent widths of the 9 main rings as determined from square-well fits to groundbased occultation profiles. The trend of increasing equivalent width with ring width is well matched by a many-particles-thick model (smooth curves) in which the equivalent *depth* is conserved (i.e., is independent of ring width). In contrast, an optical monolayer model, for which the equivalent width is conserved, gives a poorer match to the observations (figure from French et al. 1986a).

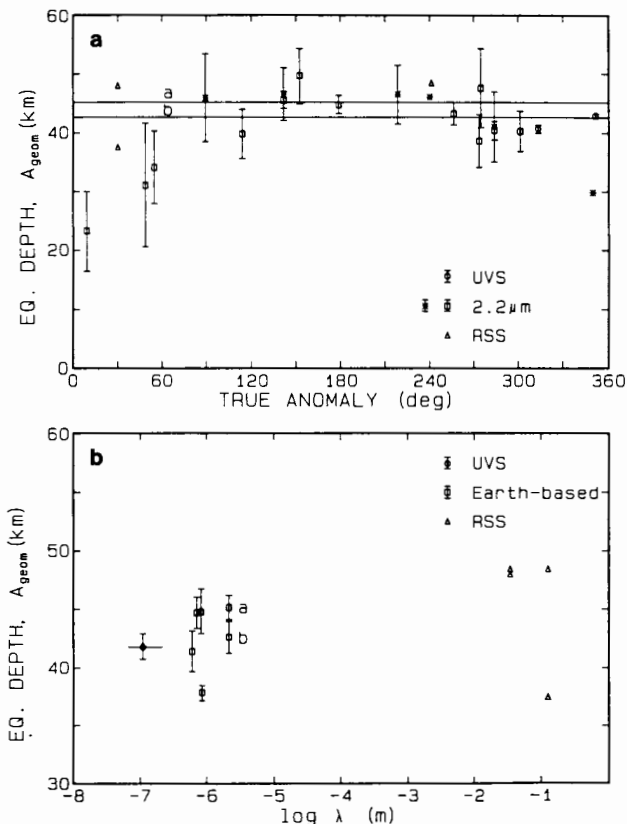


Fig. 8. The equivalent depth of the ϵ ring as a function of (a) true anomaly, and (b) wavelength. The mean integrated equivalent depth at 2.2 μm (i.e., calculated using Eq. 14) is indicated by line "a," while line "b" depicts the mean value obtained from square-well fits. No significant variation with either true anomaly or wavelength is apparent (figure from Holberg et al. 1987).

in the integrated visual brightness of the rings as a function of orbital longitude in Voyager images (Svitek and Danielson 1987). Their best fit for the ϵ ring was obtained for an equivalent depth 38 ± 5 km, consistent with the 42 km observed at ultraviolet wavelengths in the Voyager stellar occultations.

A useful opportunity to test the validity of the square-well model approach to estimating equivalent depths was provided by the Voyager radio occultations. The raw X-band data, before filtering to remove the effects of diffraction, have a radial resolution of ~ 2 km, comparable to that of ground-based data at 2.2 μm (although the latter are also affected by finite stellar angular diameters). These raw X-band intensity data were subjected to the same square-well fitting procedure used for groundbased data, ignoring the phase measurements that are critical to the diffraction reconstruction (French et al. 1988a, Table X). Subsequent comparison with the "true" ring widths

and equivalent depths calculated from the diffraction-corrected profiles by Gresh et al. (1989) led to the following conclusions:

1. As anticipated, the square-well model did a fairly good job of estimating equivalent depths, even for unresolved rings: the mean ratio of fitted to true equivalent depth was 0.92 (excepting only the almost opaque γ ring egress and ϵ ring ingress cuts) with a modest scatter about this value of 0.82 to 0.96;
2. The model was less successful in estimating the true widths of narrow rings: the mean ratio of fitted to true width was 0.81, with a rather large scatter (0.55 to 0.90). Not surprisingly, the best width results were obtained for sharp-edged, high optical-depth rings (e.g., γ ring ingress and ϵ ring egress), and the worst for transparent rings with diffuse edges (e.g., ring α ingress and both β cuts).

C. Wavelength Variations and the Particle Size Distribution

The most direct information on the particle size distribution comes from comparisons of the ring optical depths at different wavelengths. The limited wavelength coverage available from groundbased occultations indicated that the optical depths were constant between 0.5 μm and 2.2 μm (Elliot et al. 1984). With the availability of the Voyager occultation and imaging data, this range has been greatly extended. In terms of the differential size distribution $n(r)$ defined such that $n(r)dr$ is the vertically integrated number density of particles per unit ring surface area between radii of r and $r + dr$, the normal optical depth for a many-particle-thick ring is given by

$$\tau(\lambda) = \int_{r_{\min}}^{r_{\max}} Q_{ext}(r, \lambda) \pi r^2 n(r) dr \quad (17)$$

where $Q_{ext}(r, \lambda)$ is the (dimensionless) extinction efficiency. Here, r_{\min} and r_{\max} represent the smallest and largest sizes in the distribution. The sensitivity of $\tau(\lambda)$ to the size distribution stems principally from the rapid decrease in Q_{ext} in the Rayleigh scattering limit, i.e., for $r \ll \lambda$; in practice, there is little contribution to τ from particles with $r \leq \lambda/3$.

An additional complication in comparing groundbased and Voyager results is the dependence of the *effective* value of Q_{ext} for the large particles ($r \geq \lambda$) on particle sizes and experimental geometry (Cuzzi 1985). For such particles, $Q_{ext} \approx 2$ if the light diffracted by individual particles is effectively lost from the incident beam, whereas $Q_{ext} \approx 1$ if the diffracted light is detected along with the attenuated incident beam. For a mean particle radius $\langle r \rangle$, a ring width W , and distance from ring to observer D , $Q_{ext} \approx 2$ if

$$\langle r \rangle \ll \frac{\lambda D}{W} \quad (18)$$

and (for noncoherent optical experiments) $Q_{ext} \approx 1$ for $\langle r \rangle \geq \lambda D/W$. (Radio-occultations preserve phase as well as amplitude information, which permits discrimination between the direct and scattered signal even in the latter situation.)

Holberg et al. (1987) showed that, as expected, $Q_{ext} = 2$ for ground-based stellar as well as Voyager radio-occultation observations of the ϵ and δ rings, while $Q_{ext} \approx 1$ for the UVS stellar occultation of σ Sgr. They concluded from this that the effective particle size in the ϵ ring must exceed 3 mm, and in the δ ring exceeds 1 cm. For 3 mm radius particles in the ϵ ring, the angular diameter of the forward-scattering lobe in the particle phase function (due to diffraction) is comparable to the angular width of the ring as subtended at the spacecraft, so that light losses from the direct beam due to diffraction can be made up by light diffracted from nearby particles. For smaller particles, the diffracted light lost is only partially replaced, and the effective value of Q_{ext} would increase from unity towards the single particle value of 2 (van de Hulst 1957).

Holberg et al. (1987) then compared the equivalent depth of the ϵ ring, adjusted to $Q_{ext} = 1$, at wavelengths of 0.11 μm , 0.5 μm , 2.2 μm , 3.6 cm and 13 cm, and found *no* evidence for any variation over this range of a factor of 10^6 in wavelength. By comparison, the rings of Saturn typically show variations of 20 to 40% over this same range (Tyler et al. 1983). Tyler et al. (1986) and Gresh et al. (1989) found negligible variations in equivalent depth for all 9 classical rings between 3.6 cm and 13 cm in the Voyager radio-occultation experiment.

In Table V, the mean equivalent depths for each ring from each Voyager occultation experiment are tabulated and compared with the mean equivalent depths determined from groundbased 2.2- μm data by French et al. (1986a) using square-well fits. The equivalent depth ratios, normalized to the Voyager 3.6-cm values, are also given in Table V and plotted as a function of ring semimajor axis in Fig. 9. In making such intercomparisons, it is implicitly assumed that, at any particular wavelength, the equivalent depth of each ring is independent of longitude (cf. Fig. 7 above). The Voyager data in Table V were obtained from Gresh et al. (1989) (radio science), Holberg et al. (1987) (UVS), and from raw data generously provided by A. L. Lane (PPS principal investigator). The 13 and 3.6 cm entries are averages of values measured at the two observation longitudes (see Gresh et al., 1989, Table VI). Details of the calibration of the PPS equivalent depths are given in Sec. IV below.

An examination of the equivalent depth ratios in Table V and Fig. 9 leads to the following conclusions:

1. The mean 13-cm/3.6-cm equivalent depth ratio of 0.95 ± 0.13 is not significantly different from unity (see also Gresh et al. 1989, Fig. 30), in contrast to the Saturnian rings (Tyler et al. 1983), implying a lack of significant numbers of particles between 1 and 4 cm in size. Gresh et al.

TABLE V
Average Equivalent Depth (km)

Ring	$Q_{eq}=2$			$Q_{eq} \approx 1$		
	13 cm	3.6 cm	2.2 μm	0.27 μm B Per	0.27 μm σ Sgr	0.11 μm σ Sgr
6	0.85 \pm 0.26	0.93 \pm 0.07	0.83 \pm 0.04	0.52 \pm 0.14 ^a		
5	1.80 \pm 0.42	2.00 \pm 0.12	1.78 \pm 0.08	0.95 \pm 0.23		
4	1.53 \pm 0.34	1.47 \pm 0.16	1.35 \pm 0.04	0.62 \pm 0.14		
α	6.24 \pm 1.12	6.39 \pm 0.43	5.99 \pm 0.16	3.10 \pm 0.66		
β	3.57 \pm 0.98	4.16 \pm 0.14	3.84 \pm 0.08	1.93 \pm 0.55		
η	0.66 \pm 0.24	0.95 \pm 0.09	0.81 \pm 0.05	0.62 \pm 0.16 ^a		
γ	8.6 \pm 4.5 ^c	8.2 \pm 2.1	6.63 \pm 0.27	3.43 \pm 0.44 ^b		
6	5.57 \pm 0.67	4.8 \pm 0.8	4.14 \pm 0.19	1.72 \pm 0.46		
λ	? ^d	\leq 0.1	\leq 0.1			
ϵ	88.8 \pm 11.3 ^d	95.2 \pm 2.8	83.8 \pm 0.15	55.2 \pm 6.1	42.1 \pm 4.1	41.8 \pm 1.6

TABLE V (continued)

Ring	13 cm/ 3.6 cm	Equivalent Depth Ratios			$0.11 \mu\text{m}/$ 3.6 cm	σ Sgr
		2.2 $\mu\text{m}/$ 3.6 cm	β Per	0.27 $\mu\text{m}/3.6\text{cm}$		
6	0.91 ± 0.29	0.89 ± 0.08		$0.56 \pm 0.16^*$		
5	0.90 ± 0.22	0.89 ± 0.07		0.48 ± 0.12		
4	1.04 ± 0.26	0.92 ± 0.10		0.42 ± 0.11		
α	0.98 ± 0.19	0.94 ± 0.07		0.49 ± 0.11		
β	0.86 ± 0.24	0.92 ± 0.04		0.46 ± 0.13		
η	0.69 ± 0.26	0.85 ± 0.10		$0.65 \pm 0.18^*$		
γ	1.05 ± 0.61^d	0.81 ± 0.21		0.42 ± 0.12^c		
δ	1.16 ± 0.24	0.86 ± 0.15		0.36 ± 0.11	0.53 ± 0.10	0.51 ± 0.09
ε	0.93 ± 0.12^d	0.88 ± 0.03		0.58 ± 0.07	0.44 ± 0.04	0.44 ± 0.02
Average:	0.95 ± 0.13	0.88 ± 0.04		0.49 ± 0.09	0.49 ± 0.06	0.48 ± 0.05
	0.93 ± 0.15^e			0.46 ± 0.07^c		

*Egress profile only; ingress identification uncertain.

^Egress only; ingress profile opaque.

^Excluding rings 6 and η .

^Uncertain value; one profile near-opaque in 13-cm data.

^Excluding rings γ and ε .

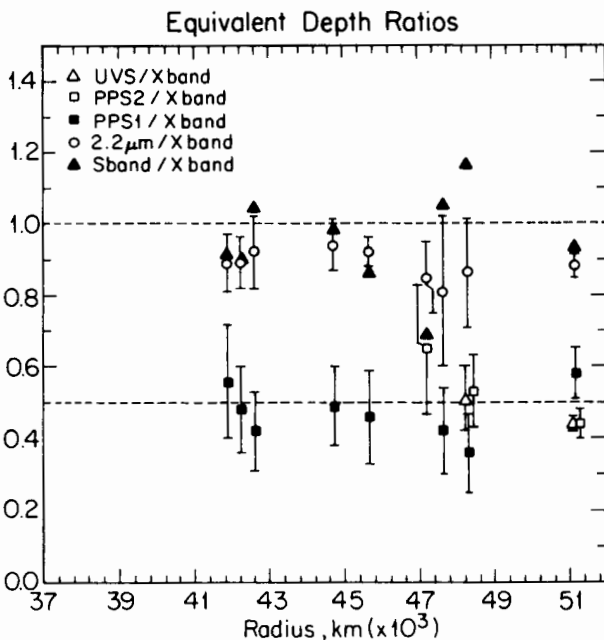


Fig. 9. Mean equivalent depth ratios at various wavelengths for the 9 main Uranian rings, plotted as a function of mean ring radius. Mean equivalent depths for each ring from the UVS σ Sgr (UVS), PPS σ Sgr (PPS2), PPS β Per (PPS1), groundbased (2.2 μm) and RSS S-band occultations are compared with the mean RSS X-band equivalent depth (see Table V). The horizontal dashed lines indicate the anticipated ratios for large (>1 cm) particles of 1.0 (2.2 $\mu\text{m}/\text{X}$ and S/X) and 0.5 (UVS/X and PPS/X). Within the experimental uncertainties, the data are consistent with these values.

(1988a,b; see also Gresh 1990; chapter by Esposito et al.) concluded that, for a plausible icy particle composition and a power-law size distribution of index $q \sim 3$ similar to that in Saturn's rings (Marouf et al. 1983; Zebker et al. 1985), the radio-occultation data constrain the "effective" particle radius a_{eff} to values exceeding about 70 cm. This implies a surface mass density $\Sigma > 80 \text{ g cm}^{-2}$ for material of density $\rho = 1 \text{ g cm}^{-3}$, large compared to $\Sigma \sim 30 \text{ g cm}^{-2}$ inferred from the self-gravity model discussed below in Sec. IV. Porous particle material or particles composed of loose aggregates of smaller particles would have smaller ρ , hence proportionately smaller Σ . Smaller a_{eff} and Σ are also possible if $q < 3$ and if the minimum particle size is much smaller than a centimeter (see the chapter by Esposito et al., Fig. 9). The latter condition is unlikely in view of the nearly identical equivalent depth observed at much shorter wavelengths (Table V) and considering the efficiency of exospheric drag in removing these small particles. A more detailed analysis of these data is given in the chapter by Esposito et al.

2. The mean 2.2 μm equivalent depths are slightly *less* than the 3.6-cm values, (average ratio = 0.88 ± 0.04) rather than greater as might be expected. (Recall that $Q_{ext} = 2$ for both data sets.) In fact, the average deficiency at 2.2 μm is identical, within the uncertainties, to the amount by which the square-well model was found to underestimate systematically the true equivalent depths of the radio data (see above), so that the true integrated optical depths at 2.2 μm can be assumed to be equal to the 3.6-cm values, at least to within a few percent. We can conclude that, for the 9 classical rings, the fraction of total surface area due to particles in the size range 1 μm to 1 cm is less than $\sim 5\%$.
3. For the δ and ϵ rings, the mean equivalent depths at 0.11 μm and 0.27 μm are essentially identical (although this conclusion is slightly weakened by adjustments of the PPS stellar flux calibration to assure this equivalence for the ϵ ring—see Sec. IV). It thus appears that there are also relatively few particles in the 0.03 to 0.1 μm size range in these 2 rings, a conclusion reinforced and extended to the other 7 classical rings by high phase angle Voyager imaging data (see chapter by Esposito et al.).
4. For the 9 main rings, the equivalent depths at 0.27 μm (PPS) and 0.11 μm (UVS) are found to be almost exactly half the 2.2 μm and 3.6 cm values. The mean ratios are 0.46 ± 0.07 for 0.27 μm /3.6 cm and 0.48 ± 0.05 for 0.11 μm /3.6 cm (rings δ and ϵ only). This is consistent with an effective $Q_{ext} \approx 1$ for the Voyager stellar-occultation data, as expected (Cuzzi 1985), and implies a lack of any true variation in optical depth between wavelengths of 0.11 μm and 3.6 cm. It appears that, within the errors of the data, the findings of Holberg et al. (1987) for the δ and ϵ rings can be extended to all 9 rings. For the PPS occultation of β Per, at a mean space-craft range of 130,000 km, the diffraction constraint for the narrowest rings imposed by $Q_{ext} \approx 1$ requires effective particle sizes that exceed 2 cm. For rings α and β , the minimum size is ~ 0.5 cm. It is likely that any appreciable population of subcentimeter size particles would increase the 0.27- μm / 3.6-cm ratio of equivalent depths for two reasons—by increasing the available number of absorbing or scattering particles in the ultraviolet, and by increasing the effective value of Q_{ext} for the ultraviolet observations, because of the broad scattering lobe for smaller particles.

An additional datum on the wavelength independence of the equivalent depths comes from the study of azimuthal brightness variations in Voyager images by Svitek and Danielson (1987), who concluded that the best fit to the ϵ ring was obtained for an apoapse mean optical depth of 0.40 ± 0.05 , corresponding to an equivalent depth of 38 ± 5 km. (The effective $Q_{ext} = 1$ for observations of reflected sunlight [Cuzzi 1985].) This is slightly less than the average equivalent depths for this ring obtained from occultation data at 0.11 μm (41.8 ± 0.2 km), 0.27 μm (49 ± 6 km) and 2.2 μm (45.2 ± 1.1 km, corrected to $Q_{ext} = 1$; see Holberg et al. 1987). Their analysis, however, assumed a square-well model for the ring, which resulted in a 10 to 15%

underestimate of the true equivalent depth because of the internal optical depth variations (cf. Eq. 16 above).

An exception to the usual situation is provided by the newly discovered λ ring, for which the equivalent depth is observed to be strongly wavelength dependent (see Fig. 10). The mean PPS equivalent depth of 0.19 ± 0.06 km (Table V) is appreciably less than the mean UVS value of 0.31 ± 0.06 km. This rapid decrease of optical depth with increasing wavelength probably accounts for failure to detect the λ ring either in groundbased occultations at $2.2 \mu\text{m}$, or in the RSS data at 3.6 cm . Kangas and Elliot (1987) examined the data from 10 groundbased occultations and placed an upper limit of 6% on the contribution of large particles to the optical depth at a wavelength of $0.11 \mu\text{m}$. A search of several groundbased lightcurves that have highest signal to noise (see Fig. 11 for an example) yields an upper limit of 0.1 km on the equivalent depth of the ring at $2.2 \mu\text{m}$. Gresh et al. (1989, Fig. 29) gave a similar upper limit on the equivalent depth at 3.6 cm , from data processed to a resolution of 200 m. It has also been observed that the ring is azimuthally clumpy (Ockert et al. 1987; Colwell et al. 1990), which is a potentially complicating issue. A predominance of small particles in this ring is consistent with its greatly enhanced brightness in the forward-scattering direction, as compared with the other narrow rings (Smith et al. 1986; Ockert et al. 1987). For further discussion of this ring, the reader is referred to the chapter by Esposito et al. Note that, for μm -size particles, $Q_{ext} \approx 2$ even for the PPS and UVS observations of this ring.

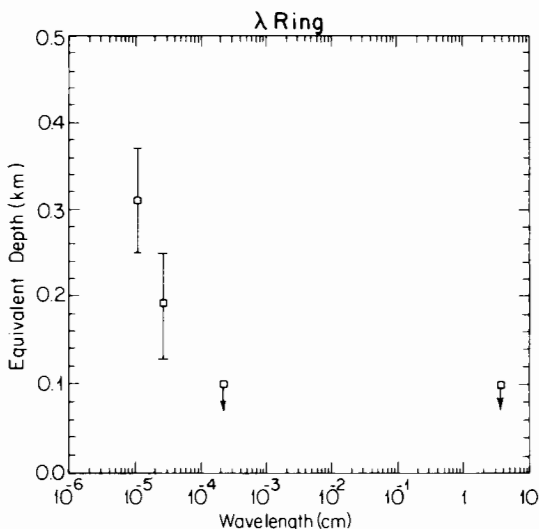


Fig. 10. Observed equivalent depth of the λ ring as a function of wavelength. The 2 points with error bars correspond to the UVS and PPS observations at 0.11 and $0.27 \mu\text{m}$, respectively. The two upper limits correspond to the absence of the λ ring in $2.2 \mu\text{m}$ groundbased and X-band RSS occultations (figure after Holberg et al. 1987).

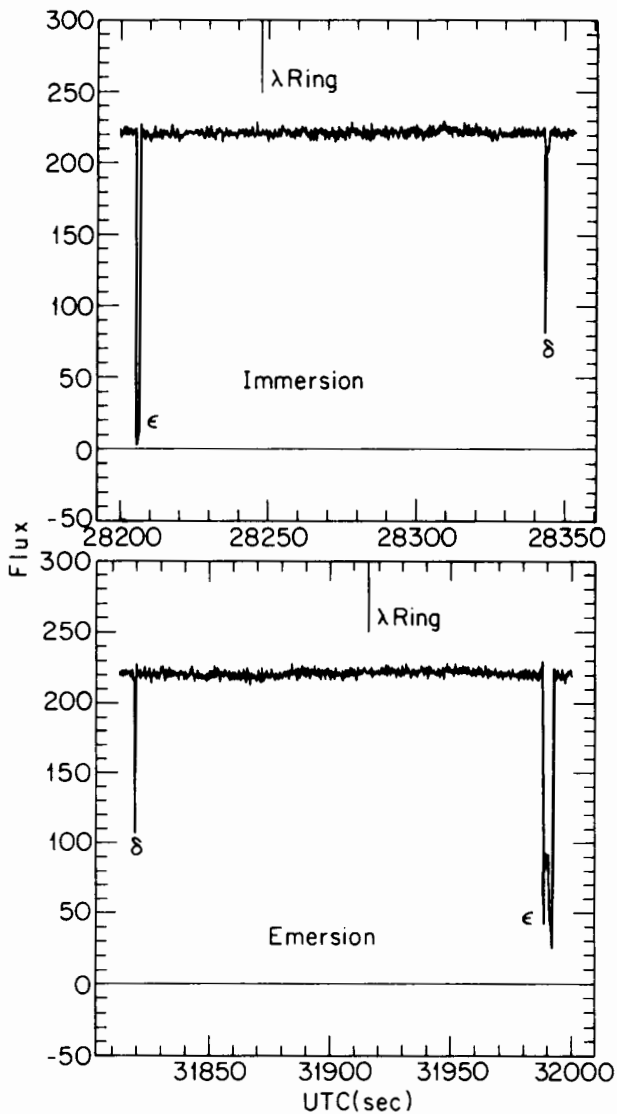


Fig. 11. Search for the λ ring in groundbased observations of the 24 May 1985 occultation of U36 as observed from Palomar Observatory. Ingress and egress traces of the outer ring region between the δ and ϵ rings are shown. No dips are seen at the locations predicted from the orbit solution of Table I, giving an upper limit of 0.1 km on the equivalent depth at 2.2 μm .

D. Other Constraints on Ring Thickness and Particle Size Distribution

While the vertical distribution of particles within the rings cannot be inferred directly from any of the available remote-sensing observations, the PPS stellar occultation of σ Sgr, with 10-m radial samples, was used to set an upper limit of 150 m on the thickness of the ϵ ring at its outer edge (Lane et al. 1986). This can be compared with the RSS lower limit of 30 m estimated from the constancy of ϵ ring equivalent depths at 3.6 cm, and a thickness of ~ 15 m inferred from the *rms* velocity dispersions for the α and β rings derived from their inferred apsidal shifts (French et al. 1986a; see also Sec. IV), although the validity of these results depends on the applicability of the extended self-gravity model (Borderies et al. 1983a) to these rings.

A possible additional source of information on the volume packing fraction is the optical phase function of the rings near opposition. Observations by Herbst et al. (1987) at 2.2 μm indicate that the Uranian rings do indeed show an “opposition surge” at phase angles below $0^\circ 5$. They concluded, however, that the volume filling fraction required by the observations is implausibly low ($\sim 5 \times 10^{-4}$) for the classical inter-particle shadowing model, and that the observed brightening probably arises in the surfaces of the particles themselves.

Showalter and Nicholson (1987, 1990) analyzed the statistical properties of the PPS stellar-occultation data for Saturn’s rings and characterized the additional variance in these data (beyond that due to pure Poisson photon counting statistics) in terms of a dimensionless parameter Q (not to be confused with Q_{ex}) defined by

$$Q = \frac{\int (\pi r^2)^2 n(r) dr}{A \mu \int \pi r^2 n(r) dr} = \frac{\pi R_{\text{eff}}^2}{A \mu} \quad (19)$$

where R_{eff} is comparable to the upper size cutoff in the size distribution and A is the effective sampling area of a single PPS measurement. For Saturn’s rings, on the assumption that the additional variance is attributable to the presence of the largest particles in the ring particle size distribution, they obtained values of Q ranging from <0.01 in the C Ring and inner Cassini Division, to 0.25 in the inner A Ring, corresponding to values for R_{eff} of ≤ 2 m to 11 m. The results for the C Ring and Cassini Division were in general accord with Radio Science estimates of particle size (Zebker et al. 1985), but the much larger value of R_{eff} found for the A Ring is inconsistent with radio data for that region. A possible explanation is that Q may reflect, in part, gravitational clustering of smaller particles, expected to be more important near the Roche limit.

A similar analysis was applied to the PPS data for the Uranian rings (Showalter and Nicholson 1988), with meaningful results obtained for the σ Sgr cuts of the δ and ϵ rings, and the β Per ϵ ring ingress cut. A mean value of $R_{\text{eff}} = 3.8 \pm 0.5$ m was obtained for ϵ , and 2.9 ± 0.6 m for δ . These results, when compared with the Saturnian data, suggest that the largest particles in the Uranian rings are comparable to those found in Saturn's C Ring and in the outer Cassini Division, but perhaps smaller than those in the A Ring. The inferred upper size cutoff in the δ and ϵ rings is ~ 10 m, for a power-law index $q = 3$ and a minimum particle radius of 10 cm. However, at least one assumption of the analytic development is violated for such large particles, so this conclusion is subject to possible revision (Showalter and Nicholson 1990).

An R_{eff} of 3 to 4 m is inconsistent with estimates of the surface mass densities for the δ and ϵ rings based on the Goldreich-Tremaine self-gravity model: with $q = 3$, the implied surface density at quadrature for the ϵ ring, $\Sigma \epsilon \sim 150$ g cm $^{-2}$ for particles of density 1 g cm $^{-3}$. This is to be compared with self-gravity model predictions of ~ 25 g cm $^{-2}$ for ϵ and ~ 7 g cm $^{-2}$ for δ (see Sec. IV below). In general, we have for a power-law size distribution with $q = 3$

$$\frac{r_{\max}}{R_{\text{eff}}} = \left[2 \ln \left(\frac{r_{\max}}{r_{\min}} \right) \right]^{1/2} \quad (20)$$

and

$$\frac{\Sigma}{\tau} = \frac{4}{3} \rho \left[\frac{2}{\ln \left(\frac{r_{\max}}{r_{\min}} \right)} \right]^{1/2} R_{\text{eff}} \quad (21)$$

where ρ is the particle density. More specific models for the size distribution in the rings, incorporating information derived from both the phase delays and differential optical depths observed at 3.6 and 13 cm, are reported by Gresh et al. (1988a,b) and Gresh (1990) and discussed in more detail in the chapter by Esposito et al.

E. Discussion

We have seen that the Uranian rings transmit and scatter optical and microwave radiation in the manner expected for a classical, many-particle-thick ring. Evidence for this conclusion comes from the observed constancy of equivalent depths despite substantial width and mean optical depth variations, the unusually large peak optical depths seen in the γ and ϵ rings, and the variation of ring brightness with longitude. For the ϵ ring, the true thick-

ness probably lies in the 50 to 150 m range, although lower values are possible away from periape.

Ring particle sizes are likely to be in the range 10 cm to 10 m, with effective mean radii in the ϵ ring being 0.7 to 3 m. Here the primary evidence is the absence of a discernable wavelength dependence in the optical depths of the 9 main rings between 0.11 μm and 13 cm, backed up by the observed $Q_{ext} \sim 1$ for the Voyager ultraviolet occultations and by $R_{eff} \sim 3$ to 4 m derived from the PPS data.

This picture of the rings is compatible with that proposed for Saturn's rings by Cuzzi et al. (1979), in which the largest particles are distributed in a layer several particle diameters in thickness. Several outstanding discrepancies should be noted, however. One is the unexplained differential phase delay between 3.6 and 13 cm observed for the inner 5 rings (Gresh et al. 1989). Second is that a key assumption of the "radiative transfer" model for ring optical depths fails to be satisfied, by many orders of magnitude, at ultraviolet and infrared wavelengths: to avoid shadowing of 1-m particles at $\lambda = 1 \mu\text{m}$, an inter-particle distance of 10^3 km is necessary. The third caveat concerns the present lack of any comprehensive study of the effects of closely packed particles on the propagation of electromagnetic radiation (however, see Gresh 1990); it is possible (albeit unlikely) that a closely packed ring would also conserve equivalent depth despite substantial width variations. Finally, we note that both the minimum ring thickness and surface mass density implied by these results are inconsistent, by factors of 4 to 10, with the predictions of the "standard" self-gravity model of Goldreich and Tremaine.

IV. STRUCTURE OF THE RINGS AND SYSTEMATIC WIDTH VARIATIONS

A. Ring Structure

With respect to the kinematics and dynamics of the Uranian rings, the Voyager observations have supplemented the data obtained from groundbased stellar occultations, but have not radically revised our understanding of the system. This circumstance stems from the fact that kinematical models of the rings depend only on accurate determinations of ring occultation midtimes, which can be reliably estimated to a few tens of milliseconds in high-quality groundbased data. The corresponding radial precision is typically on the order of 100 m, comparable with the precision of Voyager occultation data (Lane et al. 1986; Tyler et al. 1986; Holberg et al. 1987).

The situation is quite different when it comes to investigating the internal structure of individual rings: here the resolution limits imposed on ground-based occultation data by diffraction and finite stellar angular diameters severely hampered pre-Voyager studies of ring structure. At the customary ob-

serving wavelength of 2.2 μm , the Fresnel scale for groundbased occultations is 3.5 km, comparable to the widths of all but the α , β and ϵ rings. In fact, only the ϵ ring is effectively resolved in groundbased data, although hints of internal structure have been reported for the α and β rings, and low optical-depth components of the η and δ rings were identified (see Elliot and Nicholson [1984] for a discussion of these results). For the remaining 6 rings, the only structural characteristics available from groundbased data were estimates of ring width and mean optical depth, inferred at first from the measured occultation profile width (FWHM) and the fractional drop in stellar intensity (Nicholson et al. 1982), and subsequently from square-well model fits.

Catalogs of groundbased ring occultation profiles were provided by Elliot et al. (1984), Elliot and Nicholson (1984), French et al. (1986a) and French et al. (1988a), together with estimates of individual ring widths and mean optical depths derived from square-well model fits. Among the highest-quality groundbased data to date were those obtained from the occultations of stars U16 on 4 June 1982 (P. D. Nicholson and K. Matthews, unpublished data), U25 on 24 May 1985 and U28 on 26 April 1986 (both presented by French et al. 1988a). (The stellar designations are from the prediction list published by Mink and Klemola [1985] and its predecessors.) The ring profiles obtained from the U28 occultation are particularly noteworthy because of the very small stellar angular diameter (0.09 milliarcsec, or 1.2 km projected at Uranus). Figure 12 presents the egress ring profiles for this event, along with square-well models and the corresponding diffraction profiles, and illustrates the high signal-to-noise ratio and diffraction-limited resolution characteristic of the best groundbased observations. These data show evidence for internal structure in the α ring, a well-resolved width but little internal structure for the β ring, low optical depth components extending some 55 km exterior to the η ring and 12 km interior to the δ ring, and the well-known interior structure in the ϵ ring, first described by Nicholson et al. (1982). French et al. (1986a) summarized average ring widths and equivalent depths inferred from the groundbased data, and discussed models for the pronounced width variations exhibited by all 9 rings known at the time. These models are discussed further in Sec. IV.B below.

New information on ring structure, and on the associated systematic variations of ring width with longitude, have come from the Voyager imaging and occultation data. At a resolution of ~ 10 km/line pair, however, even the best Voyager images resolve only the ϵ ring and the faint component of the η ring. The great value of these data for ring studies has been the discovery of new features unsuspected from groundbased data (including the λ ring and the ϵ ring shepherds, as well as broad sheets of very low optical depth material), and characterization of the photometric behavior of the rings at optical wavelengths. These results are largely discussed in the chapter by Esposito et al. although some structural observations are described below.

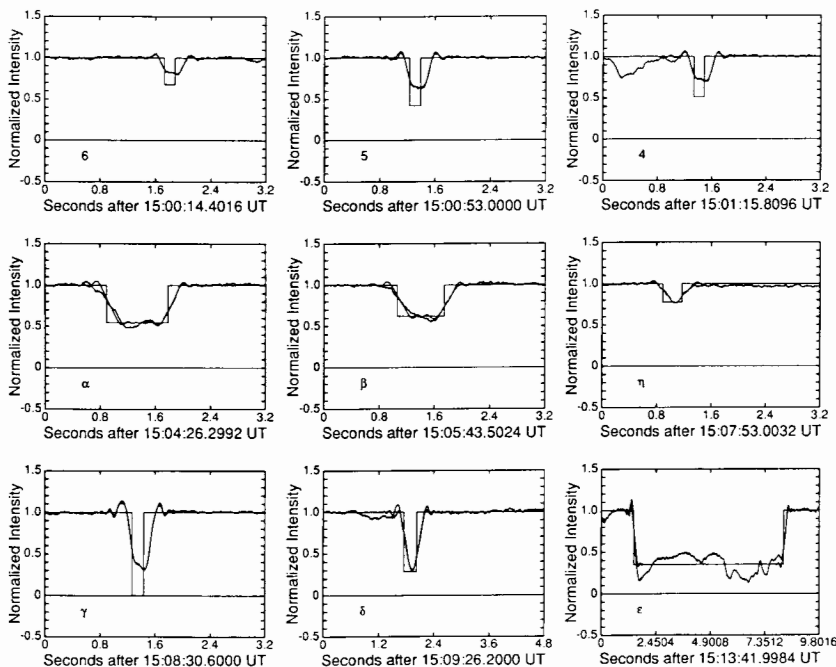


Fig. 12. Earth-based egress occultation profiles of the 26 April 1986 occultation of U28 obtained from the IRTF at 2.2 μm . Superimposed on each profile is the best-fitting square-well model, both uncorrected and corrected for diffraction, finite stellar angular diameter, and instrumental response time. The fits are remarkably good for most of the narrow rings, but little structural detail can be seen for these rings because of the considerable smoothing inherent in ground-based occultations. The photometric stability permits clear identification of low optical depth regions adjacent to the η and δ rings (figure from French et al. 1988a).

The stellar and radio occultation experiments performed by the Voyager spacecraft provided the first view of the Uranian rings at sub-kilometer resolution. Table VI summarizes the pertinent geometric quantities for all Voyager ring profiles, based on the post-Voyager orbit model of French et al. (1988a). Tabulated for each ring event, where appropriate, are the true anomaly (i.e., angle from perapse) for eccentric rings, phase (for the γ and δ ring normal mode perturbations of $m = 0$ and $m = 2$, discussed in Sec. II above), radius in the individual ring's orbit plane, radial width and equivalent depth. All equivalent depths in Table VI were obtained by integrating the normal optical depth profiles, following Eq. (14).

Figures 13 through 22 present a complete gallery of the Voyager occultations, with all data for a given ring presented (where feasible) at a uniform radial and normal optical depth scale. The RSS ingress and egress 3.6-cm profiles are shown at 50-m resolution (200 m for the ϵ ring), while the β Per ingress and egress profiles from the PPS experiment have been binned at a

TABLE VI
Voyager Ring Occultations^a

Ring	Event	True Anomaly	Phase ^d	Radius	Width	Equiv. Depth	Width (UVS)	Equiv. Depth (UVS)
6	RSSI	144.3		41871.6	1.5		0.96 ± 0.07	
	RSSE	2.6		41794.9	1.7		0.90 ± 0.07	
	BPI	197.7		41875.7	2.8 ^b		0.40 ± 0.22 ^b	
	BPE	265.6		41840.3	1.4		0.52 ± 0.14	
5	RSSI	149.9		42304.0	2.8		1.93 ± 0.08	
	RSSE	7.9		42155.3	2.6		2.07 ± 0.09	
	BPI	202.8		42308.7	1.6		0.81 ± 0.17	
4	BPE	271.9		42232.0	2.1		1.08 ± 0.21	
	RSSI	71.2		42556.5	2.0		1.57 ± 0.08	
	RSSE	288.8		42556.1	2.7		1.36 ± 0.08	
α	BPI	123.3		42595.4	2.4		0.64 ± 0.20	
	BPE	193.7		42614.7	2.2		0.61 ± 0.19	
	RSSI	124.4		44737.2	10.6		6.17 ± 0.15	
β	RSSE	340.2		44686.7	4.2		6.60 ± 0.60	
	BPI	171.7		44752.0	13.3 ^c		3.45 ± 0.70	
	BPE	249.7		44730.4	10.5 ^c		2.75 ± 0.54	
η	RSSI	13.9		45641.3	7.0		4.24 ± 0.12	
	RSSE	228.9		45674.3	11.2		4.08 ± 0.13	
	BPI	59.4		45650.9	8.1		2.16 ± 0.56	
β	BPE	140.3		45676.7	11.5 ^c		1.70 ± 0.68	
	RSSI			47176.3	1.5		1.00 ± 0.07	
	RSSE			47176.2	1.5		0.90 ± 0.07	

BPI							
BPE							
RSSI	288.7	285.1	47175.9	47175.9	1.7	0.62 ± 0.16	
RSSE	142.2	64.6	47621.6	47621.6	3.8	9.62 ± 0.28	
BPI	330.7	224.9	47628.5	47628.5	1.6	6.68 ± 0.87	
BPE	57.0	275.1	47626.0	47621.3	0.6	≥1.48 ± 0.36	
RSSI		109.7	47621.3	2.6	3.43 ± 0.44		
RSSE		37.0	48301.3	6.7	5.34 ± 0.13		
SSI	255.6	255.6	48297.5	2.7	4.21 ± 0.13		
SSE	233.1	233.1	48300.5	6.8	2.56 ± 0.35	2.39 ± 0.05	
BPI	249.9	249.9	48301.9	7.0	2.48 ± 0.35	2.45 ± 0.05	
BPE		15.5	48300.8	5.0 ^c	1.43 ± 0.25		
SSI			48296.6	3.3	2.01 ± 0.32	0.30 ± 0.10	
SSE			50024.3	2.5	0.20 ± 0.08	0.31 ± 0.05	
RSSI	30.0		50023.6	1.9	0.18 ± 0.08		
RSSE	241.2		50796.9	22.4	≥93.4 ± 2.1		
SSI	313.0		51342.2	74.9	97.0 ± 0.6		
SSE	351.8		50870.3	30.5	43.8 ± 4.2	42.9 ± 0.4	
BPI	66.9		50748.1	21.2	40.4 ± 5.0	40.6 ± 0.6	
BPE	161.7		50986.9	41.3	≥57.5 ± 7.3		
			51533.8	93.1	52.9 ± 7.3		
					92.8		

^aCodes: RSS = radio occultation (3.6 cm data only); SS = σ Sgr stellar occultation (PPS and UVS data); BP = β Per stellar occultation (PPS data); I = ingress; E = egress occultations.
All angles are in degrees and all lengths are in km.

^bIdentification uncertain; deepest feature near predicted position measured.

^cIdentification uncertain; see Colwell et al. (1990).

^dPhase of internal mode oscillation: $m = 0$ for γ ring; $m = 2$ for δ ring.

^eWidth uncertain because of unsharp edge(s).

resolution of 500 m, chosen as a compromise between resolution and signal-to-noise considerations. In addition, for the δ and ϵ rings a second set of panels presents the UVS and PPS profiles from the σ Sgr occultation. For λ , only σ Sgr data are shown, as this ring was not detected in the RSS experiment, and is below the detectability threshold of the β Per PPS data. The σ Sgr data are shown at full resolution for UVS (120 m, 280 m and 320 m, for δ , λ and ϵ respectively), and averaged to resolutions of 50 m, 85 m and 100 m, respectively, for PPS. The RSS data are from Gresh et al. (1989) and the UVS data from Holberg et al. (1987), replotted from data tapes kindly provided by the experimenters.

The PPS profiles were generated for this review from raw data provided by the PPS team and calibration data given by Colwell et al. (1990). There is some uncertainty in the more opaque PPS profiles, notably for the ϵ ring, because of the rather uncertain and variable background flux levels in the PPS data (Colwell et al. 1990). For these figures, and the equivalent depth results discussed in Sec. III, the nominal PPS stellar flux levels of 43 ± 2 cts (σ Sgr) and 15.2 ± 0.5 cts (β Per) have been adjusted slightly so that the UVS and PPS equivalent depths for the ϵ ring are in agreement (the shorter-wavelength UVS data for σ Sgr show no detectable background signal due to scattered light from Uranus; see Holberg et al. 1987), so the most opaque ring profiles do not drop below the background level. For future reference, the stellar count rates adopted were 45 ± 1 cts/integration for σ Sgr, and $15.8 (15.1) \pm 0.5$ cts/integration for β Per ingress (egress). These values were used to reduce all PPS ring occultation data and to calculate the equivalent depths in Tables V and VI. The uncertainties in stellar flux are reflected in the quoted equivalent depth uncertainties in Table VI.

In comparing occultation data from different experiments, one must take note of the effective extinction efficiency for each data set (Cuzzi 1985). As discussed in Sec. III, $Q_{ex} \approx 2$ for groundbased and spacecraft radio-occultation observations of the Uranian rings, but $Q_{ex} \approx 1$ for spacecraft stellar occultations at ultraviolet wavelengths. This effect was taken into account in Figs. 13 through 22 by plotting the RSS normal optical depth data at half the vertical scale of the PPS and UVS data; in neither case have the reported experimental optical depths been altered. In visualizing the opacity of the rings, note that it is the PPS/UVS optical depths which most closely represent the geometric integrated cross section of ring particles per unit area, while the RSS optical depths represent the "true" extinction, including removal of energy by diffraction effects.

The maximum optical depth measurable in the stellar-occultation experiments is a function of stellar count rate, the nonstellar background flux and the radial resolution at which the data were binned. For the σ Sgr occultation, the PPS background and adjusted stellar count rates were ~ 55 and 45 photons per 0.01 s integration, respectively, giving a threshold normal optical depth of 2.6 at a resolution of 100 m (i.e., a region of this opacity could not be

distinguished from a completely opaque region, at the 70% confidence level, simply due to photon shot noise). The corresponding threshold level for the β Per data, at background and stellar count rates of ~ 2 and 15, respectively, is ~ 2.4 at a resolution of 500 m. These limits are exceeded by the β Per γ ring ingress profile and by the most opaque regions of the ϵ ring in 3 of the 4 cuts. The smallest detectable optical depths in these two experiments, at the resolution of Figs. 13 through 22 and calculated at the $1-\sigma$ level, are 0.07 (σ Sgr) and 0.12 (β Per). Of course, less opaque material can be recognized if it extends over a sufficiently wide range. The threshold optical depth for the very low background UVS σ Sgr data is ~ 4.0 (Holberg et al. 1987), a value reached only in a very narrow part of the ϵ ring egress profile. The minimum detectable optical depth in the UVS data ranges from 0.03 to 0.07 (λ ingress) because spacecraft limit cycle motion displaced the star from the center of the spectrometer slit. For the diffraction-corrected RSS data presented here, the optical depth threshold is 5.2 at 50 m resolution and 6.6 at 200 m, while the minimum detectable optical depth is 0.02, set by unmodeled experimental gain variations (Gresh et al. 1989).

The structure revealed in each ring by these Voyager data sets is discussed next. Comments are based, in part, on the discussions by Gresh et al. (1989) and Colwell et al. (1990). The systematics of the observed width and mean optical depth variations are addressed in the following section.

Rings 6, 5 and 4. In many respects, these three inner rings of the Uranian system are quite similar. Each exhibits substantial eccentricity and inclination to Uranus' equatorial plane (see Table I). French et al. (1986a) found evidence for substantial width variations in rings 4 and 5, with inferred square-well widths ranging from 1 to 7 km. A somewhat smaller range of 1.0 to 2.5 km was found for ring 6, whose integrated optical depth is evidently the smallest of all the 9 classical Uranian rings. No correlation between width and orbital phase has been established for any of these 3 rings. The substantial width variations are especially surprising in view of the very small (~ 300 m) residuals obtained in fitting simple Keplerian ellipses to the rings' center lines (Table I).

The Voyager data in Figs 13, 14 and 15 reveal significant internal structure in even these extremely narrow features, calling into some doubt the underlying assumption of the square-well fits to the groundbased data. In at least 7 out of 12 cases, the outer edge of the ring is appreciably sharper than the inner edge. In 2 cases (BPI-5 and BPI-4), the edges appear comparably sharp, given the signal to noise of the profiles. In only a single case, BPE-6, does the inner edge of the ring appear sharper than the outer. (BP = β Per, SS = σ Sgr, RSS = radio science X band, with appended I for ingress and E for egress profiles.) Most curious of all is the BPI cut across ring 6, in which the ring is almost undetectable, with its center ~ 1.7 km interior to the predicted radius, indicated by an asterisk in Fig. 13. (Neither this observa-

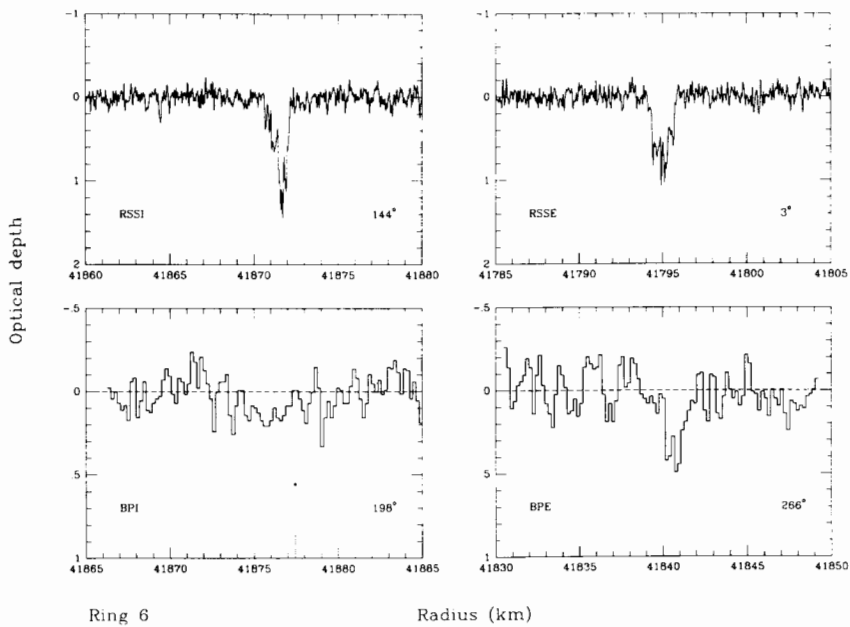


Fig. 13. Normal optical depth profiles of ring 6 from Voyager RSS X-band and β Per PPS occultations. An asterisk indicates the predicted radius for the BPI cut, ~ 2 km exterior to the most prominent feature in the lightcurve. The RSS profiles shown here and in Figs. 14 through 21 have been processed to a radial resolution of 50 m, whereas the PPS β Per data were binned at a resolution of 500 m. For the measurably eccentric rings, the true anomaly is given for each cut. Note the differing optical depth scales used for the radio and stellar profiles, chosen to reflect the factor of 2 difference in extinction efficiency between the two experiments.

tion, nor the BPI η ring cut discussed below, was included in the latest ring model solution.) The low optical depth and ~ 3 -km width of this profile appear uncharacteristic, to judge from the remaining three cuts, and may be artifacts of noise in the data. The PPS experimenters concluded that the probability that the ingress and egress cuts corresponded to identical true equivalent depths is $\sim 2\%$, given uncertainties stemming from photon-counting statistics alone.

Rings α and β . Both α and β rings are frequently resolved in ground-based data, and quasi-sinusoidal variations of width with true anomaly were established by Elliot et al. (1981) and Nicholson et al. (1982), and updated by French et al. (1986a). The width ranges inferred from these observations were 4.5 to 10.5 km and 5.5 to 12 km, respectively. The widest groundbased profiles of the α ring show evidence for a “double-dip” or W structure, which is seen much more clearly in the Voyager RSSI and BPI profiles. The most noticeable feature of the Voyager profiles, however, is the almost complete absence of sharp edges for both rings. Only the RSSE- α cut, which lies

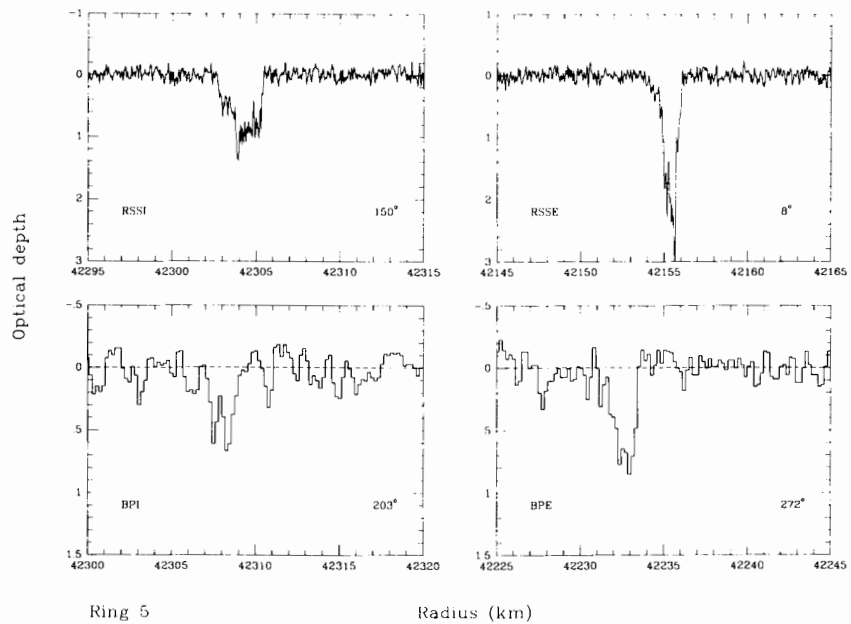


Fig. 14. Normal optical depth profiles of ring 5 from Voyager RSS X-band and β Per PPS occultations.

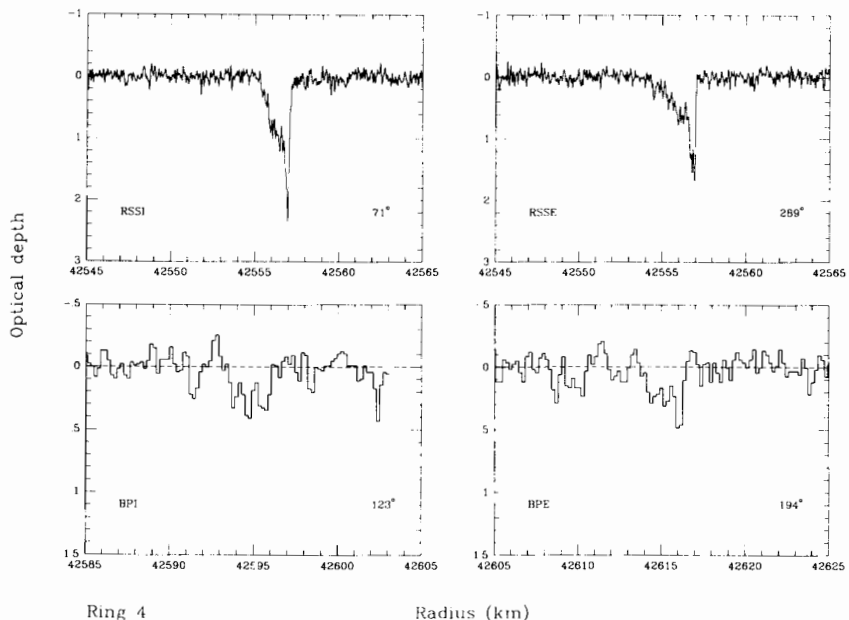


Fig. 15. Normal optical depth profiles of ring 4 from Voyager RSS X-band and β Per PPS occultations.

within 20° of periapse, and BPE- α exhibit outer edges with a sharpness comparable to those seen for rings 6, 5 and 4. The edges of the broad BPI- α and BPE- β profiles, both near apoapse, are in fact impossible to define with any accuracy. A second noteworthy feature is the relatively low optical depth shoulder seen at the inner edge of the α ring, noted independently by Gresh et al. (1989) and Colwell et al. (1990), although this feature is near the noise in the PPS data. Near apoapse, its width is ~ 3.5 km. The same shoulder may also appear in the RSSE cut near periapse, but compressed into a sharp, narrow spike. The outer edge of the β ring appears generally to be sharper than the very diffuse inner edge, although this relation is contradicted by the BPI profile, which shows a sharp inner edge and a suggestion of a diffuse shoulder at the outer edge.

The comparison of widths obtained from the profiles in Figs. 16 and 17 with the groundbased model is complicated by the presence of the α ring shoulder and the diffuse edges of the β ring. Attempts to fit a square-well model to the raw RSSI- α profile, uncorrected for diffraction, yielded models that compromised at the inner edge between the sharp feature at $\sim 44,734$ km and the shoulder extending to $\sim 44,731$ km. The square-well widths for this ring have little physical significance. Similarly, Colwell et al. (1990) reported widths of 9.6 and 7.1 km for the BPI and BPE cuts across the α ring, which now appear to refer only to the dense central part of the ring. Comparison

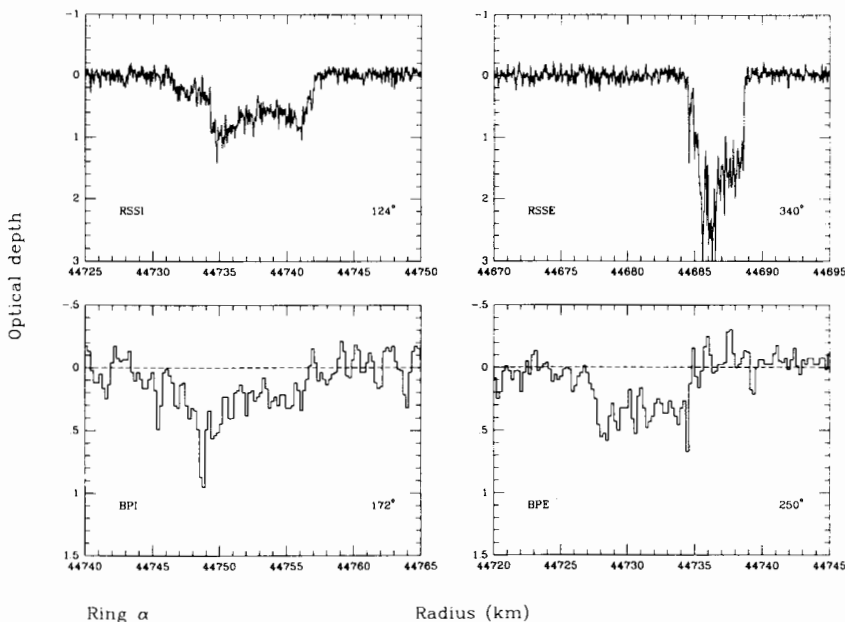


Fig. 16. Normal optical depth profiles of the α ring from Voyager RSS X-band and β Per PPS occultations.

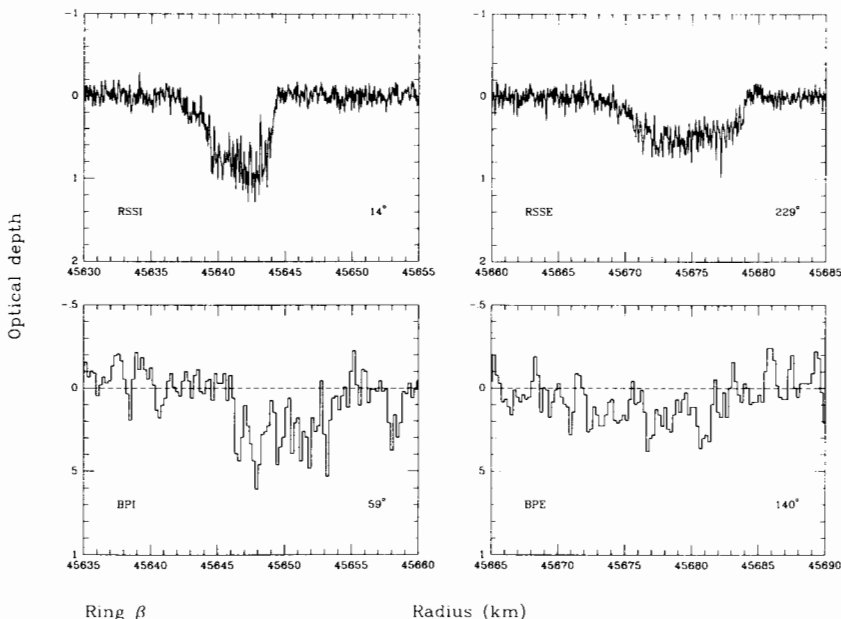


Fig. 17. Normal optical depth profiles of the β ring from Voyager RSS X-band and β Per PPS occultations.

with the RSSI profile in Fig. 16 leads to estimates of the total widths for these 2 cuts of ~ 13.3 and ~ 10.5 km, respectively, although the latter is somewhat uncertain.

A faint ring-like feature was observed just outside the β ring in at least 3 images taken in backscattered light (Smith et al. 1986). Its radius was estimated at $\sim 45,736$ km; no further information is available at this time, other than an estimate of its integrated brightness as $\sim 10\%$ of that of the β ring. If one can infer an equivalent depth of ~ 0.4 km at visible wavelengths from this observation, then this feature should have been seen readily in ground-based occultations at $2.2 \mu\text{m}$, unless, like the λ ring, it is composed principally of submicron particles. The feature was not detectable in the high signal-to-noise RSS occultation data (Gresh et al. 1989).

Ring η . The characteristics of the η ring place it in a class by itself, although in width and optical depth it resembles the inner trio, rings 6, 5 and 4. Unlike these three rings, the η ring exhibits neither a sensible eccentricity nor an inclination to Uranus' equatorial plane (see Table I). Furthermore, the η ring is composed of 2 distinct components: a sharp inner feature (to which the orbital elements in Table I apply, and which is shown in Fig. 18), and a low optical depth component which extends ~ 55 km exterior to the sharp feature. The latter was first seen in groundbased data (see Elliot and Nichol-

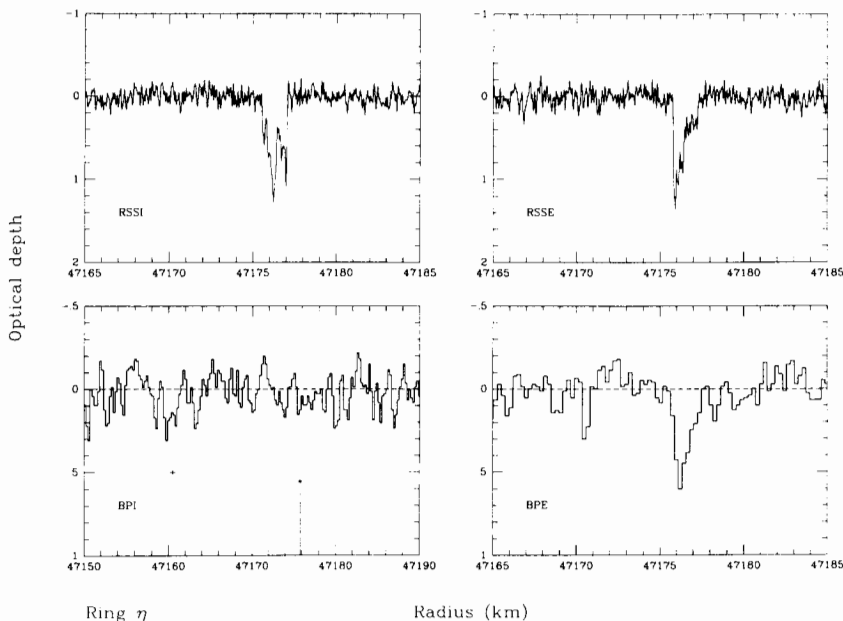


Fig. 18. Normal optical depth profiles of the narrow component of the η ring from Voyager RSS X-band and β Per PPS occultations. This ring was not convincingly detected in the β Per ingress occultation (Colwell et al. 1990); its predicted radius is indicated by an asterisk, and falls ~ 16 km exterior to the only significant feature in this part of the lightcurve, indicated by the +. Note the compressed radial scale of the BPI plot.

son [1984] for a discussion), and also appears clearly in the Voyager RSS data (Fig. 23a below). This broad feature is abruptly terminated at its outer edge, and shows a mean optical depth of 0.03 at 3.6 cm (Gresh et al. 1989) and 0.025 to 0.035 at 2.2 μm . (The signal to noise ratio of the β Per PPS data is too low to show this ring component at all.) Apparent variations in its structure and mean optical depth were reported by Elliot et al. (1983), but may be due more to low-frequency photometric noise than to real variations in the ring itself; the two RSS cuts, separated by 147° in longitude, show no significant variations in width or optical depth (Gresh et al. 1989). The integrated optical depth of the broad component was found to be 1.4 to 2.0 km at 3.6 cm, comparable to values of 1.4 to 1.7 km measured at 2.2 μm .

Inferred widths for the narrow component of the η ring, based on groundbased data, range from 1.3 to 3.5 km (French et al. 1986a). The three Voyager cuts shown in Fig. 18 show a more consistent pattern, with a mean width of 1.6 km. Unlike rings 6, 5 and 4, the η ring's inner edge is observed to be sharper than the outer in 2 of these cuts. The RSS profiles show evidence for considerable internal structure, with the BPE cut closely mimicking the RSSE cut, although they are separated by 86° in inertial longitude.

Most perplexing, however, is the apparent complete disappearance of

the η ring in the β Per ingress lightcurve (Colwell et al. 1990). The BPI panel in Fig. 18 shows a 40-km region centered on the expected location of the ring, with an asterisk indicating the predicted radius of 47,175.8 km. No feature is visible within a few km of this location, at an upper limit of 0.2 km in equivalent depth or 30% of the measured egress value (Table VI). The nearest interesting dip in the lightcurve is at a radius of 47,160 km (indicated by the cross in Fig. 18), with a width of 1.9 km and an equivalent depth $A \approx 0.37$ km, or $\approx 60\%$ of the measured egress value. There is no evidence at all from groundbased data, however, for such a large radius residual from the current kinematical model. The PPS experimenters concluded that there is less than a 1% probability that the ring is present in the egress lightcurve at the same equivalent depth as in the ingress cut, but reduced by random photometric noise to $A < 0.4$ km. This mystery is presently unresolved.

Rings γ and δ . The γ and δ rings belong to a third distinct class, exhibiting both kinematical and structural features that are unique in the Uranian system. As discussed in Sec. II, the kinematics of the γ ring involve both an $m = 0$ radial oscillation mode and an orbital eccentricity of comparable amplitude, while the δ ring appears to be dominated by an $m = 2$ normal mode of oscillation. The phases of these modes are given in Table VI for the 4 Voyager observations of the γ ring and 6 observations of the δ ring, shown in Figs. 19 and 20.

Structurally, the γ ring is the more peculiar. Both inner and outer edges appear to be extremely sharp, with the optical depth rising from zero to unity or more in ~ 100 m (Gresh et al. 1989; Colwell et al. 1990). Two cuts (RSSI and BPE) show moderate widths of 3.8 and 2.6 km, but optical depths which are far greater than those of any of the 6 interior rings. These two profiles are almost mirror images: the outer region of RSSI is more opaque than the inner region, while the opposite is the case for the BPE cut. The RSSE cut is only 1.6 km wide, with the optical depth at some places exceeding the threshold value for this experiment of 6.6 at 200 m resolution (Gresh et al. 1989). Most extreme of all is the BPI cut, that reveals a total width of only 0.6 km (poorly resolved in Fig. 19, at 500-m resolution) and an optical depth probably well above the threshold value of ~ 2.5 . A comparison with the equivalent depth of the ingress cut suggests that the mean optical depth at this ring longitude exceeds 5. This extremely narrow aspect presented by the γ ring may not be unique: in an image taken by the Voyager wide-angle camera 30 min before closest approach, which shows the rings silhouetted against the planet's disk, the γ ring appears much less prominent than either ring δ or even the η ring (Smith et al. 1986, Fig. 12). This image was taken at a longitude within 30° of the narrow BPI cut, though no careful geometric analysis is available. Groundbased data have yielded extremely variable widths for the γ ring, ranging from ~ 1 km to 8 km (French et al. 1986a) and averaging about 4 km. Either the larger groundbased values have been significantly contami-

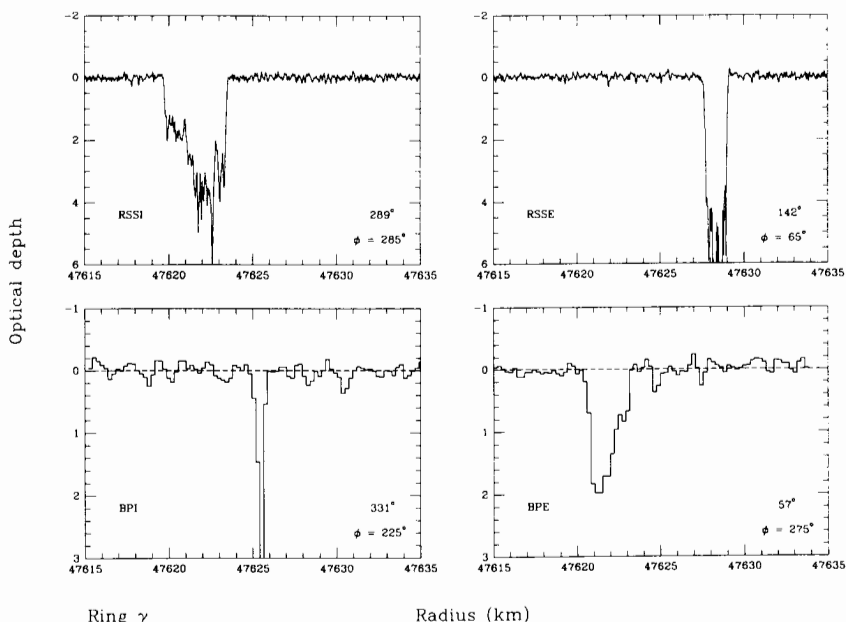


Fig. 19. Normal optical depth profiles of the γ ring from Voyager RSS X-band and β Per PPS occultations. Both the true anomaly and the $m = 0$ phase (designated ϕ) are given for each cut. The 600-m wide BPI profile is only barely resolved at the 500-m resolution used here.

nated by poorly modeled stellar diameter effects, or the total range in γ ring widths is much greater than even that represented by the Voyager sample. There appears to be no obvious relation between the width of the γ ring and either its true anomaly or $m = 0$ phase; this is discussed further below.

The δ ring is represented by 6 independent Voyager occultation profiles, with the PPS data from σ Sgr being comparable in resolution and signal to noise with the RSS data. All 6 cuts show a sharp outer edge and gradational inner edge, although the detailed internal structure varies considerably. Most similar are the RSSI, SSI and SSE cuts, all with widths of ~ 7 km. The BPI cut is fairly similar to these three, although the diffuse inner edge is closer to the noise level here. (Colwell et al. [1990] give a width of 2.47 km for this cut, but the full width appears to be ~ 5.0 km in Fig. 20a.) The RSSE and BPE cuts are significantly narrower, at 2.7 and 3.3 km, respectively, and appear to show reversed morphology, with the bulk of ring opacity near the outer edge for RSSE and near the inner edge for BPE. Widths inferred from groundbased data range from 2 to 8 km, comparable to the range of the Voyager sample.

Horn et al. (1988b) identified a regular wave-like feature in both σ Sgr profiles, which they interpret as a density wave driven by an unseen, nearby moonlet. Marouf et al. (1988b) have computed an eccentricity gradient profile

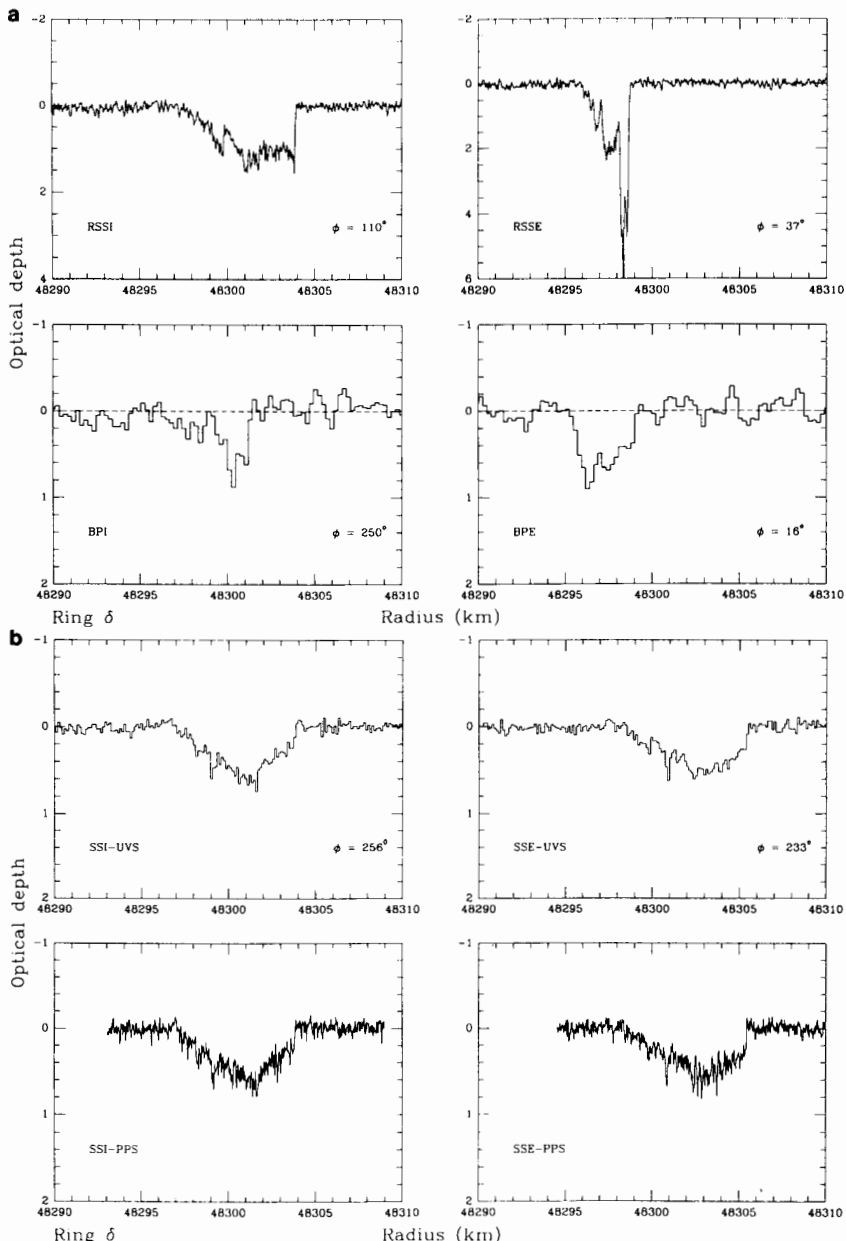


Fig. 20. Normal optical depth profiles of the narrow component of the δ ring from (a) Voyager RSS X-band and β Per PPS occultations, and (b) Voyager σ Sgr UVS and PPS occultations. The σ Sgr profiles are shown at radial resolutions of 120 m (UVS) and 50 m (PPS). The $m = 2$ phase (designated ϕ) is given for each of the 6 independent cuts across this ring.

of the ring and concluded that the $m = 2$ streamlines within the corresponding region in the RSS profiles are disturbed in a manner that appears to be consistent with a wave-like distortion (see the chapter by Esposito et al.). The sharp outer edge of the δ ring is believed to be controlled by a 23:22 resonance with Cordelia (see Table III; also Porco and Goldreich 1987).

Apart from the narrow feature illustrated in Fig. 20, high signal-to-noise profiles of the δ ring also reveal a low optical depth component located interior to the main ring (Elliot et al. 1985; Nicholson et al. 1985; French et al. 1988a, Figs. 2, 4 and 5). Unlike the exterior low- τ component of the η ring, the δ ring companion does not appear to be sharply terminated and its width is correspondingly difficult to define with any accuracy. The best groundbased observations yield widths of 9.5 to 10.8 km, with an average optical depth of 0.04 to 0.06. There appears to be a narrow gap between this feature and the main δ ring, at least at some longitudes. This low- τ companion is clearly seen in the Voyager RSS data (Gresh et al. 1989; see also Fig. 23b), with similar characteristics: a width of 10 km and a mean τ of 0.06; it is also just visible in the UVS σ Sgr δ ring profile (see Holberg et al. 1987, Fig. 4). A preliminary study indicates that the inner edge of the companion feature may remain fixed at a radius of $\sim 48,284$ km, and thus does not share in the $m = 2$ distortion of the main ring, although this result has yet to be confirmed in a careful investigation. The equivalent depth at 3.6 cm (0.60 ± 0.08 km) is similar to that at 2.2 μm (0.54 ± 0.14 km), suggesting that typical particle sizes are large and similar to those in the main ring (Gresh et al. 1989). This is unlike the situation found for Saturn's F ring, where only a very narrow core was detectable at 3.6 cm while a much wider feature was observed in Voyager images and in the PPS occultation.

Ring λ . An examination of Voyager pre-encounter images revealed the presence of a single, previously unsuspected, unresolved narrow ring located between the δ and ϵ rings (Smith et al. 1986). This new ring, previously known by its provisional IAU designation of 1986U1R, was subsequently observed during the σ Sgr occultation by the PPS and UVS instruments (Fig. 21). Based on these meager data, it appears to be circular with a radius of 50,024 km. The structure of the λ ring varies somewhat between the σ Sgr cuts, although they are separated by only 33° in inertial longitude. At ingress, the full width is 1.3 to 2.5 km, with no sharp edges evident in the higher resolution PPS data (85 m in Fig. 21). The egress profile is ~ 1.8 km wide, but shows a very narrow (≤ 0.5 km) dense core. This core is not well resolved in the UVS data, at 320 m resolution, but appears to be only ~ 300 m wide in the PPS cut. The peak optical depth in the core may exceed 0.5, although the average optical depth of the ring is ~ 0.1 at 0.27 μm . Colwell et al. (1990) estimated that 80% of the obscuring material is in the core, a situation reminiscent of the F ring at Saturn, albeit on a much smaller radial scale (Lane et

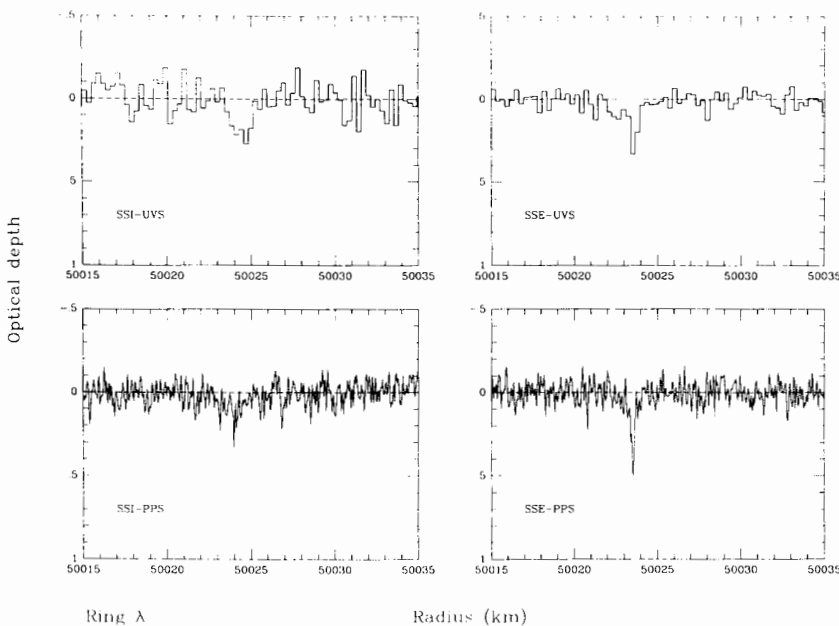


Fig. 21. Normal optical depth profiles of the λ ring from Voyager & Sgr UVS and PPS occultations, at radial resolutions of 280 m (UVS) and 85 m (PPS).

al. 1982). Ockert et al. (1987) reported a clumpy appearance of the ring in an image taken at a phase angle of $\sim 172^\circ$.

The λ ring has not been detected in groundbased occultation data at a wavelength of $2.2 \mu\text{m}$ (Kangas and Elliot 1987), nor in the Voyager radio-occultation data at 3.6 or 13 cm (Gresh et al. 1989). Figure 11 shows data obtained at Palomar Observatory on 24 May 1985, covering the interval between the δ and ϵ rings; no trace of the λ ring is seen, at an equivalent depth limit of $\sim 0.1 \text{ km}$.

Ring ϵ . With a well-resolved width that varies from $\sim 20 \text{ km}$ to $\sim 96 \text{ km}$, the ϵ ring has been studied extensively in groundbased occultation data (Nicholson et al. 1978; Nicholson et al. 1982; Elliott and Nicholson 1984). It is the prototype for variable width, eccentric rings, and its discovery prompted the first theoretical investigations of mechanisms whereby differential apsidal precession might be counteracted in such a ring (Goldreich and Tremaine 1979a; Dermott and Murray 1980). Groundbased data revealed a consistent pattern of internal structure within the ϵ ring, which to first order appears to expand and contract uniformly with the ring as a whole. The integrated optical depth of the ring was found to remain essentially constant, despite the five-fold variation in width and thus in mean optical depth (French

et al. 1986a). Groundbased observations were, however, unable to probe the narrowest and most opaque region of the ring near periapse owing to the extremely small transmitted flux ($\tau \approx 4.0$ at $Q_{ext} = 2$) and uncertainties in the corrections for background flux from Uranus itself.

In this respect, the distribution of the 6 Voyager occultation cuts was extremely fortunate: 3 observations fell within 50° of periapse, and 2 (RSSI and SSE) within 30° . The narrowest Voyager profile was obtained from the σ Sgr egress lightcurve, at a true anomaly of 352° and a width of 21.2 km. A nice balance is provided by the RSSE and BPE cuts at 241° and 162° , respectively, which sample the apoapse region of the ring. Figure 22 shows all 8 profiles (RSS, UVS and PPS for both β Per and σ Sgr), although it has been necessary in this figure to adopt variable radial and optical depth scales in order to present adequately the range of ring widths encountered. Portions of the RSSI, BPI, SSI (PPS only) and SSE profiles fall below the relevant experimental optical depth thresholds, but these account for only relatively small fractions of the total ring width, even near periapse. This situation is due in part to the extremely high dynamic range of the RSS experiment, for which the threshold optical depth is 6.6 for 200 m resolution, and in part to the reduction of a factor of 2 in Q_{ext} in going from groundbased to spacecraft stellar occultations.

A prominent characteristic of all the Voyager profiles is the sharpness of both inner and outer edges of the ϵ ring. The PPS data from the σ Sgr occultation, sampled at resolution of 10 m, reveal the inner edge to have a width of ~ 500 m, while that of the outer edge is ~ 40 m (Colwell et al. 1990). The extreme sharpness of the outer edge is also evident in the RSS data (Gresh et al. 1989), where the RSSI optical depth decreases from ~ 4 to zero in ~ 50 m. Both edges are believed to be controlled by resonances: see Table III and Sec. V. The internal structure of the ring is found to vary somewhat in detail between the different Voyager cuts, while retaining its characteristic large-scale features. A comparison with a typical groundbased profile, scaled in width and optical depth to match the UVS SSI and SSE cuts, reinforces this impression (Holberg et al. 1987, Fig. 8). The greatest deviations from a simple linear scaling of the groundbased profile occur near periapse, especially near the inner edge of the ring and within the dense narrow core (see Fig. 29 below). The very prominent optical depth maximum seen clearly at the inner edges of the RSSE, BPI, BPE and SSI profiles is greatly reduced or absent in the SSE cut at 352° . Marouf et al. (1987) used the RSS profiles to determine empirically the eccentricity gradient across the ϵ ring, for comparison with the predictions of the self-gravity model of Goldreich and Tremaine (1979a). Their results are discussed below.

A particularly puzzling feature of the ϵ ring is an anomalous scattered signal observed during radio-occultation egress. In contrast to stellar occultations, the coherent nature of the radio signal illuminating the rings allows detection of the Doppler broadened signal scattered in the direction of the

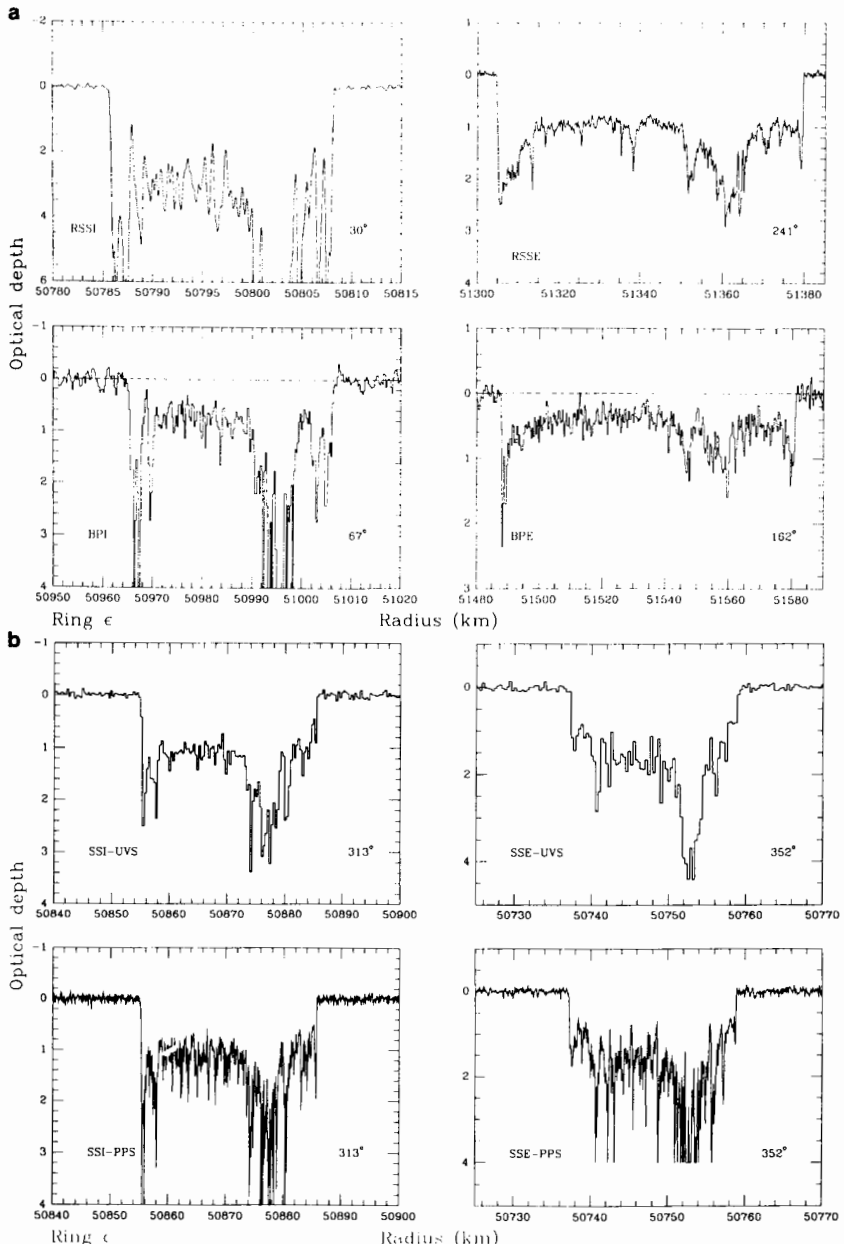


Fig. 22. Normal optical depth profiles of the ϵ ring from (a) Voyager RSS X-band and β Per PPS occultations, and (b) Voyager σ Sgr UVS and PPS occultations. The RSS data have been processed to a resolution of 200 m, while the β Per data are shown at 500 m, and the σ Sgr data at 320 m (UVS) and 100 m (PPS). Note that the five-fold variation in width exhibited by the ϵ ring has necessitated nonuniform radial scales for the individual panels. The most opaque portions of the BPI, SSI and SSE profiles exceed the threshold optical depth for the PPS data of ~ 2.5 (see text).

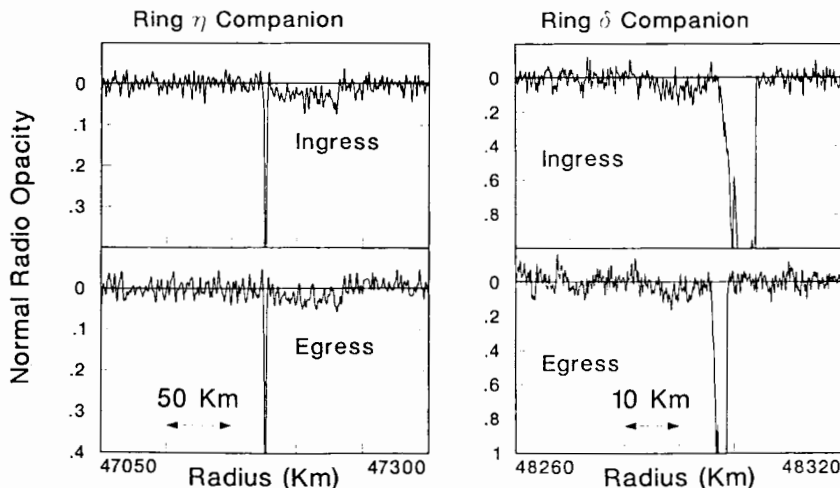


Fig. 23. Tenuous companions of (a) the η ring, and (b) the δ ring as observed in the X-band radio-occultation data (Gresh et al. 1989). Little variation in width (~ 55 km for η and ~ 10 km for δ) or average optical depth (~ 0.03 for η and ~ 0.06 for δ) with longitude is apparent.

Earth by all ring particles illuminated by the spacecraft antenna (Marouf et al. 1982). At Saturn, the scattered signal was clearly detectable and was used to obtain particle size distributions of several ring features (Marouf et al. 1983; Zebker et al. 1985). No Saturn-like scattered signal was expected at Uranus, simply because the rings are too narrow to contribute sufficient scattered signal power (radar cross-section) to overcome measurement noise.

Nonetheless, during occultation egress of the ϵ ring, a clear scattered signal was observed independently at 2 Earth receiving stations (Canberra and Parkes, Australia) for a period of about 400 s, centered on the geometric occultation time of the ϵ ring (Tyler et al. 1986; Gresh et al. 1989). The duration is approximately equal to the time that the ϵ ring was illuminated by the spacecraft antenna. As the temporal sequence of Parkes spectra in Fig. 24 shows, a single feature of bandwidth ≈ 100 Hz and peak strength ≈ 1.5 dB^a ($\sim 40\%$) above the noise baseline drifts throughout the direct signal (central feature) at a rate ≈ -4.5 Hz s⁻¹. In comparison, theoretical predictions based on a Saturn-like ring model (discrete random distribution of particles in individual Keplerian orbits) yield a bandwidth ≈ 3000 Hz, peak strength ≈ 20 dB (1%) below the noise level, and a drift rate ≈ -6.5 Hz s⁻¹ (Gresh et al. 1989).

Thus all 3 observable parameters of this "anomalous" scattered signal are totally inconsistent with a Saturn-like ring model and suggest a fundamentally different origin. The enormous strength suggests scattering by

^aSNR in dB is defined as $10 \log_{10}(P_s/P_N)$, where P_s is the signal power and P_N is the thermal noise power in a specified bandwidth (usually 1 Hz).

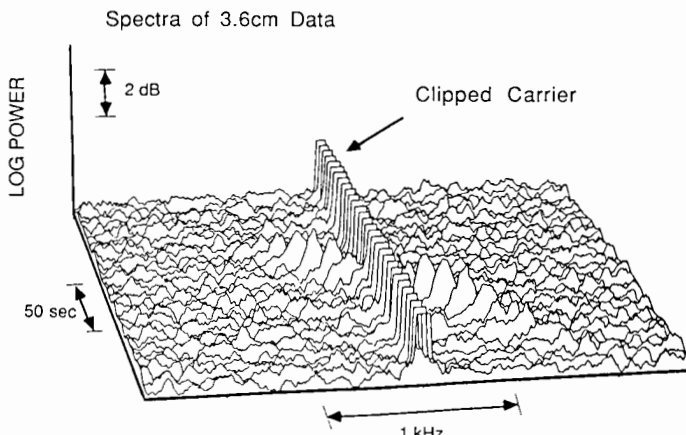


Fig. 24. Power spectra observed by the radio-occultation experiment in the vicinity of Ring ϵ at egress (Gresh et al. 1989). The "anomalous" scattered signal is the feature drifting from positive (right) to negative (left) frequency relative to the frequency of the direct signal (labeled carrier), which has been clipped in the figure for clarity. The strength, bandwidth and frequency drift rate of the feature are inconsistent with a Saturn-like scattering model.

cylinder-like structures with axial length of the order of, or exceeding the Fresnel scale (≈ 2 km) (Marouf and P. A. Rosen 1986, unpublished). The elongated axis of such structures must also be canted (in the trailing sense) by about 10 to 11° relative to the azimuthal direction to explain the observed -4.5 Hz s^{-1} drift rate. It is difficult to visualize how such elongated and canted structure could maintain its spatial coherence over distances of several kilometers in the presence of destructive Keplerian shear. No scattered signal was detectable for the ϵ ingress occultation, nor for any other ring.

Additional Ring Features. In addition to the 10 narrow rings discussed above, Voyager observations indicated the existence of other, generally low optical depth ring features in the Uranian system. In an image obtained at phase angle $\sim 90^\circ$, near ring-plane crossing, a broad sheet of material was observed inside ring 6, extending from 37,000 km to at least 39,500 km in radius. The image is badly smeared, but there are suggestions of structure within this band. The optical depth inferred from the measured surface brightness is $\sim 10^{-3}$ (Smith et al. 1986), making the feature too transparent to be recognized in groundbased or Voyager occultation experiments.

At phase angles near 180° , forward scattering greatly enhances the visibility of wavelength-size and slightly larger dust particles. A single 96-s exposure wide-angle frame at a phase angle of 172.5° revealed a bewildering array of dust features scattered throughout the Uranian ring system (see Smith et al. 1986, Fig. 13; chapter by Esposito et al.). Although the principal narrow rings are detectable in this image, many of the most prominent features

show little or no correlation with previously known rings. An exception is the λ ring, which appears as the brightest feature in the image. Although definitive results are not yet available, the optical depth of the brightest dust band revealed here (other than ring λ) is believed to be $\sim 1.5 \times 10^{-5}$, for a mean particle size of $\sim 1 \mu\text{m}$ inferred from the slope of the phase function near 172° (Ockert et al. 1987). The dusty component of the Uranian system, and its relation with the narrow rings, is discussed more completely in the chapter by Esposito et al.

Prompted by the discovery of ring material (then suspected to be incomplete rings, or arcs) around Neptune (Hubbard et al. 1986), an attempt was made to search for such arcs at Uranus using the PPS occultation data sets (Lane et al. 1986; Colwell et al. 1990). These searches were also used to identify any potential complete rings that were too narrow and/or transparent to detect from the ground. Although two candidates for new complete rings (at radii of 50,660 km and 38,280 km) and several arc candidates were identified in the initial report (Lane et al. 1986), subsequent analyses have not established the reality of any of these individual features beyond a reasonable doubt (Colwell et al. 1990). Several dips that occur in the β Per and σ Sgr lightcurves are more significant than the upper limits established for the BPI- η and BPI-6 occultations, but no individual feature (ring or arc) in the real data is more significant than similar features in the test data. It is not clear from the reported analysis whether the number of such dips is statistically significant. Furthermore, any of the putative β Per features would have been seen readily in the σ Sgr data, had that star crossed the relevant radius, as well as in the best groundbased occultation data. Reliable upper limits on the equivalent depths of undiscovered rings or arcs in the PPS data have been estimated by Colwell et al. (1990) at 0.4 km for β Per and 0.1 km for σ Sgr. No potential arcs or additional complete rings were detected in the RSS occultation data (Gresh et al. 1989). A comprehensive search for evidence of Uranian ring arcs in Earth-based occultation observations has not yet been performed.

B. Systematic Width Variations

Soon after the discovery of the Uranian rings, it was established that the eccentric ϵ ring exhibits a systematic variation in width with orbital longitude (Nicholson et al. 1978). This width variation was interpreted in terms of a differential eccentricity between the inner and outer edges of the ring, with the outer edge more eccentric than the inner. The observed range in width for the ϵ ring of ~ 20 to ~ 96 km implied an eccentricity variation of 10% across the ring. Soon afterward, similar systematic width variations were established for the α and β rings, implying similar fractional eccentricity gradients, although the measured widths for these two rings showed much more scatter about the best-fitting models (Elliot and Nicholson 1984). In terms of the mean semimajor axis a , and eccentricity e , and the corresponding differences

between inner and outer edges, $\delta a = a_{\text{outer}} - a_{\text{inner}}$ and $\delta e = e_{\text{outer}} - e_{\text{inner}}$, the variation of width W , with true anomaly θ , is given to first order in e by:

$$W(\theta) = \delta a [1 - q_e \cos \theta - q_{\dot{\omega}} \sin \theta - 2eq_e \sin^2 \theta - eq_{\dot{\omega}} \sin 2\theta + O(e^2)] \quad (22)$$

where $q_e = a \delta e / \delta a + e$, $q_{\dot{\omega}} = ae \delta \dot{\omega} / \delta a$, and $\dot{\omega}$ is the longitude of pericenter. The terms involving $q_{\dot{\omega}}$ allow for the possibility that the apsidal lines of the two bounding ellipses are mis-aligned: $\delta \dot{\omega} = \dot{\omega}_{\text{outer}} - \dot{\omega}_{\text{inner}}$. The term proportional to eq_e is significant only for the ϵ ring, where it amounts to 0.6 km; the $eq_{\dot{\omega}}$ term is negligible for all Uranian rings.

The very existence of a narrow, eccentric ring implies that somehow the tendency of the inner and outer edges of the ring to precess differentially due to the gradient in the quadrupole component of the planet's gravitational field must be counteracted. Goldreich and Tremaine (1979a) proposed the most widely accepted solution to this problem, invoking the ring's self-gravity. This model requires that δe be positive, in agreement with the observations of rings α , β and ϵ , and permits the calculation of ring mass and mean surface density Σ from the observed values of δa and δe . Extension of the self-gravity model to include the effects of a finite "viscosity" in the rings (due to random non-Keplerian velocities induced by collisions between the ring particles) led to the prediction of a negative apsidal shift, $\delta \dot{\omega}$, that is proportional to the random velocity dispersion σ (Borderies et al. 1983a).

Rings α , β , and ϵ . Fits of Eq. (22) to groundbased measurements of width variations in the α , β and ϵ rings have been published by Nicholson and Matthews (1983) and French et al. (1986a), the latter employing widths obtained from square-well fits. Both analyses were in substantial accord in finding nonzero values of $\delta \dot{\omega}$ for the α and β rings (-2° and -5° , respectively), but no measurable apsidal shift for the ϵ ring. The dimensionless eccentricity gradient q_e was found to be 0.36 ± 0.06 and 0.30 ± 0.04 for α and β , respectively, and 0.67 ± 0.01 for ϵ . The corresponding mean surface mass densities Σ and *rms* random velocities σ , based on a simple two-streamline model, were (French et al. 1986a); $\Sigma = 2.0 \pm 0.4$, 1.5 ± 0.2 and 32.7 ± 0.6 g cm⁻² and $\sigma = 1.5 \pm 0.3$, 1.7 ± 0.2 and < 6.0 mm s⁻¹, for α , β and ϵ , respectively. More realistic multistreamline models for the ϵ ring give somewhat lower mass density estimates of 25 g cm⁻² (Goldreich and Tremaine 1979a). The *rms* velocities derived in this way imply typical ring thicknesses of ~ 15 m (French et al. 1986a).

Using data obtained from more recent groundbased occultations, described in French et al. (1988a), together with the square-well fits to the Voyager RSS occultation data, and omitting several early groundbased measurements of doubtful accuracy, these width-longitude fits have been updated, as shown in Fig. 25 and Table VII (upper part). The new fits yield very similar results for the ϵ ring, as expected, with $\delta \dot{\omega}$ remaining insignificant. The ec-

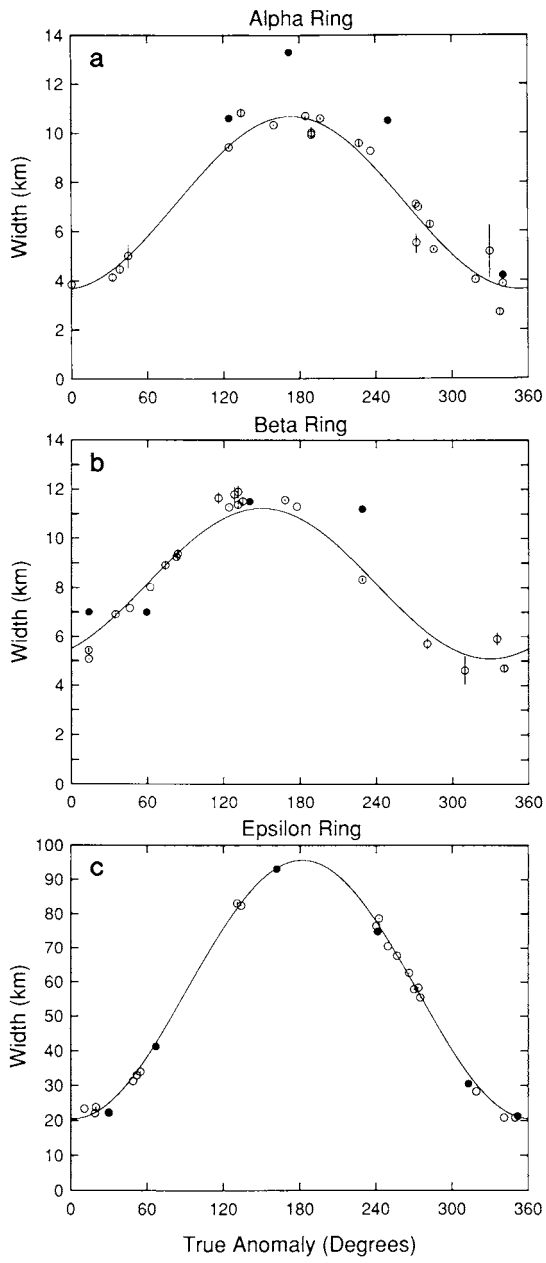


Fig. 25. Ring width vs true anomaly for (a) the α ring, (b) the β ring, and (c) the ϵ ring. The open circles are widths determined from square-well fits to groundbased data and RSS X-band profiles (uncorrected for diffraction). The solid lines show the width-longitude models fitted to these points (Table VII). The filled circles (not used in the fits) correspond to the actual ring widths measured from the Voyager profiles (see Table VI).

TABLE VII
Width-Latitude Relations

Square-well model widths*					
Ring	Mean width δa (km)	Amplitude $a\delta e$ (km)	Apsidal shift $\delta\bar{\omega}$ (deg)	q_e $a\delta e/\delta a$	$q_{\bar{\omega}}$ $a\delta\bar{\omega}/\delta a$
α	7.15 ± 0.15	3.52 ± 0.23	-0.7 ± 0.5	0.49	-0.06
β	8.15 ± 0.14	3.07 ± 0.18	-5.0 ± 0.6	0.38	-0.22
ϵ	58.1 ± 0.5	37.6 ± 0.8	$+0.16 \pm 0.09$	0.65	+0.02
Voyager widths only					
α (4 pts)	8.46 ± 0.14	4.78 ± 0.19	$+0.9 \pm 0.4$	0.57	+0.07
β (4 pts)	9.49 ± 0.04	2.59 ± 0.05	$+0.07 \pm 0.16$	0.27	+0.003
ϵ (6 pts)	57.0 ± 0.6	37.5 ± 0.8	$+0.06 \pm 0.12$	0.66	+0.01

*Groundbased and Voyager RSS data.

centricity gradients for α and β are somewhat larger, at $q_e = 0.49 \pm 0.03$ and 0.38 ± 0.02 , respectively. Rather surprising is the apsidal shift for the α ring, which has almost disappeared in the new fit ($\delta\bar{\omega} = -0.7 \pm 0.5^\circ$), though the β ring's larger shift has remained unchanged at -5° . The consequences of this result have not yet been explored, although, as indicated below, there are now other reasons to doubt the applicability of the self-gravity model to the α and β rings.

The extremely diffuse edges of the β ring and the similarly diffuse inner edge of the α ring (see Figs. 16 and 17) raise substantial doubts as to whether the square-well model fits to low-resolution groundbased data yield meaningful widths for these 2 rings. In order to begin to explore this question, Eq. (22) was fitted to the Voyager RSS and PPS occultation data alone (4 data points and three parameters each for α and β ; 6 data points for ϵ). The results, also given in Table VII (lower part), are somewhat disturbing; q_e increases to 0.57 ± 0.02 for α and decreases to 0.27 ± 0.01 for β , while insignificant apsidal shifts are found for both rings. The RSS data alone, assuming $q_{\bar{\omega}} = 0$, yield $q_e = 0.48$ and 0.27 for rings α and β , respectively (see below). These preliminary results should not be overinterpreted, given the small number of data points available, but they do suggest that the current width-latitude models for the α and β rings are only qualitatively accurate. The Voyager widths for these rings are plotted as filled symbols in Fig. 25 to emphasize the contrast with the square-well widths. Clearly, it makes little sense to combine Voyager widths for these rings with the groundbased data directly.

With the discovery of the ϵ ring shepherd satellites, Cordelia and Ophelia, and the realization that discrete resonances with these satellites control the edges of the ϵ ring (Porco and Goldreich 1987), it is likely that the ϵ ring edges exhibit wave-like perturbations with wavenumber $m = 14$ (outer edge)

and $m = 25$ (inner edge). A search of the groundbased width data has failed so far to reveal evidence of measurable perturbations with these wavenumbers (French 1987), although Horn et al. (1988a) reported that local distortions in the ring width exist in the Voyager data. A comparison of the observed Voyager edge radii with the elliptical edge model of French et al. (1986a), with the mean elements corrected to the post-Voyager model (French et al. 1988a), yields maximum residuals of 1.5 km. The width-longitude fits, using either square-well model fits or Voyager widths only (Table VII), are in substantial accord for the ϵ ring, as might be anticipated owing to the relative sharpness of the ϵ ring edges.

Elliot et al. (1987) reported the possible discovery of very small amplitude (0.1 to 0.2 km), short wavelength perturbations on both edges of the ϵ ring during a stellar occultation in 1987. These perturbations, attributed to small satellites orbiting only a few kilometers from the ring or to individual large ring particles (Kangas and Elliot 1988), are probably too small to be revealed in comparative studies of different occultation data sets, including the Voyager data, and are far too small to detect in Voyager images.

Rings 6, 5 and 4. No model for the substantial width variations exhibited by rings 6, 5 and 4 has been established to date (French et al. 1986a); the observed groundbased variations seem to be uncorrelated with true anomaly, despite the substantial eccentricities of all 3 rings. A comparison of the 4 Voyager cuts for each ring reinforces this result. Figure 26 shows the widths plotted as a function of orbital radius, using Voyager data only. For zero (or small) apsidal shift, Eq. (22) implies a positive linear relation between width and radius: $W(r) \approx \delta a + (\delta e/e)(r - a)$. No such relation is observed for any of these 3 rings, despite the evidence for substantial variations in the widths of rings 4 and 5, and perhaps ring 6 also. Plots of width vs true anomaly show no systematic trends. As specific examples of this apparently random behavior, note the very different appearance of the RSSI and BPI cuts of ring 6, both near apoapse (see Fig. 13 and Table VI for the exact true anomalies); the RSSI and BPI cuts of ring 5 (Fig. 14), also near apoapse; and the RSSI and RSSE cuts of ring 4 (Fig. 15), located 71° either side of periape (Gresh et al. 1989).

Ring η . No significant variations in width have been detected for the narrow component of the η ring (French et al. 1986a), and the 3 unambiguous Voyager observations substantiate this result (the uncertain BPI cut excluded). The mean width is ~ 1.6 km, similar to ring 6. As the ring is sensibly circular and equatorial, no width variations are expected, based on our current understanding of ring dynamics. No width variations in the broad, low optical depth component have been reported, but no careful study of this feature has been published to date.

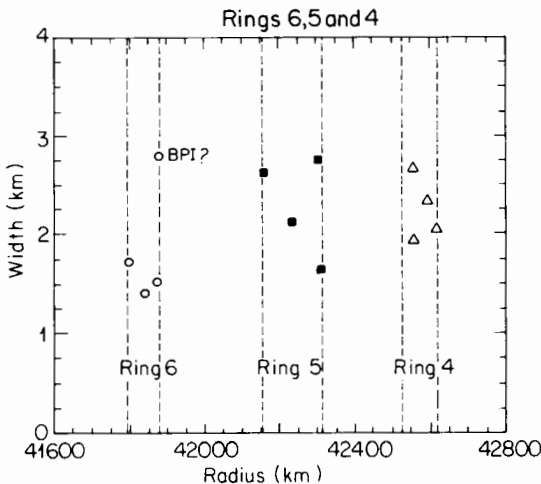


Fig. 26. Widths of rings 6, 5 and 4 from Voyager observations as a function of orbital radius. There is no evidence of a linear width-radius relation for any of these narrow rings. The uncertainly identified BPI cut of ring 6 is identified; see Fig. 13. Vertical lines indicate the pericenter and apocenter radii for each ring.

Rings γ and δ . The γ ring exhibits no obvious systematic pattern of width variations (French et al. 1986a), although its rather sharp edges, as evidenced in the Voyager profiles and in the often prominent diffraction fringes in groundbased data, suggest that the square-well widths are fairly accurate. The situation is complicated by the contributions of both $m = 0$ and $m = 1$ modes to its kinematics, with comparable amplitudes (see Sec. II). The groundbased and Voyager-derived widths for this ring have been examined as functions of true anomaly and $m = 0$ phase, but no clear pattern has emerged. In Fig. 27a, all measured widths are plotted vs orbital radius. Based on an analysis of multimode motions in narrow rings, Longaretti (1989) concluded that the $m = 0$ mode should dominate width variations, with the maximum width occurring at zero phase (i.e., minimum radius). Such a pattern is not evident in Fig. 27a. The width variations of the γ ring might be controlled by yet a third normal mode ($m = 2$ or 3, say) that does not contribute measurably to the center-line displacement (Longaretti 1988), but this possibility has not yet been numerically explored. A second possibility, alluded to above, is that the ring has a substantial out-of-plane warp, due to an inclination gradient between the inner and outer edges, although the fit in Table III yields a mean inclination of $< 0^\circ 003$.

The situation is much simpler for the δ ring, whose kinematics are well modeled by a single $m = 2$ normal mode (see Sec. II). Figure 27b, after French et al. (1988b), reveals a tight correlation of width with orbital phase. The largest widths occur near the longitudes of maximum positive radial dis-

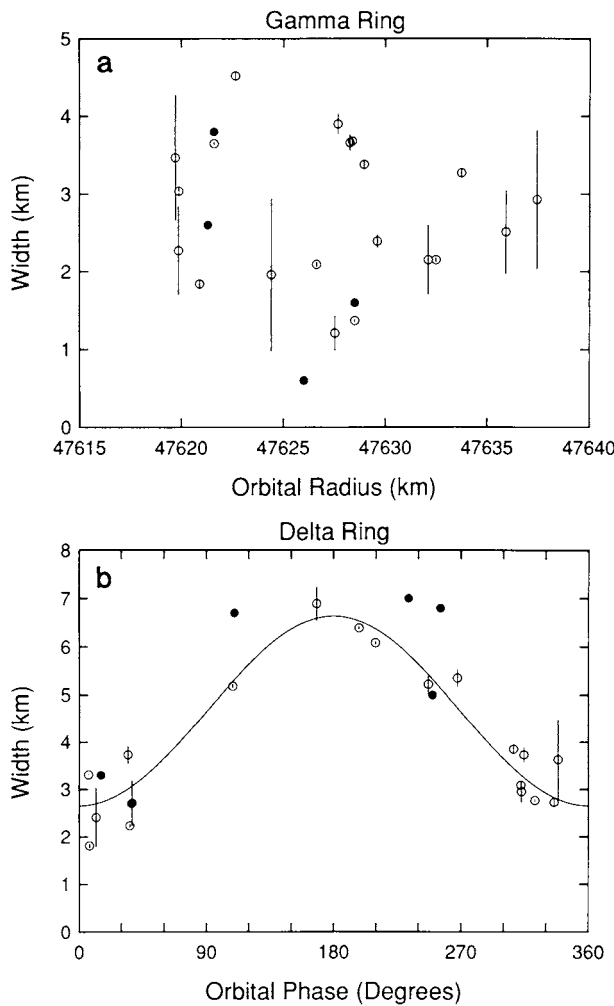


Fig. 27. (a) Ring width vs orbital radius for the γ ring. There is no hint of a linear width-radius relation. (b) Ring width vs $m = 2$ mode orbital phase for the δ ring, along with the best-fitting model curve. The open circles are widths determined from square-well fits to ground-based data and RSS X-band profiles (uncorrected for diffraction), and the filled circles (not used in the fit) correspond to the actual ring widths measured from the Voyager profiles (see Table VI).

placement, in a manner which is analogous to the width-longitude relations exhibited by the eccentric α , β , and ϵ rings (see Fig. 25), and as predicted by Goldreich and Porco (1987). The total range in width is substantial: from ~ 2.8 km to ~ 7.0 km, implying $q_e \sim 0.43$, comparable to the α and β rings. However, there is some deviation from this simple picture, as the Voyager BPI cut appears to be ~ 2 km narrower than the 2 RSS cuts that bracket it in

phase (see Table VI). Nevertheless, the overall shapes of these 3 cuts are quite similar. French et al. (1988b) estimated a mean surface density of 7 g cm^{-2} for the δ ring from the width-longitude relation in Fig. 27b and in Goldreich and Porco (1987, their Eq. 3).

C. Eccentricity Gradient Profiles

In addition to width variations, Voyager occultation profiles reveal remarkable variation in detailed ring morphology with longitude (cf., Figs. 13 through 22). For rings modeled by nonintersecting, elliptical, coplanar streamlines of the form $r = a(1 - e \cos \theta)$, this variation with longitude can be interpreted in terms of changes in the eccentricity gradient $q_e(a) \approx ade/da$ across the ring. Marouf et al. (1987) proposed a procedure that utilizes the 2 observed radio-occultation profiles for each of rings α , β , and ϵ to estimate $q_e(a)$ from simple kinematical considerations. These profiles are separated in longitude by ~ 145 to 149° and, for each ring, one profile in the neighborhood of periapsis was available (a chance event). The procedure relies on the experimental observation that integrated optical depth is nearly conserved at the two widely separated observation longitudes, and thus that τ is directly related to total particle cross section per unit area. If the particle size distribution is assumed uniform across a given ring, then the observed optical depth profiles also represent the distribution of surface mass density. One can then search the 2 observed profiles for the radii r_1 and r_2 that confine the same increment of ring mass. Presumably r_1 and r_2 belong to the same streamline, thus permitting computation of a and e (assuming $\delta\omega=0$, i.e., aligned apsidal line), and subsequently $q_e(a)$, for each streamline. No dynamical assumptions are made regarding the forces responsible for the observed $q_e(a)$ profile.

Results obtained from 500-m resolution radio-occultation profiles of rings α , β and ϵ are depicted as the solid lines in Fig. 28. The results are considered "self-consistent" if the derived $q_e(a)$ satisfies $0 \leq q_e(a) \leq 1$, consistent with the nonintersecting streamlines assumption. Also shown in Fig. 28 as horizontal dotted lines are the constant mean gradients $q_e \equiv a \delta e / \delta a$ derived from the overall ring widths alone (viz., Eq. (22); $q_{\bar{\omega}} = 0$), where $q_e \approx 0.48$, 0.27 and 0.68 for Rings α , β and ϵ , respectively. In all 3 cases, $q_e(a)$ deviates significantly from q_e . Particularly interesting in the case of the ϵ ring is the fact that while the constant gradient q_e essentially explains the overall behavior, substantial deviations from q_e characterize the dense core and many of the narrow embedded features. This is demonstrated in Fig. 29a where the ingress (Ing) and egress (Egr) 500-m resolution radio-occultation profiles are "advanced" from the observation longitude (Table VI) to 90° true anomaly (quadrature), assuming a constant gradient $q_e \approx 0.68$. A good match between the overall optical depth levels is evident; however, the opacity enhancement at the inner edge, the dense core, and prominent narrow features are clearly out of alignment. Similar results were found by Holberg et al. (1987) from a constant- q_e comparison of the UVS σ Sgr profiles.

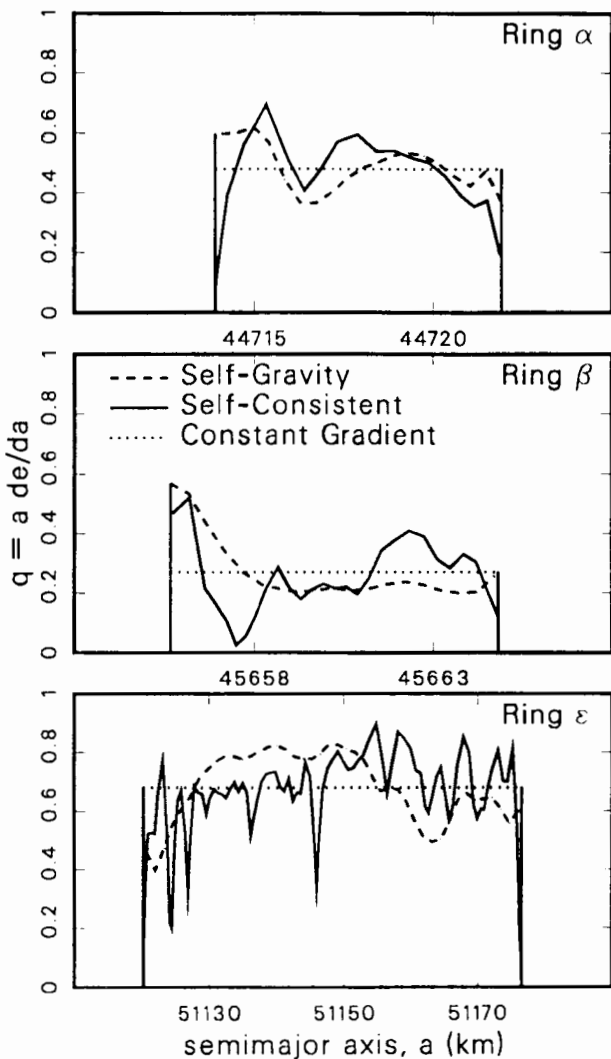


Fig. 28. Eccentricity gradient profiles of rings α , β , and ϵ (Marouf et al. 1987; Gresh 1990). The solid curves (self-consistent model) are empirically computed from the ingress and egress radio-occultation profiles. The dashed curves (self-gravity model) are computed from a single radio-occultation profile assuming that rigid precession is enforced by the ring's self-gravity (Goldreich and Tremaine 1979a); 20, 20 and 45 streamline models were used for rings α , β and ϵ , respectively. The dotted horizontal line (constant gradient) in each case corresponds to a linear taper of eccentricity between the inner and outer edge values.

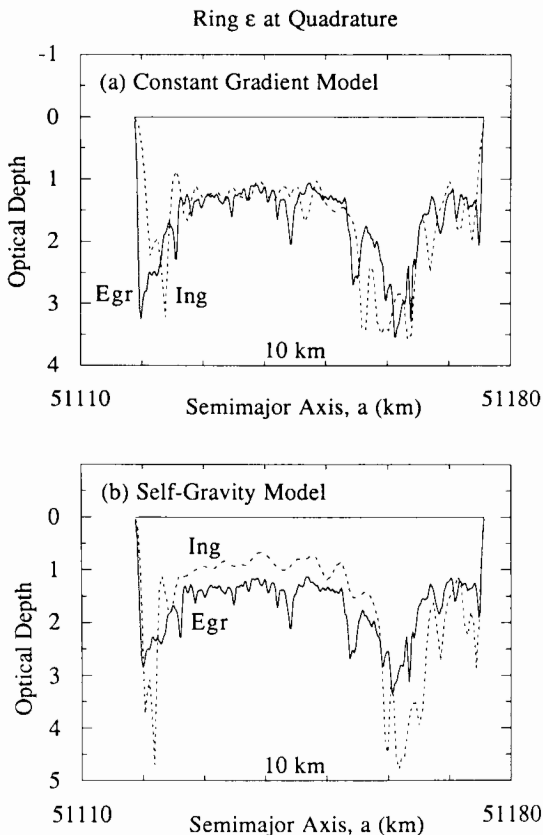


Fig. 29. Ingress (Ing) and egress (Egr) radio-occultation profiles of the ϵ ring advanced to 90° true anomaly (quadrature) using two different eccentricity gradient profiles (Marouf et al 1987): (top) constant gradient; (bottom) self-gravity eccentricity gradient. Significant differences between the ingress and egress profiles indicate that neither model is consistent with the observations.

A more physical approach to determination of the $q_e(a)$ profile was proposed by Goldreich and Tremaine (1979a). As discussed above, a ring modeled by N nonintersecting streamlines can precess as a single entity if self-gravitational forces between the streamlines are invoked to counterbalance differential precession due to the quadrupole moment of the Uranian gravitational field. Given the radial distribution of ring mass at some longitude, a discretized N -streamline model can be constructed and the corresponding $e(a)$, and hence, $q_e(a)$, profile can be calculated by enforcing such a balance (cf. Goldreich and Tremaine 1979a, Eq. 14). The balance also yields the total ring mass and precession rate. Note that for the self-gravity model, in contrast with the self-consistent approach above, only a single occultation profile is necessary for computing $q_e(a)$. Thus a second observed profile, well sepa-

rated in longitude, affords an independent means of verifying the validity of the calculated $q_e(a)$ profile.

Computational results based on the self-gravity model are shown as the dashed curves in Fig. 28 (Marouf et al. 1987). A 20, 20 and 45 streamline model is used for the α , β and ϵ rings, respectively, with individual streamline masses proportional to the local optical depth in the radio-occultation profile of highest signal-to-noise ratio (wider radio profile in each of Figs. 16, 17 and 22). For the case of the ϵ ring, 45 and 80 streamline models yield similar overall $q_e(a)$ behavior. As evident from Fig. 28, there is some agreement between the self-gravity and self-consistent $q_e(a)$ profiles of the α ring; however, prominent differences exist for rings β and ϵ . The ϵ ring result was used in Fig. 29b to advance the ingress and egress radio-occultation profiles to quadrature for comparison. Little agreement is apparent. These results strongly suggest, at least for rings β and ϵ , the presence of additional unmodeled perturbing physical mechanism(s). It is conceivable in the case of the ϵ ring that the 47:49 second-order eccentric resonance with Cordelia that falls at $\sim 51,150$ km (Porco and Goldreich 1987), appreciably influences the simple balance invoked to compute $q_e(a)$ in Fig. 28. It is possible that the large $q_e(a)$ values ($q_e \approx 0.8$ to 0.9) seen in the self-consistent $q_e(a)$ profile of the ϵ ring exterior to $a \approx 51,150$ km (Fig. 28) are a consequence of strongly perturbed streamlines rather than a "true" enhancement in $q_e(a)$ of the elliptical streamline shape. Perhaps a resonance with an undetected satellite is also responsible for the poor β ring results. At present, this is an area of active research, including investigation of alternative explanations for locked apsidal precession, such as the precessional pinch mechanism suggested by Dermott and Murray (1980).

Borderies et al. (1988) used a least-squares fit to multiple occultation profiles at various longitudes to determine the $q_e(a)$ profile of the ϵ ring. Their results agree with those of Marouf et al. (1987) if the fit is restricted to the two RSS profiles. However, they found that a simultaneous fit to the RSS and PPS profiles required relaxation of the assumption of aligned elliptical streamlines. They attributed deviations from the aligned streamlines model to a combination of perturbations due to the satellite resonances bounding the ring (and to the weaker 47:49 Cordelia resonance), to large individual ring particles, and to the neglect of the modified viscous stresses associated with these perturbations.

Comparison with Narrow Saturnian Ringlets. In Table VIII, the salient features of the Uranian α , β , γ , δ and ϵ rings are compared with those of several narrow Saturnian ringlets (Porco et al. 1984b; Porco and Nicholson 1987; Porco 1989). Each of the latter exhibits radial perturbations, some of which are suspected to be resonantly forced (the Titan and Huygens ringlets at 1.29 and 1.95 R_s , respectively). The Maxwell ringlet at 1.45 R_s and the ringlets at 1.470 and 1.495 R_s , all located in the outer C ring, appear to be

TABLE VIII^a
Comparison of Saturnian and Uranian Narrow Rings

Planet	Ring	<i>a</i> (km)	<i>ae</i> (km)	<i>m</i>	δa (km)	q_e	$\delta e/e$	Σ (g cm ⁻²)
Uranus	ϵ	51149	404	1	58.1	0.65	0.09	25
	β	45661	20.2	1	8.2	0.38	0.15	2(?)
	α	44718	34.0	1	7.2	0.49	0.10	2(?)
	γ	47627	5.2	1				
				0	5.2			
	δ	48300	3.1	2	4.6	0.43	0.64	7
Saturn	Maxwell	87491	30	1	64	0.47	1.0	17
	Huygens	117850	30	1 + ?	50	<0.6	<1.1	—
	Titan	77871	20	1	25	0.44	0.5	17
	1.495 R _s	90171	2.8	1	62	<0.05	<1.1	>28
	1.470 R _s	88716	1.4	1(?)	16	<0.5	<6.0	>0.5
				2.1	2(?)	16	<0.4	>3.0

^aAdapted from Table I of Porco (1989).

freely precessing ellipses similar to the Uranian eccentric rings. Included in Table VIII are the ringlets' mean radius *a*, mean width δa , observed radial amplitude *ae* and the *m* value for the observed radial distortions, the dimensionless eccentricity gradient q_e (where known), the fractional change in eccentricity across the ringlet, and the surface mass density inferred from the Goldreich and Tremaine (1979a) self-gravity model. Some of the gradient parameters are known only as upper limits.

From the entries in Table VIII, it is apparent that there is a considerable range in ring width δa , and in radial amplitude *ae*, but much smaller ranges in the important physical parameters of q_e and surface density Σ . Apart from specifying the fractional variation in width as a function of longitude, q_e also measures the departure of the orbital shear motion in the ring from the unperturbed Keplerian value (Borderies et al. 1983a). For $q_e = 0.75$ (almost reached by the ϵ ring), the shear approaches zero at perapse, and the ring is at that point almost in a state of "rigid rotation" about the planet. Only for the ϵ , β , α , δ , Maxwell and Titan rings have simple width-longitude relations been established, and in each case, $0.38 < q_e < 0.65$. Upper limits on q_e for the remaining rings, estimated from the maximum and minimum widths observed, are also compatible with this range, except for the ringlet at 1.495 R_s, which exhibits an unusually small width variation. Except for the α and β rings, discussed in more detail in Sec. V, the inferred surface densities fall in a rather narrow range of $7 \text{ g cm}^{-2} < \Sigma < 30 \text{ g cm}^{-2}$. These bounds must be interpreted with due caution in light of the results depicted in Fig. 28.

Beyond these two observations, few systematic conclusions can be drawn from the present data. The most frequent distortions are characterized by *m* = 1, with other values found only for the narrowest rings (γ , δ and possibly 1.470 R_s). Within the framework of the normal mode model pro-

posed by Borderies et al. (1985), in which these distortions are considered as standing density waves trapped within the ring, the prevalence of $m = 1$ for wider rings can be understood as a consequence of $m = 1$ density waves having much longer radial wavelengths than those for other m values. The radial amplitude seems to be largely uncorrelated with ring width: the ratio $ae/\delta a$ ranges from 0.05 and 0.12 for $1.495 R_s$ and $1.470 R_s$, to 7.0 for the ϵ ring. Generally, the Uranian rings exhibit larger amplitudes, relative to their widths, than do the Saturnian ringlets, which might be attributable to the confinement of the latter in fairly narrow gaps within the main ring system. The fractional variations in eccentricity show the opposite trend, being less than unity for the Uranian rings and generally greater than unity for the Saturnian ringlets. However, this might be a consequence of the relative constancy of q_e , since $(\delta e/e)(ae/\delta a) = a\delta e/\delta a \approx q_e$. The variation in $\delta e/e$ may also be due, in part, to the decrease of a factor of 5 in J_2 between Saturn and Uranus, as the required surface density scales as $J_2(e/\delta e)$.

V. SHEPHERDING OF THE URANIAN RINGS

In this section the dynamical mechanism of shepherding is discussed. The Uranian ring system was the first for which ring confinement by shepherding satellites was proposed (Goldreich and Tremaine 1979a), so it is fitting that with the Voyager discovery of the ϵ ring shepherds Cordelia (1986U7) and Ophelia (1986U8) in early 1986, this system has provided the shepherding theory its most notable success. During the Voyager encounter, 10 new satellites, ranging in radius from 13 to 85 km (Smith et al. 1986; Thomas et al. 1989), were discovered interior to the orbit of Miranda. Using the new satellites' orbital elements calculated by Owen and Synnott (1987), the latest Voyager revision of GM_U , and the ring orbital elements deduced from groundbased occultation data by French et al. (1986a), Porco and Goldreich (1987) identified several low-order resonant associations involving the 2 satellites straddling the ϵ ring and 3 of the outer rings: γ , δ , and ϵ . The close correspondence between the ring edges and the resonance locations (Table III) has confirmed beyond doubt the kinematical associations between Cordelia and Ophelia and these rings. The probability of having such close agreement by chance is quite remote, and one is thus led to examine the physics of such ring-satellite interactions. Those aspects that are relevant to the shepherding mechanism are discussed first, followed by the implications for the Uranian rings.

A. Ring-Satellite Interactions

A great deal of theoretical work has been done to illuminate the role of satellites in creating the bewildering variety of structure seen in planetary ring systems: narrow eccentric and inclined rings (Goldreich and Tremaine 1981; Borderies et al. 1983a; Borderies et al. 1984a), spiral density and bending

waves (Goldreich and Tremaine, 1978a, 1979b, 1980; Shu et al. 1985a,b; Borderies et al. 1986), and sharp edges (Borderies et al. 1982). The essential feature of all these interactions is the transfer of angular momentum between satellite and rings, the variety arising from the differing ring-satellite distances and ring environments in which this transfer occurs. The point of origin for discussion of the shepherding mechanism is the gravitational resonance at which such exchange commonly takes place. Detailed descriptions of the physics and phenomenology of resonant behavior have been incorporated into several recent reviews of planetary rings (Goldreich and Tremaine 1982; Dermott 1984; Esposito et al. 1984; Franklin et al. 1984; Shu 1984).

The direction of angular momentum flow in an unperturbed disk of particles on Keplerian orbits about a planet is positive outward and its magnitude is defined by the viscous torque, $T_v \equiv L_H^*$, where L_H^* is the angular momentum luminosity, arising from particle collisions and differential rotation (Lynden-Bell and Pringle 1974):

$$T_v \approx 3\pi\Sigma\nu n a^2 \quad (23)$$

where ν is the kinematic viscosity, n is the mean motion, a is the radius, and Σ is the surface mass density. Left to itself, a ring spreads under the influence of viscosity. Material on the inside, depleted in angular momentum, spirals inward; material on the outside, enhanced with angular momentum, spirals outwards. As an explanation for the existence of the narrow Uranian rings, Goldreich and Tremaine (1979a) originally proposed that torques exerted by small satellites on either side of a ring would, via gravitational resonances, supply at the inner edge and remove at the outer edge the angular momentum which viscous stresses transport outward through the ring.

In the theory as originally proposed, the satellites and ring are sufficiently close that several resonances fall within the ring. Now, after the Voyager encounters with Saturn and Uranus, there is observational evidence for an entire spectrum of satellite-induced disturbances that have the effect of confining ring material and shepherding individual ring edges. At one end is the small satellite which has carved out the Encke gap (Cuzzi and Scargle 1985; Showalter et al. 1986), transferring angular momentum from its inner to its outer edge, and creating disturbances of limited azimuthal extent but smoothly varying in semimajor axis for a sizeable distance from the gap edges. At the other end, the outer edges of the A and B rings of Saturn are shepherded by discrete resonances with distant satellites (Porco et al. 1984a) that remove at these locations the viscous angular momentum flowing through these rings, thereby defining their edges and, in the former case, the extreme outer limit of the main Saturn ring system. Falling between these two extremes are examples in the Uranian system, in which the satellites are close to the ring and yet shepherd by discrete resonances.

In a circular equatorial ring, three types of resonances exist that are

associated with a perturbation potential varying in time t , and azimuthal angle ϕ , as $\cos(\omega t - m\phi)$. The pattern speed of the potential $\Omega_p = \omega/m$, where m is the azimuthal wavenumber. At co-rotation resonances, which occur where the particle's mean motion $n = \Omega_p$, the particles undergo slow variations in semimajor axis and longitude only; eccentricity is damped at co-rotation resonances. Inner and outer Lindblad resonances, ILR and OLR, are located where the particle's epicyclic frequency $\kappa = \pm m(n - \Omega_p)$. Orbital eccentricities are excited at such resonances since the perturbation oscillates with the particle's natural radial frequency κ . Inner and outer vertical resonances, IVR and OVR, are the vertical equivalents of ILR's and OLR's: they exist where the vertical frequency $\mu = \pm m(n - \Omega_p)$, and are the sites of excited out-of-plane particle motions. Examples of both Lindblad and vertical resonances occur in Saturn's rings. However, to date, vertical resonances in the Uranian ring/satellite system have not received much attention and will not be discussed here.

The number of resonances falling within a ring depends on the resonance spacing Δa_{res} , and the ring's mean width δa . It can be shown easily from the Lindblad resonance condition that, for small satellite-ring distances (i.e., $a - a_s << a$, where a and a_s are the ring and satellite semimajor axes, respectively), $m \approx 2a/3(a - a_s) \gg 1$ and $\Delta a_{\text{res}} \approx 2a / 3m^2$. If $\delta a > \Delta a_{\text{res}}$, then multiple resonances exist within the ring. Two additional length scales are relevant. One is the scale over which the satellite's perturbation is significant, given by the distance from resonance within which nested periodic orbits begin to cross:

$$w_p \approx \left(\frac{M_s}{M_u} \right)^{1/2} a_s \quad (24)$$

where M_s and M_u are the satellite and planetary masses, respectively. The other is the distance over which the ring's own self-gravity can enforce rigid precession of periodic orbits and essentially prevent streamline crossing. It is given by the length of the first wave that would propagate away from resonance, were there no ring edge to interrupt it:

$$w_\lambda \approx 5 \left(\frac{a^2 \Sigma}{m M_u} \right)^{1/2} a. \quad (25)$$

If Δa_{res} is significantly greater than the larger of w_p and w_λ , the resonances are isolated. For the first-order Lindblad resonances (see below) of Ophelia falling near the outer edge of the ϵ ring, $m = 14$ and $\Delta a_{\text{res}} \sim 175$ km; for Cordelia's resonances near the inner ϵ ring edge, $m = 24$ and $\Delta a_{\text{res}} \sim 59$ km. Equations (24) and (25) yield a maximum resonance width of $w_\lambda \sim 7$ km, significantly smaller than the mean width of the ϵ ring of 58 km (Table

VII). Therefore, not only are the first-order resonances of both satellites clearly isolated, but for each satellite's resonances, $\Delta a_{\text{res}} > \delta a$. These circumstances led Porco and Goldreich (1987) to conclude that the ϵ ring must be shepherded by single, discrete resonances at each edge.

The behavior of ring particles will depend on the type of resonance (if any) near which the particles find themselves. A pure Lindblad resonance falling within a ring will be replaced by the more complex eccentric resonance when the ring's unperturbed eccentricity exceeds the perturbation excited by the resonance. At eccentric resonances, variations in semimajor axis and orbital longitude, which are characteristic of co-rotation resonances, are accompanied by the excursions in eccentricity and longitude of periape that are characteristic of Lindblad resonances. The pure co-rotation resonances maintain their identities in an eccentric ring. The resonances falling within the ϵ ring, for example, are truly eccentric: the maximum perturbation one could expect near the resonances of either Cordelia or Ophelia is $a_e \leq 7$ km, yet the amplitude of the ϵ ring's distortion is $a_e = 404$ km. However, Goldreich and Porco (1987) showed that in the Uranian rings, the co-rotation torques associated with eccentric resonances and those associated with isolated resonances turn off or "saturate"; viscous diffusion appears too feeble to prevent the azimuthal concentrations of particles that result at a co-rotation resonance. Once these concentrations do form, the actual co-rotation torque is severely reduced in much the same way as the torque associated with a Lindblad resonance is reduced once a ring edge or gap forms (see below). Consequently, co-rotation resonances are unimportant in the Uranian rings.

B. The Dynamics of Shepherding

The kinematical associations between satellites and rings are clearly established in the Uranian system. Still open to question, however, is the capability of the satellites to supply sufficient torque to confine the ring against its tendency to spread. All relevant torques are estimated below. It should be kept in mind during the following discussion that several quantities of interest are poorly known. For example, the satellite masses are estimated by adopting the density of the 5 major Uranian satellites (Tyler et al. 1986) which may in fact not be applicable to the shepherd satellites. Moreover, the generalized formulae for the Lindblad torque T^L , particularly the nonlinear torque, exerted by a satellite on a smooth uninterrupted disk is accurate only to order of magnitude, and it represents the *maximum* torque that the satellite can exert at a ring edge. If $T_v \gg T^L$, a spiral wave, rather than a gap, will form and carry away the added angular momentum luminosity due to the satellite. If $T_v \ll T^L$, then ring material will recede from resonance, a gap (and edge) will form, and equilibrium will be reached when Σ , the kinematic viscosity v , and the distance of the ring's edge from resonance have been altered sufficiently to insure that $T_v = T^L$. An additional complication in the case of the Uranian rings is the discovery of the distended Uranian atmosphere (Broad-

foot et al. 1986) that exerts a substantial drag torque T_D on the ring particles orbiting within it. In determining the viability of satellite shepherding for the Uranian rings, one must verify whether, at each resonance, T^L is sufficient to balance all competing torques acting to spread or move the ring.

At first- and second-order Lindblad resonances, the generalized satellite torque formulae, in a form appropriate for $m \gg 1$, are (Goldreich and Porco 1987):

$$T_1^L = \mp 8.6m^2 \left(\frac{M_s}{M_U} \right)^2 \Sigma n^2 a^4 \quad (26)$$

$$T_2^L = \mp 3.0e_s^2 m^4 \left(\frac{M_s}{M_U} \right)^2 \Sigma n^2 a^4 \quad (27)$$

where e_s is the satellite's eccentricity. The angular momentum luminosity supplied by these torques is $T_v \equiv L_H^v$, and is negative at inner eccentric resonances (IER's) and positive at outer eccentric resonances (OER's). Hence the upper and lower signs on the Lindblad torques apply to IER and OER, respectively. These formulae are derived from linear theory. A disturbance produced by a satellite is nonlinear when the fractional surface mass density perturbation becomes of order unity. For first-order resonances, semi-quantitative estimates of the critical torque at which nonlinear behavior sets in, and the nonlinear torque have been given by Borderies et al. (1984b):

$$T_{1,c}^L \approx \frac{\pi^2 \Sigma^3 n^2 a^8}{6M_U^2} \quad (28)$$

$$T_{1,nl}^L \approx \mp \frac{3.7 m M_s \Sigma n^2 a^6}{M_U^2}. \quad (29)$$

In explaining the sharpness of shepherded ring edges on length scales much shorter than the width of the resonance w_p , Borderies et al. (1982) were led to the discovery that satellite perturbations could be strong enough to produce local reversals in the direction of viscous angular momentum flux, while the total viscous angular momentum luminosity, averaged in azimuth around a ring, remains positive. In the case of a ring with aligned apses, sizeable eccentricity gradient, and narrow width and eccentricity maintained by a shepherding satellite, flux reversal would occur first at periape where the ring is narrowest. The dissipation associated with enhanced viscous stresses at this location acts to damp the ring's eccentricity; the shepherding torques, however, act to maintain it. Flux reversal might also occur in

strongly perturbed regions associated with nonlinear density waves launched at satellite resonances falling within the ring, leading to the possibility that, throughout a large range in semimajor axis, the angular momentum luminosity may be greatly reduced.

In any case, if the viscous torque is reduced well below its unperturbed value owing to local flux reversals, then the physics of shepherding becomes substantially different. Satellites will shepherd a ring not so much by providing the natural L_h^* required by the ring in its confined and predominantly unperturbed state, but by *reducing* the requirement. The satellites in this new form of shepherding can be a factor of $[\delta a / (a - a_s)]^2$ smaller in mass than in the standard shepherding model, in which each satellite is assumed to have several resonances within a ring (Goldreich and Porco 1987).

For reasons given above, it is essential to know the viscous stresses T_v operating in the rings. Estimates of the kinematic viscosity ν in Saturn's rings are obtained from the analysis of spiral density and bending waves (vertical resonances). Only a marginal wave-like feature is detectable at the inner edge of Uranus' δ ring (Horn et al. 1987; Marouf et al. 1988b; see the chapter by Esposito et al.). Estimates of ν for the Uranian rings can be derived, however, from the possible presence of apsidal shifts in the α and β rings (see Sec. IV). As no apsidal shift is detectable in any of the other rings, an estimate of T_v must be obtained by other means. The ϵ ring and its attendant shepherds represent the only example in the Uranian system in which both the source and sink of angular momentum luminosity flowing through the ring are known. In this case, one can derive an upper limit to the viscous torque presently exerted by the ring on the shepherds by assuming that both satellites started out at the ring at a time $t_\epsilon = 4.6$ Gyr ago and evolved to their present positions through the exchange of angular momentum (Goldreich and Porco 1987). If the system is much younger, this upper limit is increased. For the other rings, one can estimate the minimum viscosity that is achieved when the particles are very close packed and behave like an incompressible fluid:

$$\nu_{\min} \approx n \left(\frac{\Sigma}{\rho} \right)^2 \quad (30)$$

where ρ is the bulk density of the ring material (Borderies et al. 1985). The mass of a ring, and hence Σ , can be determined from the assumption that self-gravity counteracts the effect of either differential precession (for rings in which $m = 1$) or differential mean motion (for $m \geq 2$).

As mentioned above, Uranus' distended and presumably rigidly rotating hydrogen atmosphere, with a period of ≈ 17 hr, presents an additional inwardly directed torque on the ring particles. The number density of hydrogen atoms, extrapolated from the model of Broadfoot et al. (1986), is sufficiently large throughout the rings that even at the ϵ ring the torque exerted by hydro-

gen atoms colliding with ring particles is comparable to the viscous torque. Any satellite, like Cordelia, that confines a ring's inner edge via an OER must balance the loss of angular momentum suffered by the particles via collisions and atmospheric drag. The hydrogen atoms collide with the particles of the ring, exerting a torque

$$T_D \approx -\pi N_H(a) m_H v_T a^3 \Delta a \Delta n \quad (31)$$

where v_T is the average thermal speed of the hydrogen atoms of mass m_H , N_H is the hydrogen density number, Δa is the ring width, and $\Delta n = n_r - n_{atm}$ is the difference in the mean motion between the ring particles and the rigidly rotating atmosphere. Equation (31) assumes that the ring optical depth is larger than unity, a supposition that is true for most of the Uranian rings.

Goldreich and Porco (1987) investigated the dynamical relationships between satellite, atmospheric and viscous torques within the Uranian system. Subsequent revisions in the satellite radii (Thomas et al. 1989), and hence the estimated satellite masses, have changed the initially derived numerical values but not the conclusions. Values for all of the pertinent torques computed from the revised satellite masses are given in Table IX. It appears that the standard theory of shepherding is marginally adequate for the ϵ ring. The best estimates for the maximum nonlinear torques exerted by Cordelia and Ophelia on the inner and outer edges of the ring are large enough, within all considered uncertainties, to balance both T_D and T_v . However, the possibility cannot be dismissed that there are significant nonlinear perturbations in a ring whose $q_e \sim 0.7$, and that the shepherding mechanism is proceeding to some degree via flux reversal. One candidate ring region is the dense narrow core near the outer edge where the $q_e(a)$ profile constructed from the radio-occultation measurements (Fig. 28 above) shows an unusually large $q_e \sim 0.7$ to 0.8. In addition, the second-order resonance with Cordelia at $\sim 51,150$ km (47:49 OER), whose strength is comparable to the nonlinear torques at the first-order resonances, might be the site of a nonlinear wave which, together with the large eccentricity gradient across the ring, distorts the particle streamlines sufficiently to lead to flux reversal. A wave-like feature at this location was noted in the PPS data but does not appear to exhibit the wavelength variation of a density wave (Yanamandra-Fisher and Esposito 1986). This wave-like feature is not detectable in the radio-occultation profiles (Fig. 22).

At the time of writing, no other satellites have been found within the ring system. A limiting radius of $R \leq 10$ km for a reflectivity of $\sim 2\%$ has been determined from the Voyager imaging experiment for any unseen shepherds (Smith et al. 1986). Confinement of ring material via gravitational resonances between ring particles and nonradial acoustic oscillations within the interior of Uranus has been investigated, but appears incapable of explaining

TABLE IX^a
Torques

Type ^b		Location (km)	Torque (erg) ^c	
ϵ ring ^d				
First-order Lindblad				
Ophelia	14:13 IER	51178.1 ± 1.8	-6×10^{16}	(-6×10^{16})
Cordelia	24:25 OER	51121.2 ± 0.3	$+9 \times 10^{16}$	$(+7 \times 10^{16})$
Cordelia	23:24 OER	51180.3 ± 0.3	$+9 \times 10^{16}$	$(+7 \times 10^{16})$
Viscous ^e		—	$+1 \times 10^{16}$	
Atmospheric		—	-2×10^{16}	
Critical		—	6×10^{16}	
δ ring ^d				
First-order Lindblad				
Cordelia	23:22 IER	48302.5 ± 0.3	-2×10^{16}	(-5×10^{15})
Atmospheric		—	-5×10^{15}	
Critical		—	1×10^{15}	
γ ring ^d				
First-order Lindblad				
Ophelia	6:5 IER	47625.7 ± 1.8	-3×10^{15}	(-2×10^{15})
Atmospheric		—	-3×10^{15}	
Critical		—	1×10^{15}	

^a Adapted from Table I of Goldreich and Porco (1987).

^b Code: IER = inner eccentric resonances; OER = outer eccentric resonances.

^c Nonlinear torques in parentheses.

^d Using $\Sigma_{\epsilon} = 25 \text{ g cm}^{-2}$, $\Sigma_{\delta} = 7 \text{ g cm}^{-2}$, and $\Sigma_{\gamma} = 7 \text{ g cm}^{-2}$.

^e Assuming $t_{\epsilon} = 4.5 \text{ Gyr}$. Value is larger for a younger ring.

any ring features within the Uranian system (Marley et al. 1988). Hence, for the remaining rings, one can ask what size satellite would be required to prevent a ring's inner edge from spreading inward under the viscous and atmospheric torques. Using for the δ ring a mass determined from the requirement that self-gravity is maintaining apse alignment by balancing differential mean motion associated with its $m = 2$ normal mode (Goldreich and Porco 1987, Eq. 3), one obtains $\Sigma_{\delta} \sim 7 \text{ g cm}^{-2}$. This implies that an unseen satellite small enough to have escaped detection by the Voyager cameras and placed approximately midway between δ and γ could confine the ring's inner edge against viscous diffusion and atmospheric drag. Horn et al. (1988b) cited a wave-like feature in the inner half of the δ ring as a possible density wave excited by such a satellite, although the location of this wave falls precisely on a high wavenumber IVR of Cordelia, which makes its identification as a density wave questionable. Similar torque-balancing arguments made for ring γ , assuming $\Sigma_{\gamma} \sim 7 \text{ g cm}^{-2}$, yield the same result: no observational evidence is violated by placing a small satellite between γ and η to shepherd the inner edge of γ .

However, more serious problems are encountered when the effect of at-

mospheric drag on the rings that are closer to the planet is considered. In the case of the α and β rings, for which Σ has been evaluated from the self-gravity model, a satellite of diameter ~ 62 km, midway between the α and β rings, would be required to balance the atmospheric drag on the β ring. A satellite this large would require an implausibly low reflectivity of 0.2% to have gone undetected by the Voyager cameras. (The ring particle Bond albedo is 1.4% [Ockert et al. 1987].) The minimum viscous torque is several orders of magnitude lower and poses no obstacle. The difficulty arises from the low values of $\Sigma \sim 2$ g cm $^{-2}$ implied by the self-gravity model, values that are also difficult to reconcile with the large particle sizes suggested by the apparent lack of differential attenuation of the 3.6 and 13 cm radio signals (Gresh et al. 1989; see also the chapter by Esposito et al.) for these rings. These two independent lines of evidence suggest that the self-gravity hypothesis must be yielding implausibly small ring masses. Larger masses would insure that $T_{\text{f},nl}^l > T_D$ (since $T_{\text{f},nl}^l \propto \Sigma^2$ and T_D is independent of Σ), and would not endanger the requirement that $T_{\text{f},nl}^l > T_V$.

The Uranian ring system provides a striking example of shepherding, although perhaps the ϵ ring, with its 2 companion satellites, is a better example of shepherding by flux reversal than via the standard model. Nevertheless, one is left with a number of puzzles. Foremost among these are the apparent discrepancies between dynamical and occultation inferences of eccentricity gradient profiles, surface mass densities and physical ring thickness. On the one hand, dynamical arguments indicate that the ϵ ring is no more than a few meters thick, with surface mass density $\Sigma \sim 30$ g cm $^{-2}$, comparable to values inferred for Saturn's rings (Cuzzi et al. 1984; Esposito et al. 1984). On the other hand, occultation observations favor a ring that is at least a few tens of meters thick, and cast doubt on the validity of the self-gravity hypothesis used to estimate Σ , at least in its simple originally proposed form (Goldreich and Tremaine 1979a). A lower bound $\Sigma_\epsilon > 80$ g cm $^{-2}$ (for $\rho \sim 1$ g cm $^{-3}$) from radio-occultation observations is much larger than values observed anywhere in Saturn's rings and poses potential problems for shepherding mechanisms as we currently understand them.

Especially puzzling is the case of the α ring where $q(a)$ profiles deduced from occultation and dynamical considerations are in rough accord (see top panel of Fig. 28) yet $\Sigma_\alpha \sim 2$ g cm $^{-2}$ inferred from the self-gravity hypothesis is much too small to counteract the atmospheric drag torque and also too small to be consistent with the observed large, and almost equal, 3.6 and 13 cm opacities. It is clear that identification of physical mechanisms responsible for the observed rigid precession of the α and β rings, as well as mechanisms that explain the $q_e(a)$ profiles in Fig. 28, are urgent outstanding problems. It is also clear that the simple scattering models used to infer the apparently large Σ bound also need critical examination in view of possible elaborate particle structure ($\rho << 1$ g cm $^{-3}$) or possible near-field (coherent) interactions among ring particles.

VI. UNSOLVED PROBLEMS AND FUTURE DIRECTIONS

Prior to 1977, only Saturn's rings were known, and the discoveries of Uranus' narrow rings, Jupiter's diaphanous dust belt, and Neptune's fragmented ring arcs lay ahead. In that brief span, the remarkable diversity of phenomena in planetary rings has been revealed, and it is now quite clear that life as a ring particle is not necessarily benign or placid. Formerly, Saturn's rings appeared broad, nearly featureless, and eternal; it is now known that they are richly filigreed and under siege by gravitational and erosive processes that do not augur longevity. In this chapter, the observed characteristics of the Uranian rings have been emphasized, but it is well to keep in mind that behind the striking differences among the known planetary ring systems lurk common physical processes, and perhaps a common genesis as well. The Earth-based discovery and investigation of the Uranian rings and the subsequent exploration by Voyager of the rings of Jupiter, Saturn, Uranus and Neptune have afforded an examination of the dynamics and structure of rings narrow and broad, icy and dusty, opaque and diffuse. What are the prospects for putting these pieces together to achieve a coherent understanding of the origin and evolution of planetary rings? The answer is unclear, but surely advances will come from the synergism of interpretation, observations and theory. A survey of the prospects for progress in each of these areas for the Uranian rings will close this chapter.

A. Existing Observations: Puzzles and Prospects

Voyager observations have made it possible to examine ring structure at a spatial resolution unachievable from the ground, and the observed radial and azimuthal variations are now being explored. The ring gallery in Figs. 13 through 22 shows detailed internal structure in several rings, but the limited azimuthal coverage is an obstacle to determining the particle streamlines that characterize a ring's structure and reflect the dynamics of its confinement. One promising approach is to compare the high-resolution Voyager observations with the lower-resolution groundbased occultation profiles that sample a wider range of ring azimuths. For example, the Voyager observations can be used to model the normalized eccentricity gradient of a ring $q_e(a)$, which can then be used to predict the radial structure of the rings at the azimuths observed during groundbased occultations. By constructing a suite of such model ring templates, it might be possible to test a variety of eccentricity profiles, such as the self-gravity model, the constant eccentricity gradient model, and the "self-consistent" model described in Sec. IV.C above.

Another area in which progress can be made by judicious combination of Earth-based and spacecraft data is in the refinement of ring orbit models. The kinematical model of Sec. II is sufficiently accurate that weak dynamical effects might be detectable in the data and previously ignored systematic effects should now be taken into account. For example, excited normal modes

are clearly present in rings δ and γ , but no systematic search has been made for possible lower-amplitude normal modes in the other rings or for the simultaneous presence of several modes in a single ring. As another example, the precession rates of individual rings are known to a few parts in 10^5 (Table IV), which may permit the determination of the densities of small satellites, through their forced precession of nearby rings, and J_6 , once the forced precessions due to the 5 main satellites have been taken into account.

The discovery that Cordelia and Ophelia shepherd several of the rings is of great importance for the study of ring dynamics, but to date no direct connection between the satellites and observed ring structure has been established. Initial searches for waves excited in the ϵ ring edges by the shepherds were unsuccessful (French 1987), but if such satellite-induced waves are detectable in Voyager observations (Horn et al. 1988a), then similar features might be identifiable in high-quality Earth-based data. This renews the possibility of determining the satellite orbital periods to very great precision, which in turn may permit a more accurate determination of ring orbital radii and the planetary mass, GM_U .

Although only 2 shepherds have been found in the Uranian system, one clear lesson is that a single satellite may play a role in the confinement of several rings (Table III). With this example, and ring semimajor axes that are known to better than 1 km, it is possible to conduct a numerical search for the locations of shepherds that might have resonances near several rings. Signatures of any such putative satellites could then be sought in the radial structure, widths and orbits of the affected rings. Preliminary efforts in that endeavor were reported by Marouf (1988a,b). A putative satellite at $\sim 42,901$ km radius, for example, would simultaneously shepherd the three abrupt outer edges of rings 6, 5 and 4, that all fall within 1 km of first-order IER's (27:26, 43:42 and 87:86, respectively). A second putative satellite at $\sim 47,166$ km (~ 9 km inside the sharp inner edge of the η ring) has first-order, well isolated, eccentric resonances that simultaneously influence rings 6, α , β and γ (7:6, 13:12, 21:20 and 68:69, respectively). Furthermore, the same satellite has a second-order resonance (55:57) at $\sim 48,300$ km, the approximate resonance location within the δ ring pertinent to the excitation of the wave-like feature observed near the inner edge (Marouf et al. 1988b).

Still unexplained are some enigmatic Voyager observations. Perhaps the most puzzling is the anomalous scattered signal from the ϵ ring observed during the radio-occultation experiment. It is hard to envision a mechanism that could maintain the elongated structures within the ring that appear to be necessary to account for the large measured signal strength.

B. Future Observations

For years, the Uranian rings were just below the margin of detectability from the Earth, hidden from view by virtue of their remoteness and their low albedo. Improvements in detectors and in observing techniques have made it

possible to observe the rings from the ground routinely, using stellar occultations, and it is important that such observations continue to be made. It is worth remembering that it was the *combination* of the long time baseline of groundbased observations and the high-resolution of Voyager occultation profiles that made it possible to determine accurate ring orbits, discover excited normal modes in the rings, and identify satellite-ring resonances of dynamical importance. As it appears unlikely that another spacecraft will visit Uranus in the near future, Earth-based observations must add to the factual basis upon which interpretation and theory depend.

On average, there are several stellar occultations a year that can provide useful data with intermediate sized (1.5-m class) telescopes (Mink and Kleymola 1985). Only through continued improvement of the kinematical ring orbit model will it be possible to tighten the constraints on anomalous precession rates due to small satellites and improve the chances for detecting other weak dynamical effects in the rings. Because the accuracy of the precession rates is directly related to the time span of the observations being fitted, continued monitoring of even relatively low signal-to-noise events is valuable. Worldwide observations of high signal-to-noise events, such as the notable four-day occultation of U36 in April 1987 (Elliot et al. 1987a), can be used to investigate high wavenumber variations in azimuthal ring structure, such as kinks in the edges of the ϵ ring (Kangas and Elliot 1988), that are inaccessible in the more widely separated Voyager observations.

The launch of the Hubble Space Telescope offers additional opportunities for new observations. The expected pointing accuracy of the HST should make it possible to observe ring occultations by early spectral type stars at short wavelengths (visible and ultraviolet) by using a small aperture in the photometer to exclude the bright reflected sunlight from Uranus. Observing at short wavelengths reduces the Fresnel scale, making it possible to observe more detailed radial structure in the rings than is possible at infrared wavelengths. Furthermore, the angular diameters of the early spectral type stars selected for spacecraft observation are likely to be smaller than those typical of groundbased occultations, thus avoiding additional smoothing effects due to the strip brightness distribution of the stellar disk. Finally, the short wavelengths of the observations may permit detection of the faint dusty λ ring.

C. Open Theoretical Questions

Much of the observed structure and kinematics of the Uranian rings is well-understood on the basis of shepherding models of ring confinement and self-gravity models of apse alignment. Nonetheless, despite the success of shepherding theories in accounting for many of the observed features of the rings, there are many troublesome and poorly understood elements of the dynamics of narrow rings. There is little doubt that Cordelia and Ophelia maintain the sharp edges of the ϵ ring, but the masses of these satellites are uncomfortably low and the derived torques seem only marginally capable of

TABLE X
Status of the Self-Gravity Model for Narrow Eccentric Rings

Arguments in Favor	Arguments Against	Possible Counter Arguments
The model makes specific, testable predictions of surface density, velocity dispersion, and eccentricity profile based on observable ring parameters ($a, e, \delta a, \delta e, \delta w$, optical depth profile). No other model does so.	Rings 4, 5, and 6 show no correlation between width and true anomaly, despite measurable width variations in the Voyager data and large ring eccentricities.	Width variations may be controlled by other modes ($m = 0, 2, 3, \dots$), possibly with internal radial nodes, or may be due to perturbations by unseen shepherds.
Positive $\delta e/\delta a$ predicted for all distortions (except $m = 0$), as observed for Uranian ϵ , α , β , and δ rings, and Saturnian Maxwell and Titan ringlets.	γ ring shows no correlation of width with $m = 1$ or $m = 0$ phase, despite dramatic width variations.	Width variations may be controlled by other modes ($m = 2, 3, \dots$).
Negative $\delta \omega/\delta a$ predicted for $m = 1$, as observed for the α and β rings. Small predicted $\delta \omega/\delta a$ for the ϵ ring is consistent with the absence of observed apsidal shift.	RSS 3.6/13 cm optical depth ratios and $\rho = 1 \text{ g cm}^{-3}$ imply a surface mass density $\geq 80 \text{ g cm}^{-2}$, large compared to $\Sigma \approx 30 \text{ g cm}^{-2}$ predicted from the self-gravity model.	(a) The particle density may be $<< 1 \text{ g cm}^{-3}$ (fluffy structures). (b) A smaller Σ would result if the size distribution is flatter than $q = 2.5$ and the upper size cutoff is less than 1 m.
Surface density implied by $m = 2$ δ ring width variations (7 g cm^{-2}) is similar to	PPS noise statistics imply an effective particle radius of 3 m and a corresponding ϵ	(a) The PPS noise model may not be applicable if meter-scale structure is present in

<p>that for ϵ, α, and β ($2 - 25 \text{ g cm}^{-2}$), despite very different dependencies on J_2 and $\delta\epsilon$ for $m = 1$ and $m = 2$.</p>	<p>The implied surface densities for ϵ and δ are consistent with torque constraints from shepherding and (extrapolated) atmospheric drag.</p>	<p>Perturbations due to self-gravity must be important, unless surface densities are $\leq 1 \text{ g cm}^{-2}$, which is very unlikely. (This is <i>not</i>, however, an argument for the Goldreich and Tremaine (1979a) model, <i>per se</i>.)</p>	<p>ring surface density $\approx 125 \text{ g cm}^{-2}$ for $q=3$, or 280 g cm^{-2} for a monodisperse ring. The δ ring appears similar.</p> <p>The implied surface densities for α and β rings (2 g cm^{-2}) are incompatible with (a) $3.6/13 \text{ cm}$ optical depth ratios, and (b) torque constraints from atmospheric drag.</p> <p>The ring thickness implied for the α and β rings ($2H = 15 \text{ m}$) is not consistent with observed conservation of equivalent depth with longitude, which implies $2H \geq 30 \text{ m}$ for the ϵ ring. (Note that this comparison involves different rings, which might really be different; the upper limit on the ϵ apsidal shift implies $2H \leq 60 \text{ m}$.)</p> <p>Much of the physics implicit in the self-gravity model is common to density waves, for which the theory is well substantiated by observations.</p>
			<p>(a) The particle size distribution may be flatter than $q = 2.5$, provided that the upper size cutoff is less than 1 m. (b) The atmospheric density may be overestimated.</p> <p>(a) Near-field coupling effects on measured optical depth in the presence of a particle size distribution are not well understood. (b) There may be deficiencies in the collisional model used to calculate the effective ring viscosity.</p> <p>$\delta\epsilon/\delta a(a)$ profiles predicted for ϵ and β rings from Voyager RSS opacity profiles are less consistent with observed opacity profile variation with longitude than a simple constant-$\delta\epsilon/\delta a$ model.</p>
			<p>(a) Other perturbations may also affect $\delta\epsilon/\delta a$ (<i>e.g.</i>, Cordelia 47:49 OER within ϵ ring). (b) Optical depth may not mirror mass density, even at 3.6 cm. (c) Modification of the self-gravity model to incorporate satellite perturbations and viscous effects may permit improved fits to profiles.</p>

overcoming the effects of atmospheric drag. Atmospheric drag is so large that it raises the possibility that the rings are short-lived. Shepherd satellites still have not been found for all of the rings, leaving open the possibility that other mechanisms are at work in these rings (see the chapter by Esposito et al.).

The self-gravity model of apse alignment is the only theory which has been developed in sufficient detail to permit direct comparison with observations, and although it can account for the observed width-radius relations of the α , β and ϵ rings, it has a number of serious weaknesses in its present form. It predicts unreasonably low surface mass densities for the α and β rings. The detailed structure of the ϵ ring does not match the predictions of the existing self-gravity model, which may require refinement to make it more realistic. In Table X, we have attempted to summarize the arguments, both theoretical and observational, for and against the self-gravity model. It would be useful to extend other theoretical approaches, such as Dermott and Murray's (1980) precessional pinch model for apse alignment, to the point where critical observational tests can be performed.

Dermott and Murray (1980) proposed that close packing of the ϵ ring particles as they move through pericenter would force re-alignment of their pericenters on each orbit. Their model was motivated, in part, by the observation that even a small initial mis-alignment of pericenters in an eccentric ring with $\delta a \ll ae$ results in a region of the ring near quadrature being pinched down to a width $\ll \delta a$ (cf. Eq. 22 above). At this point, self-gravity creates a positive eccentricity gradient across the ring, which then forces the pinch to move towards pericenter. In equilibrium, collisions at pericenter maintain the state of uniform precession, with zero apsidal shift, and the positive eccentricity gradient is such as to ensure the close-packing configuration.

Although the concept of the "precessional pinch" seems plausible, no attempt has yet been made to quantify the collisional processes at pericenter, or to calculate precise predictions of eccentricity gradients from the model; it thus remains observationally almost untestable. Two specific predictions by Dermott and Murray have not been borne out by subsequent observations: that the optical depths of all eccentric rings at pericenter should be large, and that rings of lower mean optical depth should exhibit greater eccentricity gradients q_e . The former prediction is not satisfied by the Uranian α and β rings, for which $\tau = 0.7$ and 0.4 , respectively, at pericenter. As for the latter prediction, the ϵ ring remains the most opaque of the 6 well-characterized narrow eccentric rings (see Table VIII), but shows the largest q_e . Finally, the accurate conservation of equivalent depth as a function of longitude exhibited by the ϵ ring (see Fig. 8) argues strongly against the ring particles being tightly packed at pericenter (Tyler et al. 1986; Gresh et al. 1989).

With the passage of Voyager through the Uranus system, we now have detailed ring profiles that can be used to stimulate and test new theoretical developments. We know how sharp the ring edges are, we have some evi-

dence for the extent of azimuthal and radial variations in their internal structure, and the overall width and optical depth variations of the rings have been well determined. Width variations of most of the narrow rings are not well understood, most notably rings 6, 5, 4 and γ , which have well-determined noncircular orbits but whose widths do not vary linearly with orbital radius. Longareti (1988) has proposed two mechanisms that might account for such anomalous width-radius relations: the simultaneous presence of two normal modes in a ring, and overstable libration. These remain to be explored in detail.

Significant progress in unravelling these and other mysteries of the Uranian rings can be expected during the coming years. The groundbased and Voyager observations described above will provide a solid foundation for new theoretical developments, and the infusion of new data from the Hubble Space Telescope and groundbased observations should allow continued refinement of orbital and structural models of the rings.